

1-1-2013

# Gold Nanoparticles and Peptoids as Novel Inhibitors of Amyloid Beta Aggregation in Alzheimer's Disease

Kelly Ann Moore  
*University of South Carolina*

Follow this and additional works at: <http://scholarcommons.sc.edu/etd>

---

## Recommended Citation

Moore, K. A. (2013). *Gold Nanoparticles and Peptoids as Novel Inhibitors of Amyloid Beta Aggregation in Alzheimer's Disease*. (Doctoral dissertation). Retrieved from <http://scholarcommons.sc.edu/etd/531>

This Open Access Dissertation is brought to you for free and open access by Scholar Commons. It has been accepted for inclusion in Theses and Dissertations by an authorized administrator of Scholar Commons. For more information, please contact [SCHOLARC@mailbox.sc.edu](mailto:SCHOLARC@mailbox.sc.edu).

GOLD NANOPARTICLES AND PEPTOIDS AS NOVEL INHIBITORS OF A $\beta$  AGGREGATION IN  
ALZHEIMER'S DISEASE

by

Kelly Ann Moore

Bachelor of Science, Engineering  
University of Hartford, 2007

---

Submitted in Partial Fulfillment of the Requirements

For the Degree of Doctor of Philosophy in

Biomedical Engineering

College of Engineering & Computing

University of South Carolina

2013

Accepted by:

Melissa Moss, Major Professor

James Blanchette, Committee Member

Robert Price, Committee Member

Tarek Shazly, Committee Member

Lacy Ford, Vice Provost and Dean of Graduate Studies

© Copyright by Kelly Ann Moore, 2013  
All Rights Reserved.

## ACKNOWLEDGEMENTS

I would like to acknowledge my advisor and mentor Dr. Moss for all of her patience, help, and understanding throughout the years. I would like to thank my committee members Dr. Blanchette, Dr. Shazly, and Dr. Price for their help and input in preparing my dissertation. I would also like to thank all of the previous and current members of Dr. Moss' lab for all their help.

I would like to thank my mother, Lynn, for her continued support of my dreams to pursue my Ph.D. Finally, I would like to thank my husband Keith who is always there to listen, encourage and support me.

## ABSTRACT

In 2012 it was estimated that one in every nine Americans over the age of 65 has Alzheimer's disease (AD) (1). These patients experience gradual loss of memory, cognition, and behavioral stability eventually leading to death (2). These symptoms were first described in 1906 by Alois Alzheimer and now are the classic signs of the number one neurodegenerative disease today. Current AD therapies delay or mitigate the symptoms associated with AD to improve the quality of life for the patient; however, there is currently no cure for those that have been diagnosed. In order to develop a possible treatment for patients with mild to severe AD, the disease pathology must first be understood. One neuropathological marker for AD is the development of amyloid plaques, which are deposited around the neurons in the brain and are associated with neuronal atrophy. The main constituents of these plaques are aggregated forms of the amyloid- $\beta$  ( $A\beta$ ) peptide. Thus, one possible therapeutic intervention for AD is to inhibit the formation of  $A\beta$  aggregates.

Numerous small molecules and peptides have been studied for their ability to inhibit  $A\beta$  aggregation, but none have proven therapeutically effective. In this study, we demonstrated the effects of two novel inhibitors of  $A\beta$  aggregation. First, we examined the ability of spherical gold nanoparticles (NP) with varying diameter and surface coatings to abrogate  $A\beta$  aggregation. Results indicated that smaller NPs with an anionic poly acrylic acid (PAA) surface coating were the most effective as inhibitors of

aggregation at concentrations as low as 20 pM. Peptoids, mimicking the hydrophobic core of A $\beta$ , were also studied for their ability to inhibit A $\beta$  aggregation. Peptoids of similar structure, but differing in a single charged residue, induced the formation of fewer, smaller oligomeric A $\beta$  aggregates. Additionally, inclusion of a neutral or positively charged residue in the peptoid sequence induced structural changes in A $\beta$ <sub>1-42</sub> oligomers. Overall, this study provides insight into the effective properties of gold NPs and peptoids as novel potential inhibitors of A $\beta$  aggregation.

## TABLE OF CONTENTS

ACKNOWLEDGEMENTS.....	iii
ABSTRACT .....	iv
LIST OF FIGURES .....	ix
LIST OF ABBREVIATIONS.....	xi
CHAPTER 1: BACKGROUND AND SIGNIFICANCE .....	1
1.1. Alzheimer’s Disease .....	1
1.2. Amyloid- $\beta$ Protein .....	2
1.3. Inflammation and AD .....	4
1.4. Inhibition of A $\beta$ Aggregation .....	7
1.5. Therapeutic Applications of Nanoparticles in Alzheimer’s Disease .....	9
1.6. Potential Therapeutic Application of Peptoids in Alzheimer’s Disease .....	10
CHAPTER 2: MATERIALS AND METHODS .....	14
2.1. Materials .....	14
2.2. A $\beta_{1-40}$ Monomer Purification .....	15
2.3. Preparation of A $\beta_{1-40}$ Fibrils .....	17
2.4. A $\beta_{1-40}$ Monomer Aggregation .....	17
2.5. Analysis of A $\beta_{1-40}$ Monomer Aggregation with ThT.....	17
2.6. Analysis of A $\beta_{1-40}$ Monomer Aggregation by Dot Blot.....	18
2.7. Quantitative Analysis of A $\beta_{1-40}$ Monomer Aggregation.....	19

2.8. Transmission Electron Microscopy .....	21
2.9. ThT Detection of A $\beta$ <sub>1-40</sub> Aggregates in the Presence of Potential Inhibitors .....	21
2.10. Preparation of A $\beta$ <sub>1-42</sub> Oligomers .....	22
2.11. Analysis of A $\beta$ <sub>1-42</sub> Oligomerization via SDS-PAGE and Western Blotting .....	22
2.12. Determination of A $\beta$ <sub>1-42</sub> Oligomer Structure by ANS Fluorescence .....	23
2.13. Cell Culture .....	24
2.14. XTT Reduction Assay.....	24
2.15. Confocal Microscopy of NF- $\kappa$ B Activation in SH-SY5Y Cells.....	25
2.16. NF- $\kappa$ B Quantification with MATLAB .....	26
2.17. Statistical Analysis.....	26
 CHAPTER 3: SIZE AND SURFACE MODIFICATIONS OF GOLD NANOPARTICLES INFLUENCE INHIBITION OF A $\beta$ AGGREGATION .....	
3.1. Introduction.....	27
3.2. Materials & Methods .....	30
3.3. Results.....	33
3.4. Discussion .....	46
 CHAPTER 4: A NOVEL PEPTOID AS AN INHIBITOR OF A $\beta$ AGGREGATION IN ALZHEIMER'S DISEASE.....	
4.1 Introduction.....	50
4.2 Methods & Materials .....	52
4.3 Results.....	56
4.4 Discussion .....	67
 CHAPTER 5: MODULATION OF A $\beta$ AGGREGATION BY PEPTOIDS IS EFFECTED BY CHARGED RESIDUES WITHIN THE PEPTOID SEQUENCE.....	
5.1 Introduction.....	70

5.2 Methods & Materials .....	71
5.3 Results.....	74
5.4 Discussion.....	84
CHAPTER 6: CONCLUSIONS .....	87
CHAPTER 7: FUTURE WORK.....	89
REFERENCES.....	91

## LIST OF FIGURES

Figure 1.1: The amyloid cascade hypothesis .....	3
Figure 1.2: APP cleavage pathways.....	5
Figure 1.3: A $\beta$ self-assembly .....	6
Figure 1.4: Activation of NF- $\kappa$ B.....	8
Figure 1.5: Schematic comparison of peptide and peptoid structure:.....	13
Figure 2.1: Purification of A $\beta_{1-40}$ monomer.....	16
Figure 2.2: Assessment of inhibition of A $\beta_{1-40}$ monomer aggregation.....	20
Figure 3.1: NP structure.....	31
Figure 3.2: Neurotoxicity of surface coated NPs.....	34
Figure 3.3: Effect of surface coated NPs on ThT fluorescence detection of A $\beta_{1-40}$ aggregates.....	36
Figure 3.4: Effect of 18 nm NPs exhibiting varying surface chemistries on A $\beta_{1-40}$ monomer aggregation .....	37
Figure 3.5: Effect of solubilized PAA on A $\beta_{1-40}$ monomer aggregation .....	40
Figure 3.6: Morphology of A $\beta_{1-40}$ aggregates formed in the presence of 18 nm NPs exhibiting varying surface chemistries.....	41
Figure 3.7: Effect of 8 nm PAA-coated NPs on A $\beta_{1-40}$ monomer aggregation .....	43
Figure 3.8: Morphology of A $\beta_{1-40}$ aggregates formed in the presence of PAA-coated NPs of varying size .....	44
Figure 4.1: Structure of peptoid PN.....	53
Figure 4.2: Effect of peptoid PN on A $\beta_{1-40}$ monomer aggregation.....	57
Figure 4.3: Effect of peptoid PN on A $\beta_{1-42}$ oligomerization.....	59

Figure 4.4: Effect of peptoid PN on the formation of A $\beta$ <sub>1-42</sub> dimers and trimers .....	60
Figure 4.5: Peptoid PN alters A $\beta$ <sub>1-42</sub> oligomer structure to expose hydrophobic regions.....	63
Figure 4.6: Activation of NF- $\kappa$ B in SH-SY5Y human neuroblastoma cells .....	64
Figure 4.7: Effect of peptoid PN on A $\beta$ <sub>1-42</sub> oligomer induced activation of NF- $\kappa$ B.....	65
Figure 4.8: Neurotoxicity of peptoid PN .....	66
Figure 5.1: Structure of peptoids P+ and P-.....	72
Figure 5.2: Effect of peptoids P+ and P- on A $\beta$ <sub>1-40</sub> monomer aggregation .....	75
Figure 5.3: Effect of peptoid P+ on A $\beta$ <sub>1-42</sub> oligomerization .....	76
Figure 5.4: Effect of peptoid P- on A $\beta$ <sub>1-42</sub> oligomerization .....	77
Figure 5.5: Effect of peptoids P+ and P- on the formation of A $\beta$ <sub>1-42</sub> dimers and trimers.....	78
Figure 5.6: Peptoid P+, but not peptoid P-, alters A $\beta$ <sub>1-42</sub> oligomer structure to expose hydrophobic regions .....	81
Figure 5.7: Effect of peptoids P+ and P- on A $\beta$ <sub>1-42</sub> oligomer-induced activation of NF- $\kappa$ B .....	82
Figure 5.8: Neurotoxicity of peptoids P+ and P- .....	83

## LIST OF ABBREVIATIONS

AD.....	Alzheimer's disease
ADDL's.....	A $\beta$ derived diffusible ligands
ANS.....	8-Anilino-1-naphthalenesulphonic acid
ApoE.....	ApolipoproteinE
APP.....	Amyloid precursor protein
A $\beta$ .....	Amyloid- $\beta$ protein
BACE-1.....	$\beta$ -site APP-cleaving enzyme
BBB.....	Blood brain barrier
BSA.....	Bovine serum albumin
CD.....	Circular dichroism
CdTe.....	Cadmium -tellurium
CSF.....	Cerebrospinal fluid
CTAB.....	Cetyltrimethylammonium bromide
DAPI.....	4',6'-diamidino-2-phenylindole dihydro-chloride
DIC.....	N,N'-diisopropyl carboniimide
DMEM.....	Dulbecco's modified Eagle's medium
DMF.....	Dimethylformamide
DMSO.....	Dimethyl sulfoxide
ECL.....	Enhanced chemiluminescent substrate
ELISA.....	Enzyme-linked immunosorbent assays

FBS .....	Fetal bovine serum
HFIP .....	1,1,1,3,3,3-Hexafluoro-2-propanol
HRP.....	Horseradish peroxidase
IAPP .....	Islet amyloid polypeptide
LSPR.....	Localized surface plasmon resonance
MALDI .....	Matrix-Assisted Laser Desorption/Ionization
NaCl .....	Sodium chloride
NaOH .....	Sodium hydroxide
NFTs .....	Neurofibrillary tangles
NF- $\kappa$ B .....	Nuclear factor- $\kappa$ B
NP .....	Nanoparticles
PAA.....	Poly (acrylic acid)
PAH.....	Poly (allylamine hydrochloride)
PBS .....	Phosphate buffered saline
PBS-T.....	PBS with Tween
PMS.....	Phenazine methosulfate
pres1 .....	Presenilin 1
pres2 .....	Presenilin 2
QD.....	Quantum dots
RP-HPLC .....	Reversed-phase high pressure liquid chromatography
SDS-PAGE .....	Sodium dodecyl sulfate polyacrylamide gel electrophoresis
SEC .....	Size exclusion chromatography
SEM .....	Standard error of the mean

SH-SY5Y .....	Human neuroblastoma cells
TEM .....	Transmission electron microscopy
TFA.....	Trifluoroacetic acid
TGA .....	Thioglycolic acid
ThT.....	Thioflavin T
TIS.....	Triisopropylsilane
TNF- $\alpha$ .....	Recombinant human tumor necrosis factor- $\alpha$
XTT.....	2,3-Bis-(2-Methoxy-4-Nitro-5-Sulfophenyl)-2H-Tetrazolium-5-Carboxanilide

# CHAPTER 1

## BACKGROUND AND SIGNIFICANCE

### **1.1. Alzheimer's Disease**

Every 68 seconds another person in the United States develops Alzheimer's disease (AD). In 2012, it was estimated that 5.4 million Americans were afflicted by AD (1). Currently, AD ranks as the sixth leading cause of death in the United States; however, it is expected to increase as the number of people diagnosed increases every year (1). These patients experience gradual loss of memory, cognition, and behavioral stability eventually leading to death (2). In 1906, Alois Alzheimer described to the scientific community a disease in which patients were disoriented and exhibited deteriorating long-term memory and communication skills as well as a gradual loss of their ability to form and maintain short-term memories. Post mortem autopsies of the brains of Alzheimer's patients showed severe neuronal atrophy along with an increased presence of intraneuronal neurofibrillary tangles (NFTs) and extracellular amyloid plaques, which have become the two pathological hallmarks of this disease (3).

NFT's are paired helical filaments that form from the hyperphosphorylation of the tau protein. Under normal conditions, tau serves in the promotion of tubulin assembly and the stabilization of microtubules in neurons. As a result of the dysregulation of the phosphorylation cascade, tau assembles into insoluble filamentous polymers that deposit as NFTs within neurons in the brain (4). These tangles are also observed in

patients with other neurological diseases, such as Pick's disease and Parkinson-dementia complex of Guam (5). Thus, while these NFTs lead to cellular atrophy in the brain, they are not the defining causative agent in AD pathology (6). According to the amyloid cascade hypothesis (Figure 1.1), hyperphosphorylated tau deposition and subsequent tangle pathology is caused by a chain of events that stems from changes in the metabolism of the amyloid- $\beta$  ( $A\beta$ ) protein.

## 1.2. Amyloid- $\beta$ Protein

$A\beta$ , the main constituent of amyloid plaques, was first isolated by Glenner et al. in 1984 (7). With varying isoforms ranging from 40-42 residues,  $A\beta$  is a naturally occurring protein in the body, whose function is still unknown. It is produced via cleavage of the amyloid precursor protein (APP), a 695 residue protein, also with uncertain functions, found in neuronal and non-neuronal cells throughout the body (8). Cleavage of APP at two sites leads to the formation of the more abundant  $A\beta_{1-40}$  (9) or the more pathogenic  $A\beta_{1-42}$  (10). Cleavage of  $A\beta$  from APP can occur via two pathways (Figure 1.2). In both pathways C-terminal transmembrane cleavage by  $\gamma$ -secretase generates  $A\beta_{1-40}$  or  $A\beta_{1-42}$  depending on the location of cleavage (11).  $\gamma$ -secretase cleavage occurs due to the aspartyl protease complex, whose main components are presenilin 1 (pres1) and presenilin 2 (pres2) (5). Scheuner et al. have demonstrated that AD causing mutations in pres1 or pres2 cause an increase in the production of  $A\beta_{1-42}$  (12). N-terminal cleavage via  $\beta$ -secretase releases the amyloidogenic  $A\beta$ . However, alternative cleavage by  $\alpha$ -secretase results in the non-amyloidogenic fragment P3. In

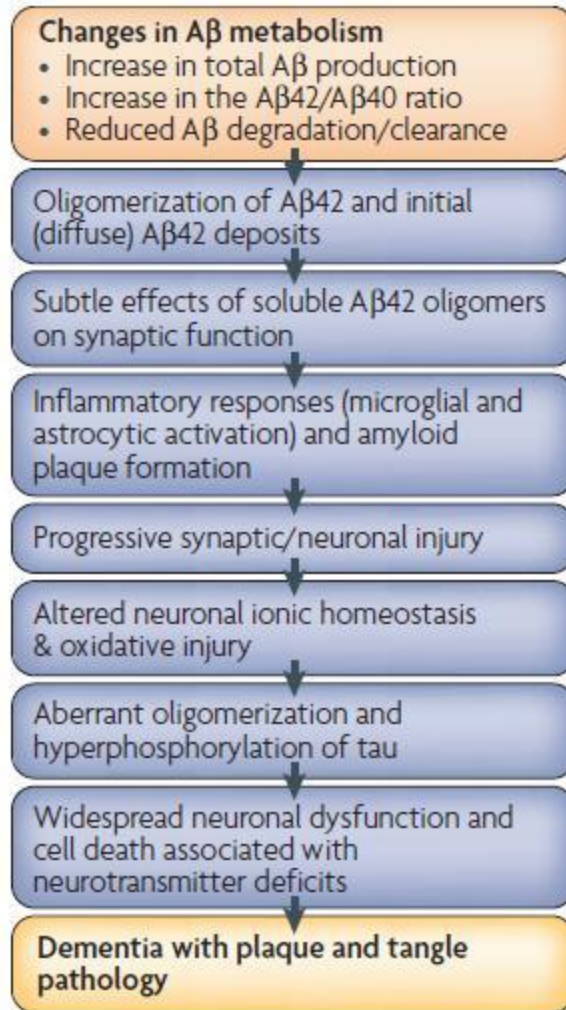


**Figure 1.1: The amyloid cascade hypothesis (13)**

mice lacking the  $\beta$ -site APP-cleaving enzyme (BACE-1), the production of  $A\beta$  is halted and only P3 species are produced (14).

The amyloid plaques commonly found in AD brains are primarily composed of insoluble amyloid fibrils. These fibrils form due to the aggregation of  $A\beta$  from its monomeric state.  $A\beta$  aggregation occurs as a nucleation dependent process exhibiting lag, growth and plateau phases (Figure 1.3A). The rate limiting lag phase occurs when  $A\beta$  monomer spontaneously forms a nucleus (15). Once nucleation has taken place,  $A\beta$  aggregate growth begins, proceeding to soluble aggregates and finally insoluble fibrils. Soluble aggregates are ~5 nm in diameter with an average length of 150 nm (16). The development of soluble aggregates into fibrils can occur via two simultaneous growth mechanisms: elongation and association (17). In soluble aggregate elongation, monomeric  $A\beta$  binds to the ends of the aggregates increasing their length. Alternatively, soluble aggregate association occurs when two or more aggregates laterally bind to one another creating an aggregate with increased radius (Figure 1.3B). Finally, in the plateau phase, equilibrium is reached among all  $A\beta$  species.

### **1.3. Inflammation and AD**

$A\beta$  aggregation and deposition is associated with an increase in inflammatory responses. As stated in the amyloid cascade hypothesis (Figure 1.1),  $A\beta$  deposition leads to the activation of brain astrocytes and microglia (13), followed by an increase in pro-inflammatory molecules, such as cytokines, chemokines and complement proteins (18). This increase in pro-inflammatory molecules in turn brings on a cyclic process of

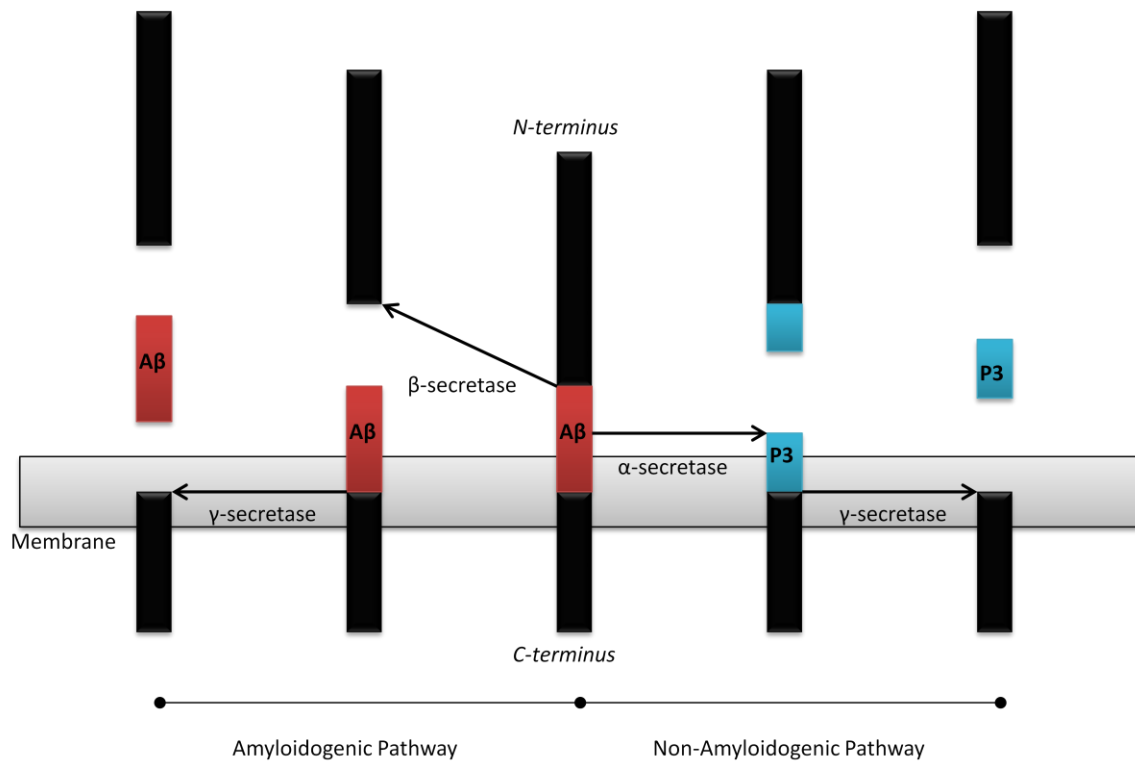


**Figure 1.2: APP cleavage pathways:** Cleavage of APP by  $\beta$ -secretase and  $\gamma$ -secretase to create  $A\beta_{1-40}$  or  $A\beta_{1-42}$ . Alternate cleavage by  $\alpha$ -secretase creates the non-amyloidogenic P3 species.

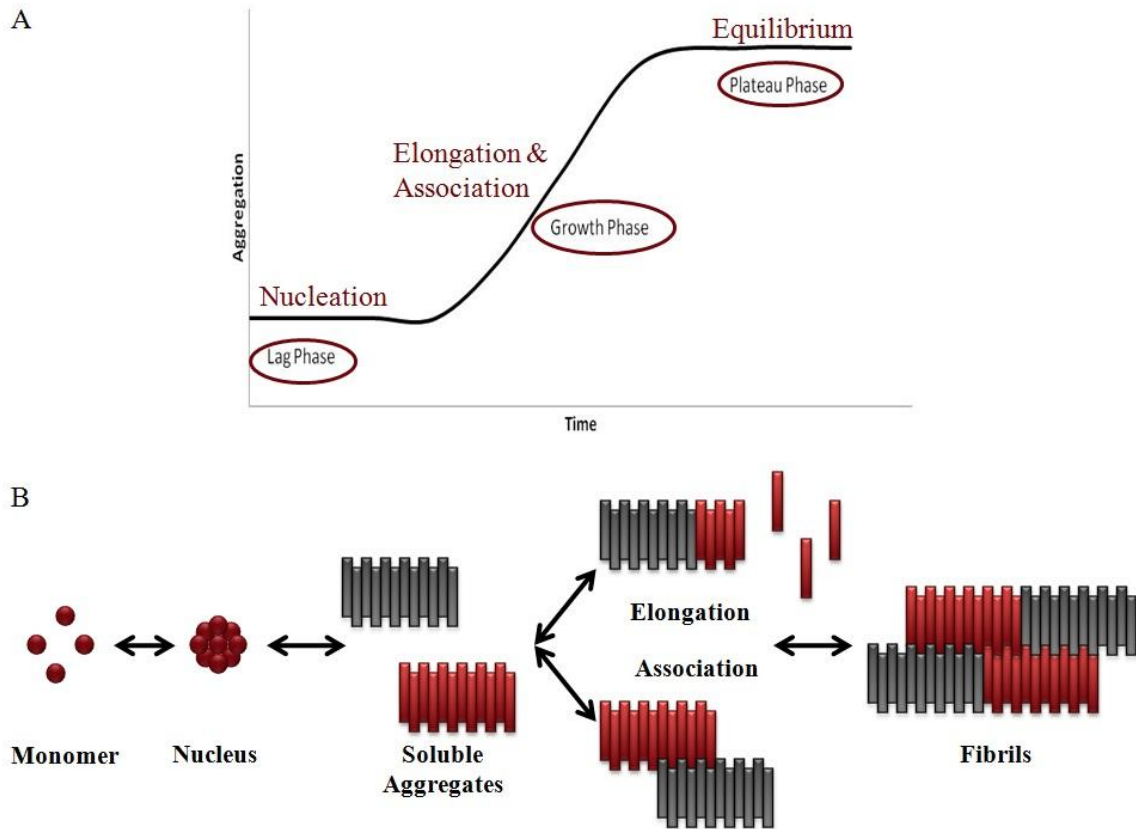


**Figure 1.3: A $\beta$  aggregation:** A) A $\beta$  aggregation begins with a rate-limiting nucleation lag phase, followed by growth of soluble aggregates and a plateau where fibrils, soluble aggregates, and monomers are in equilibrium. B) Monomeric A $\beta$  assembles into a nucleus which grows to form soluble aggregates. These soluble aggregates can then elongate or associate to form insoluble fibrils.

inflammation, leading to further activation of astrocytes and microglia, which leads to the further production of pro-inflammatory molecules (19).

One key molecule in AD-associated inflammation is nuclear factor- $\kappa$ B (NF- $\kappa$ B). NF- $\kappa$ B is a heterodimer comprised of p65 and p50 subunits that plays a central role in inflammatory regulation (20; 21). Under normal conditions, NF- $\kappa$ B is bound by I $\kappa$ B, which restricts its location to the cytoplasm. When cellular activation occurs, such as an increase in pro-inflammatory molecules, I $\kappa$ B is phosphorylated, releasing NF- $\kappa$ B to translocate into the nucleus where it begins transcription of a variety of inflammatory and immune related genes (Figure 1.4) (22).

A $\beta$  has been shown to induce NF- $\kappa$ B activation in neuronal cells (23-27). To further elucidate the role of A $\beta$  in NF- $\kappa$ B activation, researchers have examined the effects of different A $\beta$  aggregate species. He et al. examined the effects of fibrillar and oligomeric A $\beta_{1-42}$  on NF- $\kappa$ B activation in male rats. While both species were found to increase activation compared to control rats, oligomeric A $\beta$  increased activation beyond that of the fibrillar A $\beta$  (28). In corroboration with these results, Gonzalez-Velasquez et al. also observed increased NF- $\kappa$ B activation in human brain microvascular endothelial cells by soluble A $\beta_{1-40}$  but not fibrillar A $\beta_{1-40}$  (29).

#### **1.4. Inhibition of A $\beta$ Aggregation**

While it was originally postulated that insoluble A $\beta$  fibrils were the pathogenic species, later research suggests that the soluble intermediate aggregates are most toxic (30). Correlations between the degree of neuronal dysfunction and the number of amyloid plaque deposits in the brain proved weak. However, it was later observed that

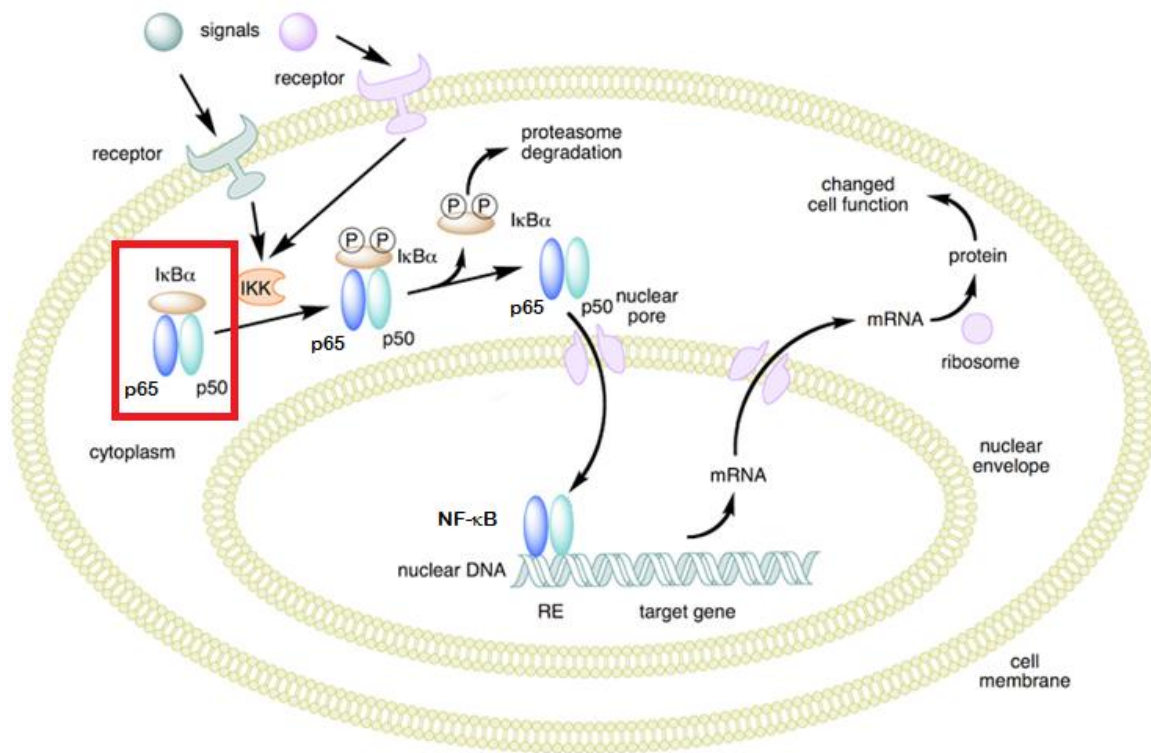


**Figure 1.4: Activation of NF- $\kappa$ B:** NF- $\kappa$ B is a heterodimer comprised of p65 and p50 subunits. Under resting conditions NF- $\kappa$ B is bound by I $\kappa$ B, restricting its location to the cytoplasm. When cellular activation occurs, such as an increase in pro-inflammatory molecules, I $\kappa$ B is phosphorylated, releasing NF- $\kappa$ B. Once NF- $\kappa$ B is released, it translocates into the nucleus where it begins transcription of a variety of inflammatory and immune related genes.

neuronal dysfunction correlated with the concentration of soluble A $\beta$  species found in AD brains (31). In addition, neuronal death in cultured cells is induced when cells are treated with soluble A $\beta$  (32). Thus, the ability to inhibit or alter the formation of these species may be imperative to disease therapies.

Inhibition of A $\beta$  aggregation can occur at multiple steps. The first stage at which inhibition can occur is during nucleation, where inhibitors can bind to individual monomeric units stopping them from coalescing, or impede already formed nuclei from growing. Inhibition can also occur during soluble aggregate growth blocking mechanisms of either association or elongation. During association, inhibitors can bind to the side of the aggregates, blocking lateral binding. During elongation, inhibitors can bind either to the free monomers or to the ends of aggregates to block monomer addition.

### **1.5. Therapeutic Applications of Nanoparticles in Alzheimer's Disease**

The biological application of nanoparticles (NP) has gained interest over the years for cellular imaging and targeted gene and drug delivery (33). NPs can range in size from a few nanometers up to hundreds of nanometers and can be synthesized from a wide variety of materials such as metals, polymers, lipids and carbon (34). In AD research, NPs are being investigated as potential biosensors for the detection of AD biomarkers. A $\beta$  derived diffusible ligands (ADDL's), which are an A $\beta$  oligomeric species, are expected to be enriched in cerebrospinal fluid (CSF) of AD patients. Haes et al. created a biosensor that can determine ADDL concentration based on a shift of the localized surface plasmon resonance (LSPR) of gold nanotriangles. As the ADDL's bind to the sensor, the LSPR wavelength shifts to the right, which can correlate to ADDL

concentration in the CSF (35). Another potential biomarker for AD is ApolipoproteinE (ApoE). Ratios between total ApoE and isoform ApoE4 are significantly different between patients with and without AD. To examine the ability to increase biomarker detection over conventional methods, such as enzyme-linked immunosorbent assays (ELISA), researchers investigated the use of core-shell quantum dots (QD) as reporters for microarrays to increase assay sensitivity. In this study it was determined that the QD's could increase ApoE detection by 7-fold over traditional ELISA (36).

An imperative feature of any treatment candidate for neurodegenerative diseases is the ability to cross the blood brain barrier (BBB). The BBB, consisting of endothelial cells and astrocytic feet, serves as the transportational gateway to protect the brain from infection. For this reason, transport across the barrier is severely restricted. To bypass this restriction, NP-mediated delivery can carry across the BBB a drug either encased within the NP or bound to its surface (37; 38). Recently, Veisheh et al. have synthesized iron oxide derived NPs coated with a tumor targeting drug that can successfully cross the BBB and bind to tumors within a mouse model (39). In another study, the transportation across the BBB of bare and peptide conjugated NPs was examined. While both types of NPs were found to successfully transport, their mechanisms of action were different. Although the transport mechanism for peptide conjugated NPs was uncertain, it was discovered that bare NPs undergo macropinocytosis to cross the BBB (40).

### **1.6. Potential Therapeutic Application of Peptoids in Alzheimer's Disease**

One of the key features of A $\beta$  aggregation is the protein's ability to bind itself. This suggests the existence of a specific binding domain within the protein that allows for

aggregation. To determine this binding region, researchers have evaluated the ability of A $\beta$  fragments to aggregate in a manner similar to as the full length protein (41-44). These studies demonstrated that fragments based on the hydrophobic core of A $\beta$  aggregate with the same propensity as the full length protein, implicating the hydrophobic core as the key region associated with A $\beta$  aggregation. With this notion in mind, researchers have investigated the ability to disrupt aggregation using peptides as inhibitors. Some studies have examined the effect of peptides, mimicking the C-terminus of A $\beta$ , which is proposed to play a critical role in the formation of A $\beta$  structure during aggregation (45-47). In particular, Fradinger et al. demonstrated that A $\beta$ <sub>39-42</sub> and A $\beta$ <sub>31-42</sub> both alter A $\beta$ <sub>1-42</sub> aggregate structure and reduce A $\beta$ <sub>1-42</sub> induced neurotoxicity in cultured mouse primary hippocampal cells (45). Studies have also examined the effects of peptides designed from the N-terminus of A $\beta$ . Findeis et al. examined multiple peptides designed from A $\beta$  with and without cholyl modification. Screening results showed that A $\beta$ <sub>1-15</sub> and A $\beta$ <sub>16-30</sub> were able to arrest aggregation, and this effect was enhanced with cholyl modification (48).

While peptides derived from the sequence of A $\beta$  have shown promise as potential aggregation inhibitors, peptides are susceptible to proteolysis when introduced to the body, leading to ineffective results as potential therapeutics. One approach to circumvent this problem is the use of peptoids. Peptoids were originally designed to maintain polypeptide structure while removing their susceptibility to degradation (49). This structural stability was accomplished by creating structures where the side-chain connectivity point is moved from the  $\alpha$ -carbon to the amide nitrogen (Figure 1.5). Movement of the side-chains leads to two distinct advantages for peptoids over peptides.

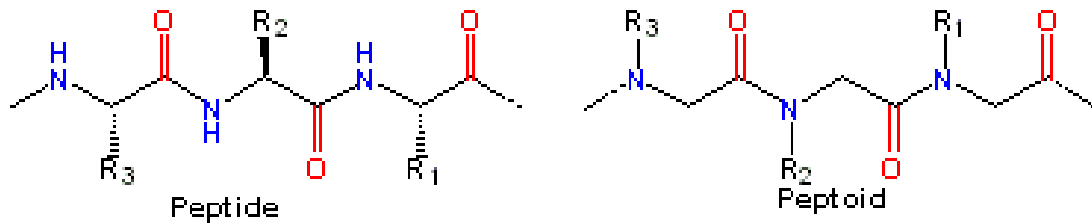


**Figure 1.5: Schematic comparison of peptide and peptoid structure:** Side chain connectivity is moved from the  $\alpha$ -carbon to the backbone nitrogen. This results in the ability of peptoids to be resistant to proteolysis and increased flexibility of the backbone.

First, protease degradation is eliminated, and secondly, movement of the side-chain allows for greater flexibility of the peptoid (50). These two advantages combined make peptoids a novel therapeutic agent for A $\beta$  aggregation with strong potential.

In this study, nanoparticles and peptoids were examined for their effects as novel A $\beta$  aggregation inhibitors. Nanoparticles, which have the ability to cross the BBB, have potential as strong therapeutic agents in AD. Their ability to attenuate aggregation of A $\beta_{1-40}$  was examined and is outlined in Chapter 4. Another potential therapeutic in AD is the use of peptoids, due to their strong resistance to proteolysis. We examined the effects of a neutral charge peptoid on A $\beta_{1-42}$  oligomerization along with its ability to alter A $\beta$ -induced NF- $\kappa$ B activation (Chapter 5). Finally, to further elucidate the effects of peptoids, charge modulation of this peptoid was examined in Chapter 5 to determine if charge can alter the effects of the peptoids on A $\beta_{1-42}$  oligomerization and NF- $\kappa$ B activation (Chapter 6).

## CHAPTER 2

### MATERIALS & METHODS

#### 2.1. Materials

A $\beta$ <sub>1-40</sub> and A $\beta$ <sub>1-42</sub> were purchased from AnaSpec, Inc. (San Jose, CA). Thioflavin T (ThT), Triton-X 100, sodium chloride (NaCl), sodium hydroxide (NaOH), phosphate buffered saline (PBS), paraformaldehyde, 1,1,1,3,3,3-Hexafluoro-2-propanol (HFIP), phenazine methosulfate (PMS) and 2,3-bis (2-methoxy-4-nitro-5-sulfophenyl)-5-[(phenylamino)carbonyl]-2H tetrazolium hydroxide (XTT) were purchased from Sigma (St. Louis, MO). Dulbecco's modified Eagle's medium (DMEM), Ham's F12K medium, fetal bovine serum (FBS), sodium bicarbonate, penicillin, streptomycin, glycine, pyruvate,  $\beta$ -mercaptoethanol, and Fluoroshield with 4', 6'-diamidino-2-phenylindole dihydro-chloride (DAPI) were also obtained from Sigma. Bovine serum albumin (BSA) and dimethyl sulfoxide (DMSO) were obtained from EMD Biosciences (San Diego, CA). Uranyl acetate and 300 square mesh formvar-carbon supported copper grids were obtained from Electron Microscopy Sciences (Hatfield, PA). Donkey normal serum was obtained from Jackson ImmunoResearch (West Grove, PA). 8-Anilino-1-naphthalenesulphonic acid (ANS) was obtained from Research Organics (Cleveland, Ohio). Surfact-Amps 20 detergent (Tween) and SuperSignal West Pico enhanced chemiluminescent substrate (ECL) were purchased from Thermo Fisher

Scientific (Rockland, IL). Recombinant human tumor necrosis factor- $\alpha$  (TNF- $\alpha$ ) was obtained from Promega (Madison, WI).

Antibodies were purchased from the following companies: rabbit anti-NF- $\kappa$ B-p65 antibody from Rockland (Gilbertsville, PA); rabbit anti-A $\beta$ -fibrils antibody (LOC) from EMD Millipore (Billerica, MA); mouse anti-A $\beta_{1-16}$  antibody (6E10) from Covance (Princeton, NJ); goat anti-rabbit IgG AlexaFluor 633 conjugate from Life Technologies (Carlsbad, CA); goat anti-rabbit IgG horseradish peroxidase (HRP) conjugate from Bio-Rad (Hercules, CA); and sheep anti-mouse IgG HRP conjugate from GE Healthcare (Piscataway, NJ).

## **2.2. A $\beta_{1-40}$ Monomer Purification**

When studying A $\beta_{1-40}$  aggregation, it is important to ensure that aggregation reactions are initiated with only monomeric species, since small aggregates can accelerate aggregation kinetics by serving as nucleation seeds. Thus, A $\beta_{1-40}$  monomer was purified using size exclusion chromatography (SEC). Lyophilized A $\beta_{1-40}$  peptide was stored desiccated at -20 °C. As described previously (51), the peptide was reconstituted to a concentration of 2 mg/mL in 50 mM NaOH to dissociate preformed small aggregates. To reduce nonspecific interactions between A $\beta_{1-40}$  and the column matrix, the Superdex 75 10/300 GL column (GE Healthcare) column was pre-treated with 2 mg/mL BSA before injection of solubilized A $\beta_{1-40}$ . Using 40 mM Tris-HCl (pH 8.0) elution buffer, a void peak (8-12 mL) containing A $\beta_{1-40}$  aggregates was followed by monomer, which elutes within the included volume at approximately 15-19 mL (Figure 2.1). The concentration of eluted monomer was determined using a Beckman Coulter DU700 UV-VIS

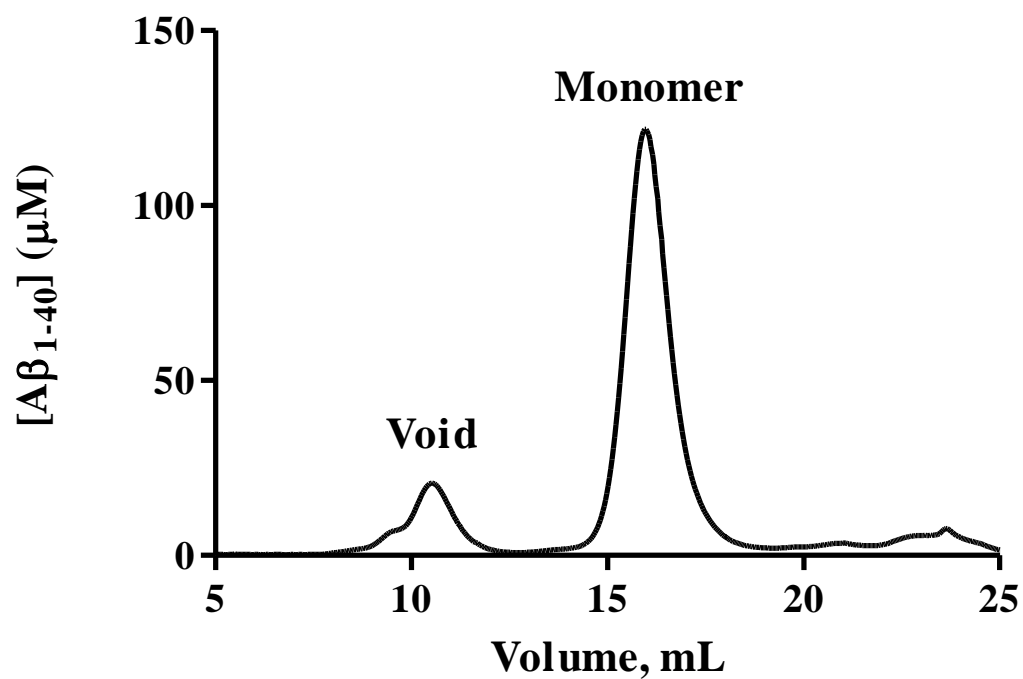


**Figure 2.1: Purification of Aβ<sub>1-40</sub> monomer:** Aβ<sub>1-40</sub> monomer is separated from small aggregates using SEC on Superdex 75. Aβ<sub>1-40</sub> aggregates elute from the column within the void peak (8-12 mL), while Aβ<sub>1-40</sub> monomer elutes in the included volume between 15-19 mL.

spectrometer (Brea, CA) at  $\lambda=276$  nm with an extinction coefficient ( $\epsilon$ ) of  $1450 \text{ cm}^{-1}\text{M}^{-1}$  (17). Purified monomeric  $\text{A}\beta_{1-40}$  was stored at  $4^\circ\text{C}$  for no longer than 7 days.

### **2.3. Preparation of $\text{A}\beta_{1-40}$ Fibrils**

Insoluble  $\text{A}\beta_{1-40}$  fibrils were prepared from SEC isolated  $\text{A}\beta_{1-40}$  monomer. As described previously (51), 60-70  $\mu\text{M}$  monomeric  $\text{A}\beta_{1-40}$  was agitated at  $25^\circ\text{C}$  for 24 h in the presence of 250 mM NaCl and 40 mM Tris-HCl (pH 8.0). Fibrils were separated from soluble  $\text{A}\beta_{1-40}$  species via centrifugation (14,000  $\times g$ , 10 min). Supernatant, containing unreacted monomer and soluble aggregates, was removed and the pellet was resuspended in 40 mM Tris-HCl (pH 8.0). Fibril concentration was calculated from the fraction of pelleted protein. Fibrils were stored at  $4^\circ\text{C}$  for no longer than 7 days.

### **2.4. $\text{A}\beta_{1-40}$ Monomer Aggregation**

Aggregation of  $\text{A}\beta_{1-40}$  monomer was carried out with 400  $\mu\text{L}$  reactions containing 20  $\mu\text{M}$  SEC-isolated  $\text{A}\beta_{1-40}$  monomer, 150 mM NaCl, and 40 mM Tris-HCl (pH 8.0) incubated alone (positive control) or in the presence of potential inhibitors (experimental samples). Reactions were incubated at room temperature ( $25^\circ\text{C}$ ) and agitated at 800 rpm to promote  $\text{A}\beta_{1-40}$  aggregation. The extent of aggregation was determined using ThT fluorescence or dot blot analysis.

### **2.5. Analysis of $\text{A}\beta_{1-40}$ Monomer Aggregation with ThT**

ThT is a benzathiole dye that binds to the  $\beta$ -sheet structure of amyloid aggregates but does not bind to unordered species, including monomer (52). When ThT is bound to

$\beta$ -sheet aggregates it experiences a shift in fluorescence excitation and emission wavelengths and an enhancement in fluorescence emission (53). To determine the extent of monomer aggregation reactions, a 20  $\mu$ L sample was periodically removed from each reaction and combined with 140  $\mu$ L of 10  $\mu$ M ThT. Fluorescence was measured using an LS-45 luminescence spectrometer (Perkin-Elmer, Waltham, MA) with excitation at 450 nm and emission at 460-520 nm. Fluorescence values were determined by integrating the area under the emission curve from 470-500 nm and subtracting the baseline (ThT alone). Results are plotted as fluorescence vs. time, and experimental samples are compared to the control.

## **2.6. Analysis of A $\beta$ <sub>1-40</sub> Monomer Aggregation by Dot Blot**

To determine the extent of monomer aggregation reactions by dot blot analysis, a 4  $\mu$ L sample was periodically removed from each reaction, dotted onto 0.1  $\mu$ m nitrocellulose membrane, and allowed to dry. After each time point the membrane was blocked until the aggregation reaction was completed ( $\geq 1$  h) at 4°C in 5% nonfat milk in PBS with Tween (PBS-T). Primary antibody LOC (1:5000) in 5% nonfat milk in PBS-T was allowed to incubate for 1.5 hrs followed by three washes in PBS-T. HRP-conjugated anti-rabbit secondary antibody (1:2000) in 5% nonfat milk in PBS-T was allowed to bind for 1.5 hrs. The immunolabeled protein membrane signal was enhanced using ECL and imaged with the Gel Doc<sup>TM</sup> XRS+ imaging system (Biorad). Blots were analyzed using Biorad Quality One software with identical area elements for each protein dot. Density values for each dot were calculated as percent of control to allow for comparison between blots and experiments.

## 2.7. Quantitative Analysis of A $\beta_{1-40}$ Monomer Aggregation

To evaluate inhibition, A $\beta_{1-40}$  aggregation in the presence of each potential inhibitor was quantitatively compared to the positive control. Extension of the lag, which occurs prior to aggregation, indicates the ability of an inhibitor to slow nucleation. Lag extension was calculated as the ratio of the time at which aggregation signal first increases for the experimental sample ( $t_E$ ) relative to that of the control ( $t_C$ ) (Equation 2.1, Figure 2.2). A lag extension of 1 denotes no change from the control.

$$LE = \frac{t_E}{t_C}$$

### Equation 2.1

Reduction of the equilibrium plateau, which occurs at the conclusion of aggregation, indicates the ability of an inhibitor to decrease the quantity of aggregates containing  $\beta$ -sheet structure present at equilibrium. Plateau reduction was calculated as the percentage decrease in the average plateau signal observed for each experimental sample ( $S_E$ ) relative to that observed for the control ( $S_C$ ) (Equation 2.2, Figure 2.2). A plateau reduction of 0% denotes no change from the control.

$$PR = \frac{S_C - S_E}{S_C} * 100\%$$

### Equation 2.2

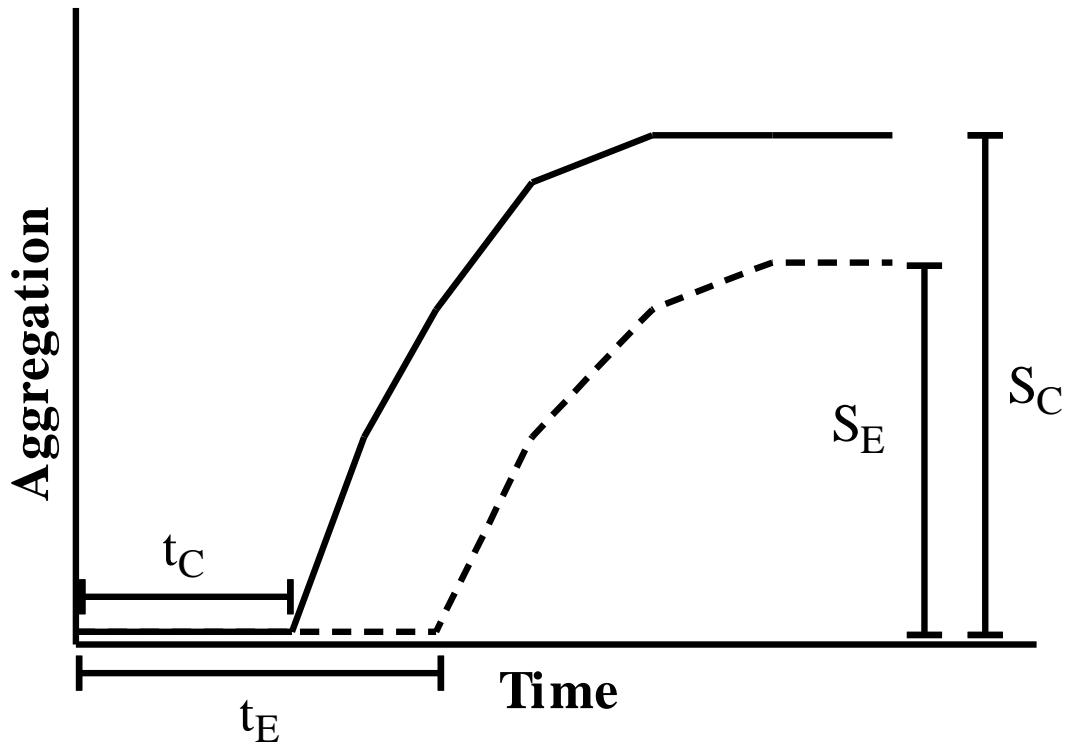


**Figure 2.2: Assessment of inhibition of  $A\beta_{1-40}$  monomer aggregation:** Monomer aggregation assays were performed in the absence (control, solid line) and presence (experimental, dashed line) of potential inhibitors, and aggregate formation was followed by ThT fluorescence or dot blot analysis to evaluate the ability of the potential inhibitors to alter lag time and plateau equilibrium. Lag time extension was evidenced as an increase in the experimental lag time,  $t_E$ , as compared to the lag time for the control,  $t_C$ , and determined by the ratio,  $t_E/t_C$ . Reduction of the equilibrium plateau was evidenced as a decrease in the average experimental plateau,  $S_E$ , relative to the average plateau observed for the control,  $S_C$ , and was determined as the percentage decrease from the control,  $[(S_C - S_E)/S_C] \times 100\%$ .

## **2.8. Transmission Electron Microscopy**

Monomer aggregation reactions were gridded for transmission electron microscopy (TEM) at time points after which the control reaction reached equilibrium. A 10  $\mu$ L sample was placed on a 300 square mesh formvar-carbon supported copper grid. After 3 min, the sample was wicked away from the bottom side of the grid using a piece of filter paper. Sample application was repeated twice in this manner, and samples were allowed to air dry for 24 h. Gridded samples were stained with 2% aqueous uranyl acetate for 10 min, excess stain was wicked away, and the grids were allowed to dry for 24 h. Imaging was performed using a JEOL 200CX TEM (JEOL Ltd., Tokyo, Japan) with an accelerating voltage of 120 kV. Blinded observation of samples with random selection of grid areas was implemented to reduce bias during imaging.

## **2.9. ThT Detection of A $\beta$ <sub>1-40</sub> Aggregates in the Presence of Potential Inhibitors**

Employing ThT for the detection of amyloid aggregates containing  $\beta$ -sheet structure is a well established technique in the field (53; 54). However, when using ThT to monitor the effects of a potential inhibitor on A $\beta$ <sub>1-40</sub> aggregation, interference in the fluorescent signal can occur (55). A false increase in fluorescent signal can be observed, due to self-fluorescence of the inhibitor, leading to the inability to identify inhibition. On the other hand, potential inhibitors can exhibit strong absorbent properties in the range at which ThT emission occurs, which leads to a quenching of the fluorescent signal and false positive results.

To identify any alterations in ThT fluorescence due to potential inhibitors, the ThT fluorescence of pre-formed A $\beta$ <sub>1-40</sub> fibrils was evaluated in the presence of potential

inhibitors.  $A\beta_{1-40}$  fibrils were diluted in 40 mM Tris-HCl (pH 8.0) to a final concentration of 5  $\mu$ M either with or without the inclusion of inhibitor and combined with 8.75  $\mu$ M ThT to reflect concentrations within diluted samples used to monitor  $A\beta_{1-40}$  aggregation. Fluorescence was measured at 0 h and 2 h using a BioTek Synergy 2 microplate reader (Winooski, VT) with excitation at 450 nm and emission at 485 nm. ThT fluorescence was found to be compromised if a significant difference in fluorescent signal was observed between samples with and without the addition of inhibitor.

### **2.10. Preparation of $A\beta_{1-42}$ Oligomers**

Lyophilized  $A\beta_{1-42}$  was stored desiccated at  $-80\text{ }^{\circ}\text{C}$  until use.  $A\beta_{1-42}$  was dissolved in cold HFIP at a concentration of 4 mg/mL and allowed to incubate for 60 min. After incubation, the peptide solution was aliquoted, and the HFIP was allowed to evaporate at room temperature resulting in the creation of thin peptide films. Once dry, peptide films were stored desiccated at  $-80\text{ }^{\circ}\text{C}$  until use. Prior to experimentation, peptide films were rehydrated in DMSO to a concentration of 1.5 mM and incubated alone (positive control) or in the presence of potential inhibitor (experimental sample). PBS with 1  $\mu$ M NaCl was added for a final  $A\beta_{1-42}$  concentration of 20  $\mu$ M. Reactions sat quiescent at  $25\text{ }^{\circ}\text{C}$  for 30 min at which point they were halted by the addition of 1% Tween.

### **2.11. Analysis of $A\beta_{1-42}$ Oligomerization via SDS-PAGE and Western Blotting**

$A\beta_{1-42}$  oligomers formed in the absence or presence of potential inhibitors were separated by size via sodium dodecyl sulfate polyacrylamide gel electrophoresis

(SDS-PAGE). After the reaction was halted via addition of 1% Tween, samples were diluted 1:1 with lamelli or tricine loading buffer and electrophoresed at 120 V across 4-20% Tris-Glycine or 16.5% Tricine gels, respectively. Following separation, protein was transferred to 0.2  $\mu\text{m}$  nitrocellulose membrane via semi-dry blot transfer on a Trans-blot SD semi-dry transfer cell (Biorad) for 15 min at 14 V. Membranes were blocked for 1 h in 5% nonfat milk in PBS-T. Primary antibody, 6E10 (1:1000) in 5% nonfat milk in PBS-T, was allowed to incubate for 1 h followed by three washes in PBS-T. HRP-conjugated anti-mouse secondary antibody (1:2000) and Precision Protein StrepTactin-HRP conjugate (1:5000) in 5% nonfat milk in PBS-T were allowed to bind for 45 min. Immunolabeled protein membrane signal was enhanced using ECL and imaged using the Gel Doc<sup>TM</sup> XRS+ imaging system (Biorad). Blots were analyzed using Biorad Quality One software with identical area elements for each range (20-100 kDa and 100-250 kDa) of molecular weights. Density values for each range were calculated as percent of control to allow for comparison between blots and experiments.

## **2.12. Determination of A $\beta$ <sub>1-42</sub> Oligomer Structure by ANS Fluorescence**

ANS is a naphthaline based compound commonly used as a fluorescent probe. When ANS is introduced to solvent exposed hydrophobic residues it undergoes a conformational change resulting in both blue shift and increased quantum yield (56). ANS was solubilized in DMSO at a concentration of 50 mM and stored at 4 °C. Stock ANS was diluted with PBS and then combined with oligomers without the addition of Tween for final concentrations of 100  $\mu\text{M}$  ANS and 1  $\mu\text{M}$  A $\beta$ <sub>1-42</sub>. Fluorescence was measured using a LS-45 luminescence spectrophotometer (Perkin Elmer, Waltham, MA)

with excitation at 350 nm, emission from 400 nm to 600 nm, and excitation and emission slits of 10 nm. Fluorescence values were determined as the integrated area under the emission curve from 400 nm to 550 nm with background (buffer or inhibitor with ANS) subtraction.

### **2.13. Cell Culture**

Human neuroblastoma SH-SY5Y cells (American Type Culture Collection, Manassas, VA) were maintained in a 1:1 mixture of DMEM and Ham's F12K medium supplemented with FBS (10%), penicillin (100 Units/mL), and streptomycin (100 µg/mL). Medium was changed every 48 hrs and cells were split 1:3 when they reached 80% confluency. All cultures were maintained at 37 °C in a humid atmosphere of 5% CO<sub>2</sub> and 95% air.

### **2.14. XTT Reduction Assay**

The neurotoxicity of inhibitor candidates was assessed using XTT reduction to evaluate cellular metabolic activity of SH-SY5Y cells, as XTT reduction is known to correlate with direct measures of A $\beta$ -induced cellular toxicity (57). When metabolically active cells are treated with XTT, a colored formazan derivative is formed, which can be detected via absorbance (58). Inclusion of PMS facilitates cellular uptake of XTT. SH-SY5Y cells were sustained as in Section 2.13 until experimentation. Cells were seeded 5x10<sup>4</sup> cells/well onto 96 well plates using reduced serum medium, containing 1% FBS, and allowed to reach a semi-confluent state (24 h). Cell culture medium was replaced with medium into which inhibitors were diluted, and cells were incubated for

24 h. Cells incubated with medium alone served as a negative control, while cells incubated with a 2% Triton X-100 in culture medium served as a positive control. Following 24 h exposure, cells were washed, treated with 0.33 mg/mL XTT in the presence of 8.3  $\mu$ M PMS diluted in cell culture medium, and incubated for 24 h. Absorbance at 450 nm, used to detect the soluble formazan XTT reduction product, was measured using a BioTek Synergy 2 microplate reader. Results are reported as a percentage of the positive control following background (medium containing XTT) subtraction.

### **2.15. Confocal Microscopy of NF- $\kappa$ B Activation in SH-SY5Y Cells**

SH-SY5Y cells were seeded onto 22x22 mm uncoated glass coverslips, and allowed to adhere for 24 hrs. Cells were treated for 15 min with A $\beta$ <sub>1-42</sub> oligomers formed in the absence or presence of potential inhibitor without the addition of Tween. Following treatment, cell cultures were washed, fixed in 3% paraformaldehyde and permeabilized with 0.1% Triton X-100 and 0.01 M glycine in PBS. Cells were then blocked with 5% normal donkey serum and 1% BSA in PBS and incubated overnight (4 °C) with rabbit anti-NF- $\kappa$ B-p65 (1:500). Cells were again blocked with 5% normal donkey serum and 1% BSA in PBS and bound primary antibody was detected via 2 h incubation with goat anti-rabbit IgG AlexaFluor 633 conjugate (1:1000). Coverslips were mounted onto slides using Fluoroshield containing DAPI for nucleic acid visualization. Image z-stacks were collected with optimal interval settings using a Zeiss LSM 510 META confocal microscope (Carl Zeiss, Thornwood, NY) with either a plan-apochromat 63X / 1.4 oil DIC or 40X / 1.3 oil immersion objective (Carl Zeiss). Images were

collected with identical settings. Blinded observation of samples with random selection of imaging areas was implemented to reduce bias during imaging.

## **2.16. NF- $\kappa$ B Quantification with MATLAB**

Custom MATLAB (MathWorks, Natick, MA) functions developed previously were implemented to quantify image data for each confocal optical series (59). First, nuclear areas were defined as the pixels in DAPI channel images with fluorescence greater than the optimal background, determined separately for each experiment. Total nuclear volumes within the z-stack were calculated from the total nuclear voxel count and the voxel size. Second, the nuclear NF- $\kappa$ B fluorescence was defined as the sum of fluorescence values for all pixels within NF- $\kappa$ B channel images colocalized to a nuclear area. Results were calculated as the total nuclear NF- $\kappa$ B fluorescence per nuclear volume and are reported as the mean  $\pm$  standard error (SEM) for 3 optical series.

## **2.17. Statistical Analysis**

Statistical analysis was performed using Prism 5 software (GraphPad Software Inc., San Diego, CA). The effect of potential inhibitors on extension of the lag time reduction of the equilibrium plateau, neurotoxicity, and oligomer size were evaluated using a one-way analysis of variance. Differences between experimental groups and controls were assessed using Dunnett's test. Inhibitor effects on ThT interference were evaluated using a two-way analysis of variance, with Bonferroni posttests, to identify differences between experimental groups and controls.  $p < 0.05$  was considered significant.

## CHAPTER 3

### SIZE AND SURFACE MODIFICATIONS OF GOLD NANOPARTICLES INFLUENCE INHIBITION OF $A\beta$ AGGREGATION

#### 3.1. Introduction

A wide array of compounds, including fluorescent dyes (60; 61), peptides (62; 63), and small molecules (64; 65), have shown positive results in disrupting the formation of  $A\beta$  aggregates. However, none have been as effective as NPs at substoichiometric ratios, a characteristic that will facilitate delivery of therapeutically effective concentrations to the brain (64; 66). This potential of NPs to serve as AD therapeutics necessitates insight into the properties of NPs that impart effective inhibitory capabilities. While each material used to create NPs has its own advantages and disadvantages, gold NPs are therapeutically desirable since they are non-toxic (67), can cross the BBB (38), and the size and shape of synthesized particles can be uniformly controlled (68). Gold NPs are also desirable for their ability to be imaged using electron microscopy (69). In addition, gold NPs absorb and scatter light in the visible region (70). This latter attribute leads to a strong surface plasmon band which varies with particle size and shape (71), which makes these NPs easy to characterize.

Many studies have examined the effects of NPs on amyloid aggregation. Bellova et al. demonstrated that  $Fe_3O_4$  magnetic NPs can inhibit the formation of lysozyme amyloid aggregates. These particles were also shown to depolymerize preformed aggregates (72). Previous studies using various inorganic NPs have shown the ability to

diminish the formation of amyloid aggregates. Using copolymeric NPs at picomolar concentrations, Cabaleiro-Lago et al. demonstrated retardation of fibrillation during islet amyloid polypeptide (IAPP) aggregation, which was dependent upon particle surface chemistry (73). Applying the same copolymeric particles, Cabaleiro-Lago et al. also observed a concentration dependent extension of lag time for A $\beta$  monomer aggregation, indicative of inhibition of nucleation (74). Yoo et al. synthesized cadmium-tellurium (CdTe) NPs stabilized with thioglycolic acid (TGA) that dose dependently prolonged A $\beta$ <sub>1-40</sub> nucleation and decreased the quantity of aggregates formed. These results were evidenced with ratios of CdTe NPs to A $\beta$ <sub>1-40</sub> as low as 0.001 (75).

However, the effects of gold NPs on A $\beta$  aggregation have not been examined as extensively as other particle types. Kogan et al. used local heat dissipated from gold NPs stimulated by an electromagnetic field to induce the disaggregation of preformed amyloid fibrils as well as to prohibit the formation of new fibrils (76). Liao et al. examined the effect of charged gold nanospheres on A $\beta$  fibrilization and demonstrated that negatively charged NPs were able to reduce the formation of A $\beta$  fibrils (77). From these studies the potential of gold NPs as A $\beta$  aggregation inhibitors is evidenced however, the characteristic of these NPs that impart strong inhibitory capabilities are still undetermined.

In this study, the effects of surface chemistry and diameter on the ability of spherical gold NPs to inhibit A $\beta$  aggregation were investigated. Gold NPs coated with cationic, CTAB and PAH, and anionic, citrate and PAA, were examined to determine if surface charge and surface chemistry influence inhibitory capabilities toward A $\beta$

aggregation. In addition, 8 nm, 18 nm, and 40 nm diameter spherical NPs were evaluated to determine if NP size alters the NP-protein interactions.

## 3.2. Materials & Methods

### 3.2.1. Nanoparticle Synthesis

Gold NPs were obtained from the laboratories of Dr. Catherine Murphy (Department of Chemistry, University of Illinois at Urbana-Champaign) and Dr. Rahina Mahtab (Department of Biological and Physical Sciences, South Carolina State University). NPs used in this study were synthesized with a spherical shape and 8 nm, 18 nm, or 40 nm diameter. Capping agents of interest in this project were sodium citrate and PAA, which impart an anionic surface charge, and CTAB and PAH, which induce a cationic surface charge (Figure 3.1). Citrate NPs were synthesized according to the Frens method (78), where  $\text{HAuCl}_4$  was heated to a boil and reduced using sodium citrate, creating monodisperse suspensions of gold NPs. CTAB, PAA and PAH surface coated NPs, were synthesized via a seeding growth protocol (79). 3 nm citrate NPs were synthesized by the reduction of  $\text{HAuCl}_4$  by sodium borohydride and then capped with sodium citrate. These particles served as nucleation centers that were used to grow larger particles. Seed diameter was increased by the reduction of  $\text{HAuCl}_4$  and CTAB with ascorbic acid. Once the CTAB particles were created to the desired size, PAA and PAH were coated on to the particles to yield the desired surface capping agent. Particle concentration was determined from UV absorbance at  $\lambda=520$  nm using an extinction coefficient that is independent of the capping ligand (80), but is a function of the particle diameter ( $D$ ).

$$\ln(\epsilon) = 3.321 \times \ln(D) + 10.805$$

**Equation 3.1**

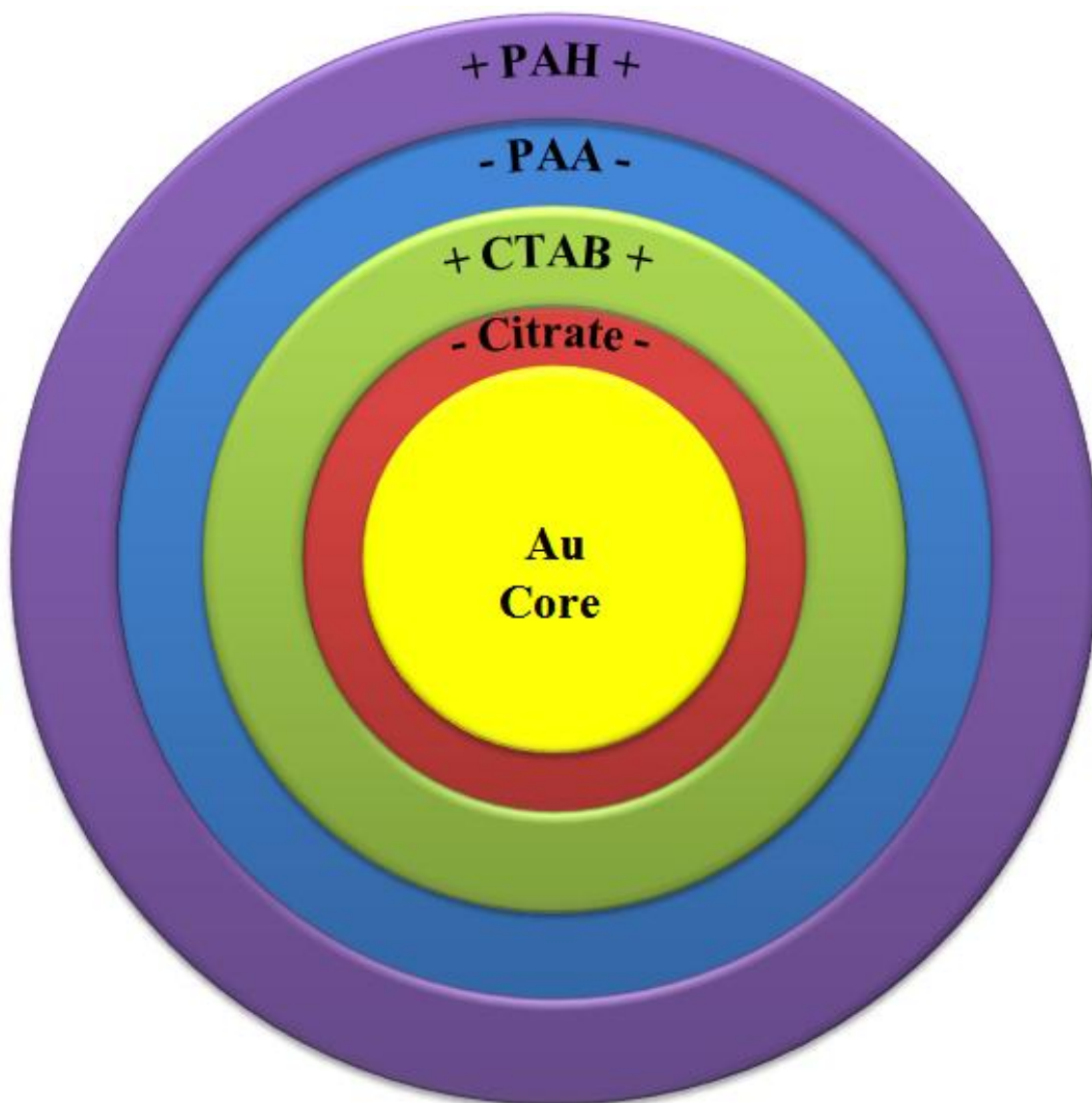


**Figure 3.1: NP structure:** Citrate stabilized NPs were synthesized using the classical Frens method. For the synthesis of CTAB, PAA, and PAH-coated NPs, a seeding growth protocol was implemented where each NP layer is overcoated onto the previous layer.

### **3.2.2. A $\beta$ <sub>1-40</sub> Monomer Aggregation**

To assess NP inhibitory capabilities monomer aggregation experiments were conducted as described in Section 2.4, with slight modification. Due to unwanted aggregation of the NPs stimulated by high salt concentrations, reactions were performed in 40 mM Tris-HCl, in the absence of NaCl, and at an A $\beta$ <sub>1-40</sub> concentration of 40  $\mu$ M to promote protein aggregation. NPs were evaluated for their inhibitory capabilities at concentrations ranging from 20 pM-200 pM. Aggregation was assessed via ThT fluorescence as described in Section 2.5, with data analysis as described in Section 2.7, and by TEM analysis as described in Section 2.8.

### **3.2.3. ThT Detection of A $\beta$ <sub>1-40</sub> Aggregates in the Presence of Gold NPs**

The possibility that NPs may interfere with the ThT fluorescent signal was evaluated as described in Section 2.9. NPs were assessed for ThT interference at concentrations ranging from 5 pM-200 pM.

### **3.2.4. XTT Reduction Assay**

Cellular viability following exposure to gold NPs was assessed via XTT reduction as described in Section 2.14. SH-SY5Y human neuroblastoma cells were cultured as described in Section 2.13 and treated with NPs at either 100 pM or 200 pM.

### **3.3. Results**

#### **3.3.1. Neurotoxicity of Surface Coated NPs**

When developing a potential therapeutic agent, it is important to determine that it will be toxicologically inert. NPs were evaluated for their ability to induce toxicity in SH-SY5Y human neuroblastoma cells. SH-SY5Y cells, cultured in low serum medium, were incubated for 24 h alone or in the presence of 100 pM or 200 pM NPs. When metabolic activity was assessed using an XTT reduction assay, cellular viability remained >95% following incubation with 18 nm NPs displaying citrate, PAA, and PAH surface chemistries (Figure 3.1). In contrast, 18 nm NPs displaying CTAB surface chemistry reduced cellular metabolic activity by  $81.2 \pm 7.2\%$  and  $85.0 \pm 5.7\%$  at 100 pM and 200 pM, respectively, indicating their ability to induce neurotoxicity. When SH-SY5Y cells were incubated in the presence of PAA-coated NPs with varying diameter, 8 nm and 18 nm NPs failed to elicit toxicity while 40 nm NPs were neurotoxic, reducing cellular viability by  $90.7 \pm 2.5\%$  and  $90.6 \pm 0.1\%$  at 100 pM and 200 pM, respectively (Figure 3.2).

#### **3.3.2. Effect of Surface Coated NPs on ThT Fluorescence Detection of A $\beta$ <sub>1-40</sub> Aggregates**

The plasmonic nature of NPs imparts an ability to absorb and scatter light, which may quench or enhance fluorescent signals (81). To ensure that observed differences in ThT fluorescence accurately reflect changes in  $\beta$ -sheet aggregate formation, ThT fluorescence of pre-formed A $\beta$ <sub>1-40</sub> aggregates was measured in the absence and presence of NPs. Representative of concentrations in diluted samples used for monitoring

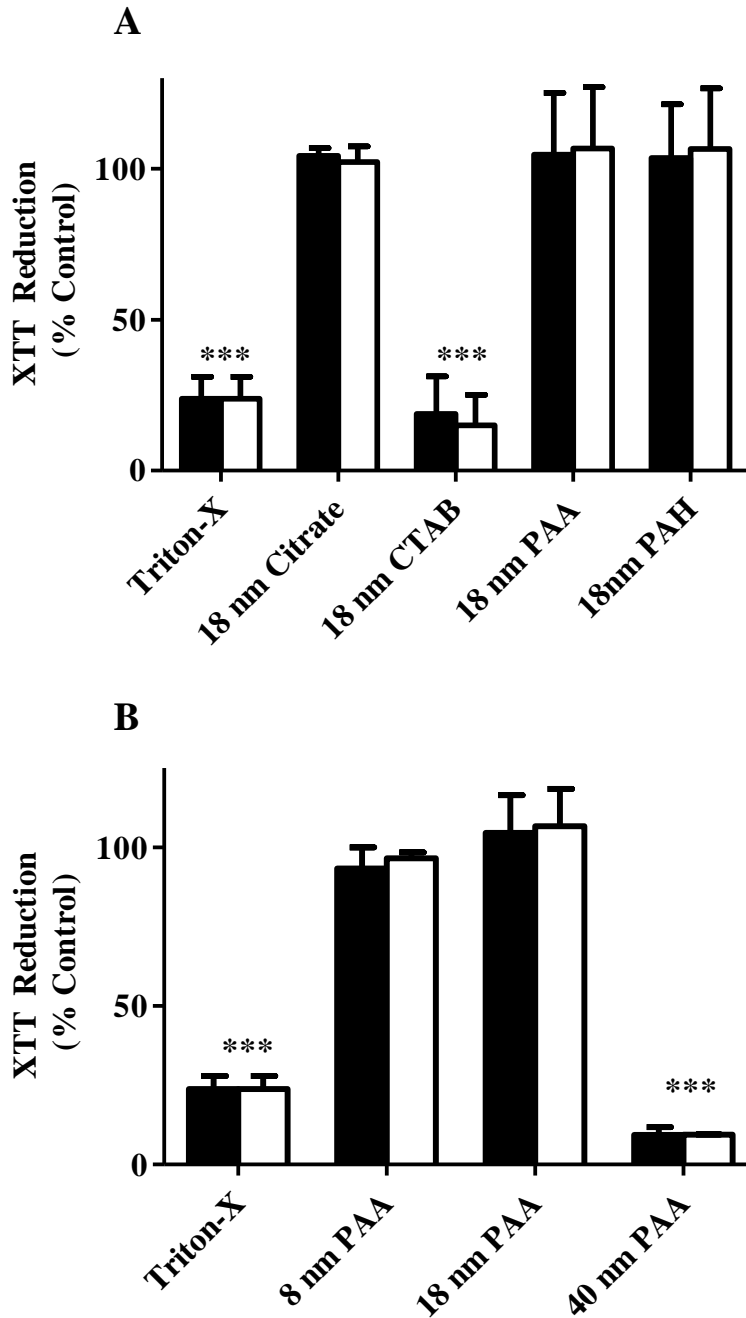


**Figure 3.2: Neurotoxicity of surface coated NPs:** SH-SY5Y human neuroblastoma cells were incubated for 24 h alone or in the presence of 100 pM (closed bars) or 200 pM (open bars) 18 nm NPs (A) or 8 nm, 18 nm and 40 nm PAA-coated NPs (B). Treatment with Triton-X served as a positive control. Cellular viability was assessed using XTT reduction. Results represent the mean of 2-3 independent experiments, each performed with 6 replicates. Error bars represent SEM. \*\*\*  $p < 0.001$  compared to control.

aggregation reactions, 5  $\mu\text{M}$   $\text{A}\beta_{1-40}$  fibrils were incubated for 2 h with 8.75  $\mu\text{M}$  ThT and 5-200 pM NPs, and ThT fluorescence was compared to  $\text{A}\beta_{1-40}$  fibrils incubated with ThT alone. ThT fluorescence detection of  $\text{A}\beta_{1-40}$  fibrils was unaltered by 18 nm NPs displaying citrate, PAA, and PAH surface chemistries (Figure 3.3A). In contrast, 18 nm CTAB-coated NPs significantly quenched ThT detection of aggregated  $\text{A}\beta_{1-40}$  at concentrations of 50 pM and higher. When PAA-coated NPs of varying diameter were compared, neither 8 nm nor 18 nm NPs altered the detection of  $\text{A}\beta_{1-40}$  fibrils by ThT; however, ThT detection was significantly compromised by the presence of 40 nm PAA-coated NPs (Figure 3.3B). As a result of these findings, assessment of the effect of 18 nm CTAB-coated NPs and 40 nm PAA-coated NPs was limited to TEM analysis.

### **3.3.3. Inhibition of $\text{A}\beta_{1-40}$ Monomer Aggregation by Surface Coated Gold NPs**

To evaluate the effect of gold NPs on  $\text{A}\beta_{1-40}$  aggregation, aggregation of monomeric protein was induced by continuous agitation, and ThT fluorescence was used to monitor the formation of  $\beta$ -sheet amyloid aggregates.  $\text{A}\beta_{1-40}$  aggregation yielded a characteristic growth pattern displaying an initial lag phase, indicative of nucleation, which was followed by rapid aggregate growth that ceased at equilibrium, as evidenced by plateau of the fluorescence signal (Figure 3.4A).

Aggregation of 40  $\mu\text{M}$   $\text{A}\beta_{1-40}$  monomer was induced in the presence of 20 pM-200 pM NPs. While none of the NPs examined were capable of impeding nucleation to extend the lag time, three types of NPs decreased the quantity of aggregates formed (Figure 3.4A). Addition of 18 nm citrate-coated NPs resulted in a  $19.4 \pm 8.0\%$  reduction of the equilibrium fluorescence plateau, and addition of 18 nm PAH-coated

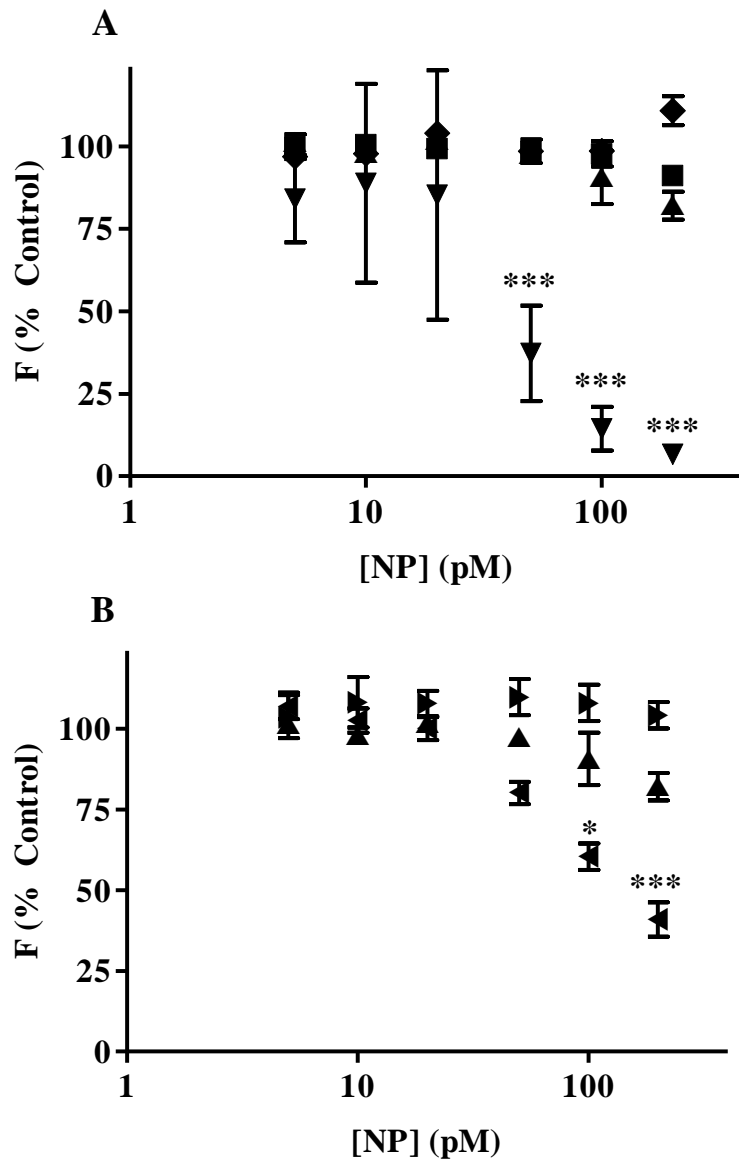


**Figure 3.3: Effect of surface coated NPs on ThT fluorescence detection of A $\beta_{1-40}$  aggregates:** A $\beta_{1-40}$  fibrils diluted in 40 mM Tris-HCl (pH 8.0) to a final concentration of 5  $\mu$ M were combined with 8.75  $\mu$ M ThT to reflect concentrations within diluted samples used to monitor A $\beta_{1-40}$  aggregation. Fibrils and ThT were incubated alone or with 20 pM-200 pM NPs for 2 h before fluorescence was evaluated. Results are expressed as the percent of ThT fluorescence detection relative to control samples. A) Incubation with 18 nm NPs displaying citrate (■), CTAB (▼), PAH (◆), or PAA (▲) surface chemistries. B) Incubation with PAA-coated NPs exhibiting 8 nm (▶), 18 nm (▲), or 40 nm (◄) diameters. Error bars represent SEM, n=3. \*p<0.05, and \*\*\*p<0.001 compared to control.

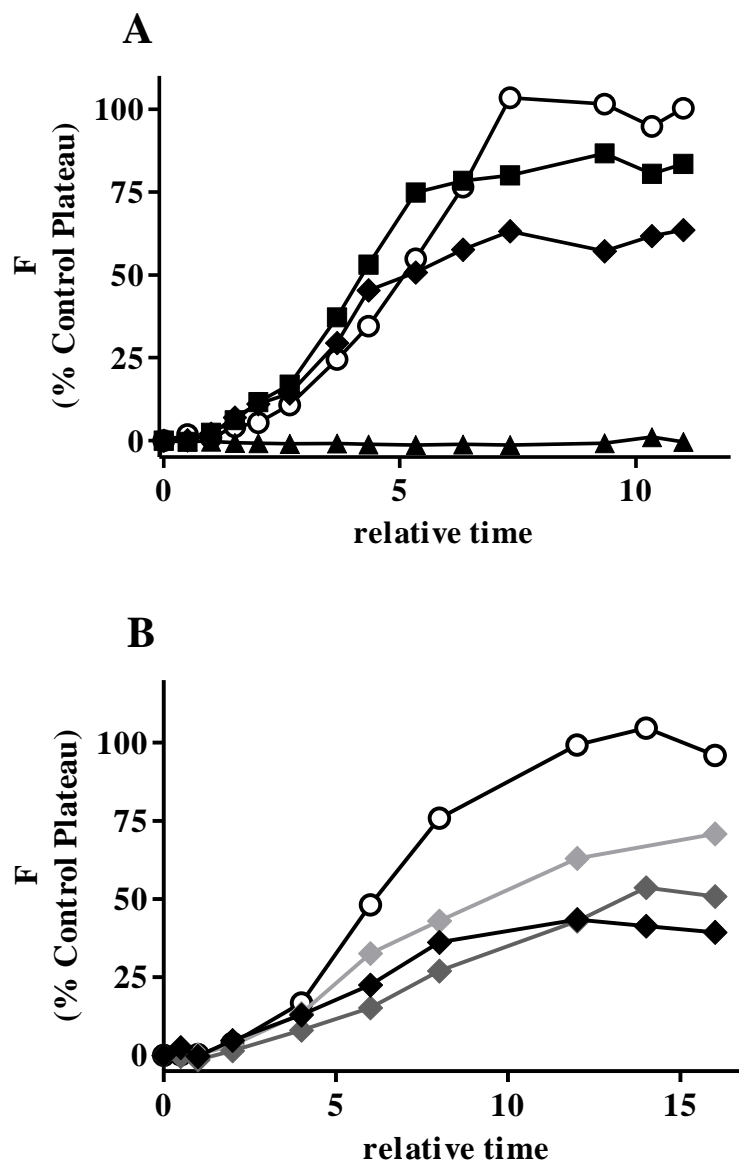


**Figure 3.4: Effect of 18 nm NPs exhibiting varying surface chemistries on  $A\beta_{1-40}$  monomer aggregation:**  $A\beta_{1-40}$  monomer diluted to 40  $\mu\text{M}$  in 40 mM Tris-HCl (pH 8.0) was incubated alone (control, ○), or in the presence of NPs. Monomer aggregation was induced under continuous agitation and monitored via ThT fluorescence (F) by periodic dilution into 10  $\mu\text{M}$  ThT. Fluorescence values are presented as a percentage of the equilibrium plateau fluorescence observed in the absence of NPs, and time is plotted as a fraction of the lag time observed in the absence of NPs. A) Aggregation in the presence of 200 pM NPs displaying citrate (■), PAH (◆), or PAA (▲), or surface chemistries. B) Aggregation in the presence of 18 nm PAH-coated NPs at 200 pM (◆), 100 pM (◆), or 20 pM (◆). Results are representative of three independent experiments.

NPs reduced  $\beta$ -sheet aggregates by  $58.5 \pm 9.3\%$  (Table 3.1). The most robust effect was observed with the addition of 18 nm PAA-coated NPs, which completely abrogated  $A\beta_{1-40}$  aggregation.

Inhibition of  $A\beta_{1-40}$  monomer aggregation by surface modified NPs was dose-dependent (Figure 3.4B, Table 3.1). 18 nm citrate-coated NPs proved ineffective at concentrations below 200 pM, and inhibition by 18 nm PAH-coated NPs decreased from  $58.5 \pm 9.3\%$  to  $46.9 \pm 4.5\%$  and  $44.8 \pm 4.4\%$  when NP concentration was reduced to 100 pM and 20 pM, respectively. 18 nm PAA-coated NPs, however, continued to impart complete inhibition at concentrations as low as 20 pM, or a 1:2,000,000 substoichiometric ratio of NPs to  $A\beta_{1-40}$ . These results confirm the superior inhibitory capabilities of PAA-coated NPs. In addition, these inhibitory effects were specific for the presence of surface coated NPs, as 100  $\mu$ M of solubilized PAA failed to elicit an inhibitory effect on aggregation of 40  $\mu$ M  $A\beta_{1-40}$  (Figure 3.5).

To confirm inhibition of  $A\beta_{1-40}$  monomer aggregation by surface coated gold NPs and further investigate changes in aggregate morphology, TEM images were acquired after aggregations reached equilibrium. In the absence of NPs, two distinct aggregates were observed: long, thin elongated aggregates and short, thick associated aggregates (Figure 3.6A). This morphology is similar to  $A\beta$  aggregates observed in other studies (17; 82). While  $A\beta_{1-40}$  aggregates formed in the presence of 200 pM 18 nm citrate-coated NPs exhibited the same morphology, the quantity of aggregates was reduced compared to the control (Figure 3.6B). A reduction in the quantity of aggregates formed in the presence of PAH-coated NPs was also evidenced as compared to the control (Figure 3.6C). These results corroborate the plateau reductions observed via ThT fluorescence.

**Table 3.1:** Inhibition of A $\beta$ <sub>1-40</sub> monomer aggregation by surface modified NPs. <sup>a,b</sup>

NP type		[NP] ( $\mu$ M)		
Diameter	Surface modification	20	100	200
18 nm	Citrate	4.3 $\pm$ 2.6	0.0 $\pm$ 0.0	19.4 $\pm$ 8.0
	PAA	96.5 $\pm$ 2.3 <sup>***</sup>	98.8 $\pm$ 0.2 <sup>***</sup>	94.8 $\pm$ 2.7 <sup>***</sup>
	PAH	44.8 $\pm$ 4.4 <sup>***</sup>	46.9 $\pm$ 4.5 <sup>***</sup>	58.5 $\pm$ 9.3 <sup>***</sup>
8 nm	PAA	95.1 $\pm$ 3.1 <sup>***</sup>	91.9 $\pm$ 4.1 <sup>***</sup>	94.4 $\pm$ 0.5 <sup>***</sup>

\*\*\*p<0.001 compared to control.

<sup>a</sup> Inhibition is expressed as plateau reduction, or the percentage of reduction in the equilibrium fluorescence plateau compared to the control, calculated as described in Section 2.7.

<sup>b</sup> Parameters are expressed as mean  $\pm$  SEM, n=3-5.

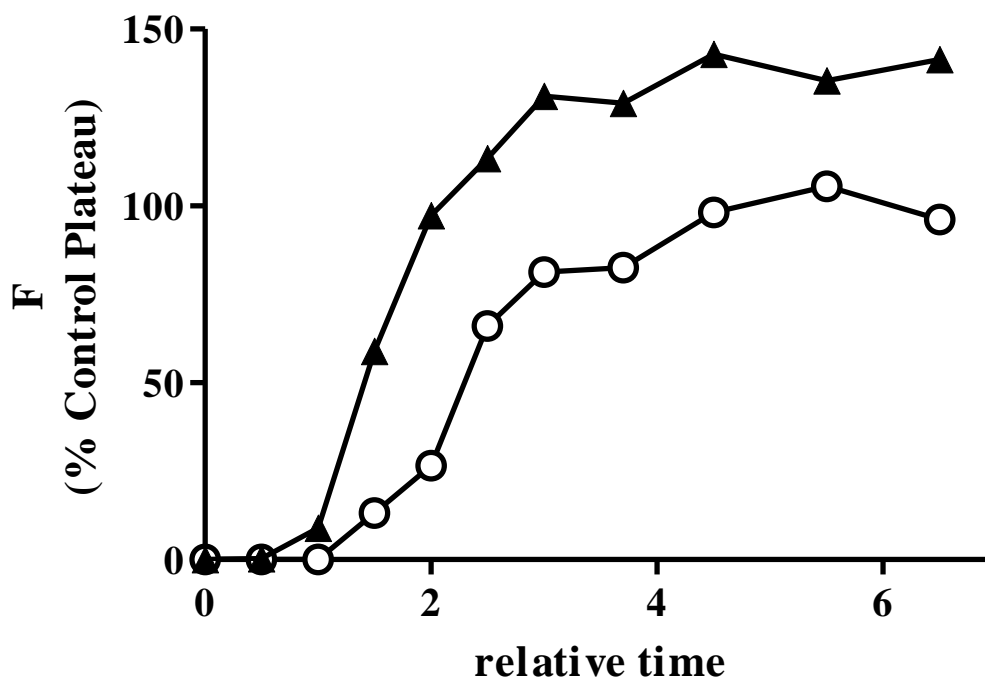


**Figure 3.5: Effect of solubilized PAA on  $A\beta_{1-40}$  monomer aggregation:**  $A\beta_{1-40}$  monomer diluted to  $40 \mu\text{M}$  in  $40 \text{ mM}$  Tris-HCl (pH 8.0) was incubated alone (control, ○) or in the presence of  $100 \mu\text{M}$  PAA (▲). Monomer aggregation was induced under continuous agitation and monitored via ThT fluorescence (F) by periodic dilution into  $10 \mu\text{M}$  ThT. Fluorescence and time values are presented as in Figure 3.4. Results are representative of three independent experiments.

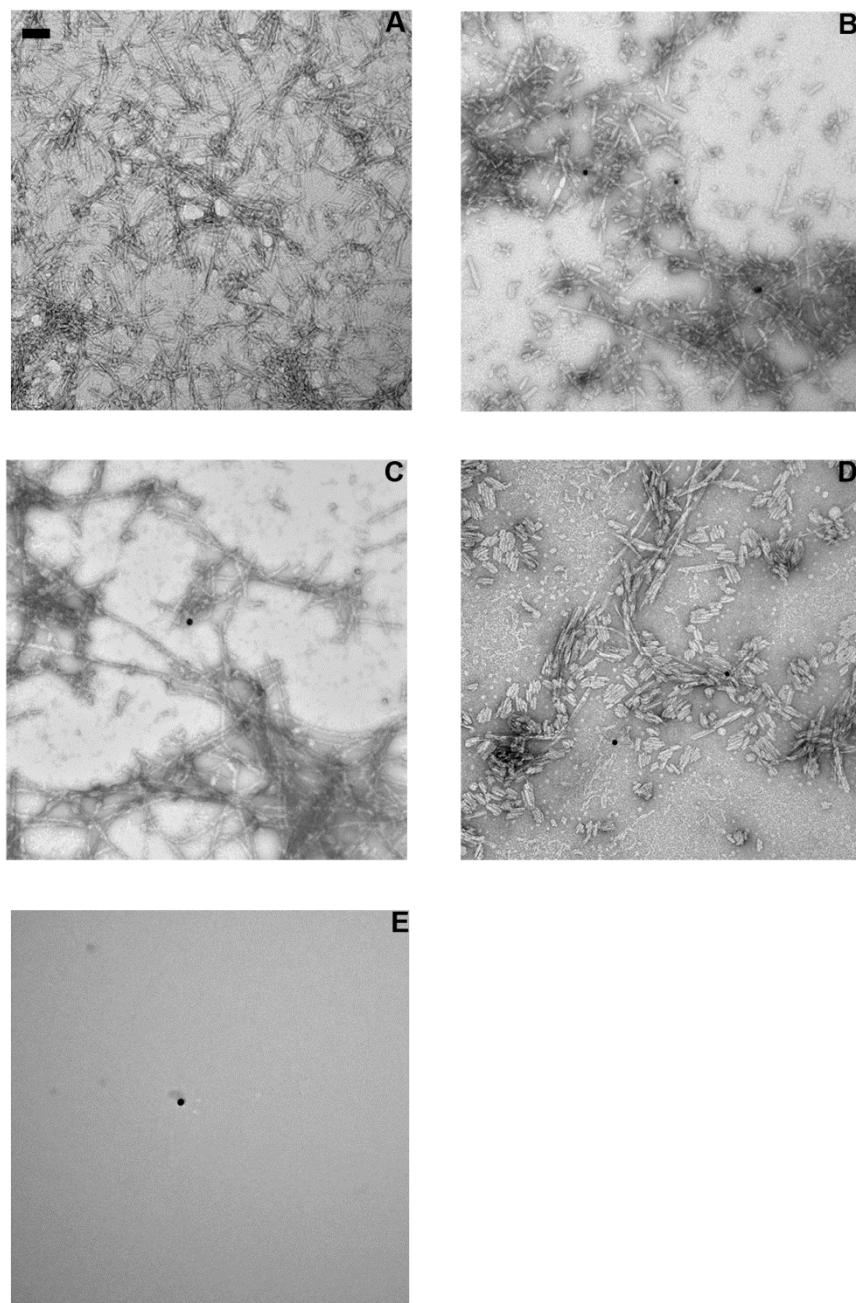


**Figure 3.6: Morphology of  $A\beta_{1-40}$  aggregates formed in the presence of 18 nm NPs exhibiting varying surface chemistries:** 40  $\mu\text{M}$   $A\beta_{1-40}$  monomer in 40 mM Tris-HCl (pH 8.0) was aggregated alone (control, A) or in the presence of 200 pM 18 nm NPs displaying citrate (B), PAH (C), CTAB (D), or PAA (E) surface chemistries. The control reaction was monitored via ThT fluorescence, and upon evidence of the equilibrium plateau samples were gridded and visualized by TEM as described in Section 2.8. Results are representative of 2 independent experiments. Images are shown relative to a scale bar of 100 nm.

Aggregates formed in the presence of CTAB-coated NPs, demonstrated a slight reduction in aggregate quantity (Figure 3.6D), however, they were not as effective as PAH-coated NPs. Furthermore, the absence of fibrillar content detected via TEM when A $\beta$ <sub>1-40</sub> monomer was subjected to aggregation conditions in the presence of 200 pM 18 nm PAA-coated NPs confirms the ability of these NPs to abrogate A $\beta$ <sub>1-40</sub> monomer aggregation (Figure 3.6E).

A $\beta$ <sub>1-40</sub> monomer aggregated in the presence of 18 nm cationic NPs, coated with CTAB or PAH, exhibited morphological changes in aggregate structure. 200 pM CTAB-coated NPs induced an increased amount of short, thick aggregates (Figure 3.6D), while aggregates formed in the presence of 200 pM PAH-coated NPs exhibited an increased content of long, thin structures (Figure 3.6E). In contrast, anionic citrate-coated NPs failed to alter aggregate morphology (Figure 3.6B). Thus, TEM images further demonstrate the ability of cationic NPs, but not anionic NPs, to influence aggregate morphology.

#### **3.3.4. Effect of NP Size on Inhibition of A $\beta$ <sub>1-40</sub> Monomer Aggregation**

Further experimentation with PAA-coated NPs was performed to elucidate the effect of NP size on inhibitory capabilities. PAA-coated NPs exhibiting diameters of 8 nm, 18 nm, and 40 nm were examined for their ability to attenuate A $\beta$ <sub>1-40</sub> monomer aggregation. Similar to 18 nm PAA-coated NPs, 8 nm PAA-coated NPs reduced the equilibrium fluorescence plateau by >90% at concentrations as low as 20 pM (Figure 3.7, Table 3.1), demonstrating their effectiveness as A $\beta$ <sub>1-40</sub> aggregation inhibitors. This result was corroborated by the absence of aggregate material observed via TEM (Figure 3.8B).

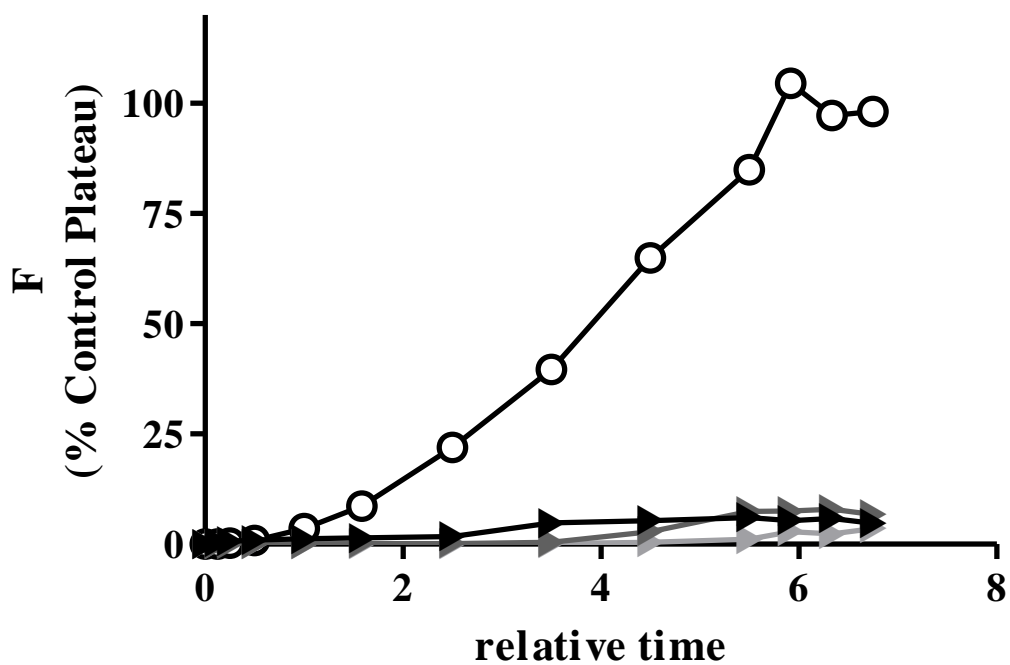


**Figure 3.7: Effect of 8 nm PAA-coated NPs on A $\beta_{1-40}$  monomer aggregation:** A $\beta_{1-40}$  monomer diluted to 40  $\mu$ M in 40 mM Tris-HCl (pH 8.0) was incubated alone (control, ○) or in the presence of 200 pM (▶), 100 pM (◀), or 20 pM PAA-coated NPs (◄). Monomer aggregation was induced under continuous agitation and monitored via ThT fluorescence (F) by periodic dilution into 10  $\mu$ M ThT. Fluorescence and time values are presented as in Figure 3.4. Results are representative of three independent experiments.

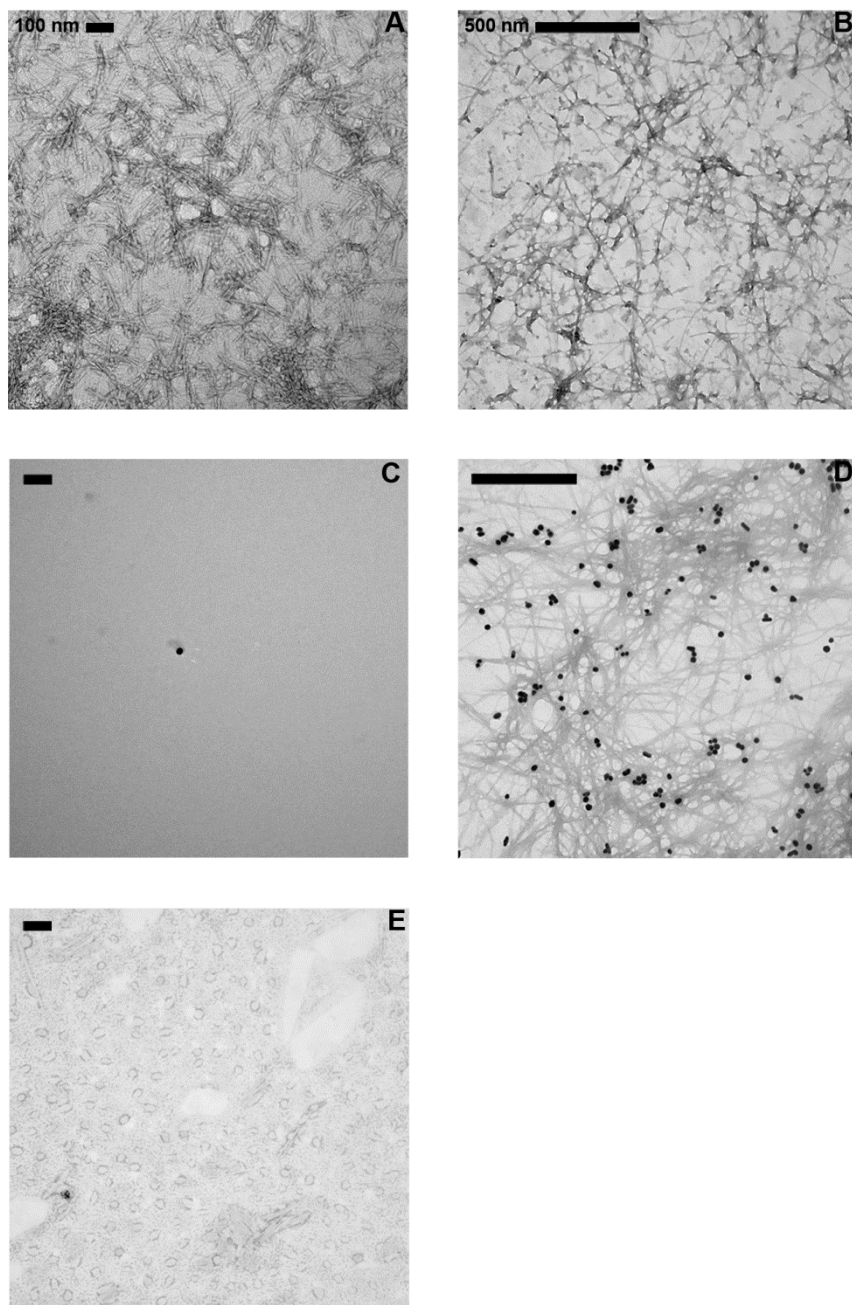


**Figure 3.8: Morphology of  $A\beta_{1-40}$  aggregates formed in the presence of PAA-coated NPs of varying size:**  $40\ \mu\text{M}$   $A\beta_{1-40}$  monomer in  $40\ \text{mM}$  Tris-HCl (pH 8.0) was aggregated alone (control, A, D) or in the presence of  $200\ \text{pM}$  PAA-coated NPs exhibiting diameters of  $8\ \text{nm}$  (B),  $18\ \text{nm}$  (C), or  $40\ \text{nm}$  (E). The control reaction was monitored via ThT fluorescence, and upon evidence of the equilibrium plateau samples were gridded and visualized by TEM as described in Section 2.8. Results are representative of 2 independent experiments. Images are shown relative to a scale bar of  $100\ \text{nm}$  (A-C) or  $500\ \text{nm}$  (D-E).

In contrast, when NP diameter was increased to 40 nm, PAA-coated NPs were ineffective at preventing the formation of A $\beta$  aggregates. Although 40 nm PAA-coated NPs quenched ThT fluorescence, their inability to prevent aggregate formation was evidenced by TEM images displaying a similar quantity of A $\beta$ <sub>1-40</sub> aggregates formed in the absence and presence of 200 pM NPs (Figure 3.8E). These results demonstrate that only smaller PAA-coated NPs are capable of serving as effective inhibitors of A $\beta$ <sub>1-40</sub> aggregation.

### 3.4. Discussion

The emergence of NPs in medicinal research has led to various applications such as photo thermal ablation (83), drug delivery (84; 85) and advanced medical imaging (86; 87). With a near limitless library of NPs that can be synthesized with varying core material, surface chemistry, size, and shape it is important with application in AD that these NP properties are explored for their therapeutic value. Various types of NPs that possess potential as A $\beta$  aggregation inhibitors have been developed (74; 75; 81). In this study, we have characterized the inhibitory capabilities of spherical gold NPs with varying surface chemistries and diameters. By examining their toxicological effects as well as their ability to attenuate A $\beta$  aggregation, we identify NP surface chemistry and size characteristics with potential as an effective AD therapeutic.

Neurotoxicity elicited by synthesized NPs was a function of both surface chemistry and size. Among 18 nm NPs, only CTAB-coated NPs elicited significant toxicological effects. Numerous *in vitro* and *in vivo* studies have been conducted on the toxicological effects of NPs (reviewed in (88-90)). While CTAB, a known cellular membrane detergent, is important in the formation of gold NPs, soluble CTAB left in the NP solution can lead to toxicity. NPs displaying an inert surface chemistry elicited varying cellular responses when particle diameter was altered. While 8 nm and 18 nm PAA-coated particles showed no toxicological effects, larger 40 nm PAA-coated particles elicited a pronounced decrease in cellular viability. Thus, maintaining a smaller size of spherical NPs prevents neurotoxicity. This result is in agreement with other reports of NP toxicity. Mironava et al. demonstrated that 45 nm spherical gold NPs were more cytotoxic to human dermal fibroblasts than their comparative 13 nm NPs (91). This

study further determined that altering NP size led to different cellular uptake mechanisms and thus varied vacuole sequestration, which led to an increase in toxicity for larger particles.

Moderate inhibitory capabilities were evidenced with the citrate-coated NPs with  $19 \pm 8\%$  inhibition of aggregation at 200 pM. PAH-coated NPs exhibited  $58.5 \pm 9.3\%$  inhibition of aggregation. The most effective inhibition was evidenced with PAA-coated NPs where complete inhibition was observed at sub-stoichiometric ratios as low as 1:2,000,000 of A $\beta$ :NP. Inhibitory capabilities of NPs are influenced to a greater extent by surface chemistry than surface charge. While both citrate-coated and PAA-coated NPs carry a negative charge, PAA-coated NPs are significantly more effective at inhibiting aggregation. Ikeda et al. discovered that anionic nanogels suppressed A $\beta$  aggregation at a greater rate than neutral nanogels (92). It was proposed that the anionic nanogels were able to electrostatically disrupt salt bridge formation resulting in the inability of fibril formation. This theory can be applied to the inhibitory effects of citrate-coated and PAA-coated NPs, with the increased surface charge density of PAA-coated NPs over citrate-coated NPs leading to increased salt bridge disruption.

Another possible mechanism in which NPs can inhibit A $\beta$  aggregation was elucidated by Cabaleiro-Lago et al. (74). When cationic polymeric particles were introduced to monomeric A $\beta$ , an extension of the lag time to nucleation was evidenced. It was proposed that absorption of monomeric protein onto the surface of the NPs depletes monomer within solution leading to an increase in the time required for nucleation to occur. In this current study, NPs were observed to have no effect on lag time to aggregate formation. Instead, the quantity of aggregates formed was reduced.

This contrast suggests that monomeric depletion may not be the mechanism by which the NPs in this study attenuate A $\beta$  aggregation. Instead, NPs may interact electrostatically with intermediate aggregates of the protein.

Gold NPs also have the ability to modify fibrillar structure of A $\beta$  aggregates. Cationic PAH-coated and CTAB-coated NPs elicited the ability to induce distinct changes in fibrillar morphology. Protein interactions with charged surfaces can have a pronounced effect on the formation of fibrillar aggregate species. Li et al. demonstrated that cationic DTAB and a cationic gemini surfactant stimulate distinct changes in fibrillar aggregate morphology due to the interaction of cationic species with anionic charged residues within A $\beta$ , leading to misfolding of the protein (93). This study is consistent with alterations in aggregate morphology induced by cationic CTAB-coated and PAH-coated NPs. Thus, electrostatic interactions between cationic NPs and anionic A $\beta$  residues may lead the protein to fold into these distinct conformations.

NP size also plays a role in inhibitory capabilities. While smaller 8 nm PAA-coated NPs were as effective as their 18 nm counterparts, 40 nm PAA-coated NPs elicited no effect on monomer aggregation. The effects of varying diameter on protein aggregation have been attributed to NP surface curvature and surface area. Lundqvist et al. found that larger diameter silica NPs had an increased surface area for human carbonic anhydrase 1 protein absorption, leading to conformation changes in the protein (94). In contrast, molecular modeling simulations of NP-protein interactions have demonstrated that smaller diameter particles can delay protein fibrilization longer than larger particles (95). Since 40 nm PAA-coated NPs were less effective than their smaller counterparts, A $\beta$  may not be absorbed onto the NP surface as demonstrated in the work of Lundqvist.

These results demonstrate that both surface chemistry and size can modulate the ability of spherical gold NPs to act as A $\beta$  aggregation inhibitors. Surface chemistry was found to influence the magnitude of inhibition, with PAA-coated NPs exhibiting the most pronounced effect. Surface chemistry can also influence in a manner in which NPs modify aggregate morphology as evidenced with the cationic NPs. Finally, NP size also influences inhibitory capabilities, as larger particles were ineffective at inhibiting A $\beta$  aggregation as compared to similarly coated smaller particles. Overall, PAA-coated NPs 18 nm and smaller are superior inhibitors abrogating aggregation at substoichiometric ratios with the protein. Together, these findings identify gold NPs as potential therapeutic agents for the abrogation of A $\beta$  aggregation and provide further insight into the characteristics needed in the rational design of highly effective NP inhibitors.

## CHAPTER 4

### A NOVEL PEPTOID AS AN INHIBITOR OF A $\beta$ AGGREGATION IN ALZHEIMER'S DISEASE

#### 4.1. Introduction

One approach to the inhibition of A $\beta$  aggregation has been the use of small peptides derived from the A $\beta$  sequence. This approach is based on the idea that the aggregation of A $\beta$  occurs via self-recognition within the peptide (96). Corroborating this hypothesis, studies have concluded that peptides homologous to A $\beta$  recognize and bind A $\beta$ , while amino acid substitutions or additions within these peptides disrupt the aggregation process. The most effective peptide inhibitors have been those mimicking the sequence KLVFF, located within the A $\beta$  hydrophobic core (97-100). Research suggests that this region of A $\beta$  is responsible for the formation of the protein's secondary structure during aggregation (101). In particular, residues 19 and 20 of A $\beta$ , a pair of phenylalanine residues, are speculated to give rise to  $\pi$ -stacking interactions that may play a key role in the assembly and stabilization of A $\beta$  aggregates (102). By disrupting these  $\pi$ - $\pi$  interactions, inhibition of A $\beta$  aggregation can occur.

One challenge in developing peptides as therapeutic agents is the ease in which they are degraded *in vivo* by proteases before reaching their therapeutic target (103). To decrease protease degradation, researchers have implemented terminal modification by acetylation or amidation (104), D-amino acid substitutions (105), and tryptophan replacement of proteolytic sites (106). In each of these studies, an increased half-life was observed for the modified peptide as compared to its natural counterpart. However, in

many cases peptide modification also decreased therapeutic activity. An alternative approach is to create a peptoid replicate of the peptide of interest. Peptoids differ from peptides in that the side-chain connectivity is moved from the  $\alpha$ -carbon to the amide nitrogen. This backbone structural modification allows for increased protection from protease degradation while preserving side chain chemistry to closely maintain the original structure. In this study, a peptoid based on the amino acid sequence KLVFF was examined for its ability to disrupt A $\beta$  aggregation. We hypothesize that the peptoid will alter A $\beta$  aggregation to reduce the physiological activity of A $\beta$  aggregate preparations. To test this hypothesis, we examined the ability of the peptoid to modulate the formation of larger A $\beta$  aggregates as well as A $\beta$  oligomers, postulated to be the primary pathogenic aggregate species, and to attenuate NF- $\kappa$ B activation, a key factor in inflammation related to AD.

## 4.2. Methods & Materials

### 4.2.1. Peptoid Synthesis

The peptoid examined in this study was synthesized in the laboratory of Dr. Shannon Servoss (Department of Chemical Engineering, University of Arkansas). This peptoid (PN) was designed after the KLVFF sequence of A $\beta$  with three additional C-terminal residues, a spacer and two phenylalanines. Peptoid PN possesses a neutral spacer residue, an isoleucine, between the two pairs of aromatic phenylalanines (Figure 4.1). PN was synthesized via the submonomer protocol on an ABI 433A automated peptide synthesizer (Invitrogen, Carlsbad, CA). The Rink amide resin (substitution rate of ~0.59 mmol/g) was swelled with dimethylformamide (DMF) and the Fmoc protecting group was removed using 20% piperidine in DMF. The secondary amine was bromoacetylated by adding 1.2 M bromoacetic acid in DMF and N,N'-diisopropyl carbodiimide (DIC) at a ratio of 4:1 and vortexing for 60 min. The reaction vessel was drained and the resin was rinsed with DMF. The desired side chain was integrated by adding 1 M of primary amine in DMF and vortexing for 90 min. After the synthesis was complete, the product was cleaved from the resin using a mixture of 95% trifluoroacetic acid (TFA), 2.5% water, and 2.5% triisopropylsilane (TIS) for 10 min.

Crude product was purified using a Waters Delta 600 reversed-phase high pressure liquid chromatography (RP-HPLC) system (Milford, MA) equipped with a Duragel G C18 150 x 20 mm column (5-95% gradient water to acetonitrile). Final purity was confirmed using a Waters 2695 Separations Module analytical RP-HPLC using a Duragel G C18 150 x 2.1 mm column (5-95% gradient water to acetonitrile) and Matrix-

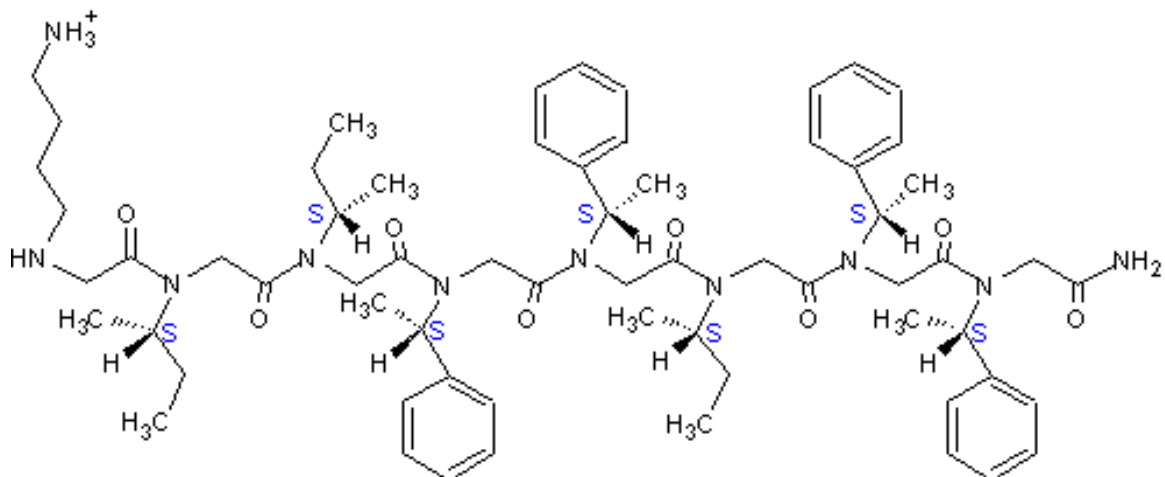


**Figure 4.1: Structure of peptoid PN:** PN was synthesized analogous to KLVFF, the hydrophobic core of A $\beta$ . The first five residues of the peptoid mimic KLVFF, while the c-terminal three residues incorporate a spacer residue, an isoleucine, followed by two additional aromatic phenylalanines.

Assisted Laser Desorption/Ionization (MALDI). The secondary structure was determined to be  $\alpha$ -helical via circular dichroism (CD) in methanol.

#### **4.2.2. A $\beta$ <sub>1-40</sub> Monomer Aggregation**

Monomer aggregations were carried out as described in Section 2.4 with the inclusion of 100  $\mu$ M PN. Aggregation was assessed via dot blot analysis as described in Section 2.6.

#### **4.2.3. A $\beta$ <sub>1-42</sub> Oligomerization**

A $\beta$ <sub>1-42</sub> oligomerization was conducted as described in Section 2.10 with the inclusion of 2  $\mu$ M-100  $\mu$ M PN. After 30 min incubation, oligomers were resolved via SDS-PAGE and Western blotting following procedures in Section 2.11.

#### **4.2.4. Determination of A $\beta$ <sub>1-42</sub> Oligomer Structure by ANS Fluorescence**

A $\beta$ <sub>1-42</sub> oligomerization was conducted as described in Section 2.10 with the inclusion of 100  $\mu$ M PN. Alterations in oligomer structure, by changes in solvent exposed hydrophobic regions, were assessed using ANS fluorescence following procedures in Section 2.12.

#### **4.2.5. XTT Reduction Assay**

SH-SY5Y human neuroblastoma cells (Section 2.13) were treated with PN at 20  $\mu$ M, 10  $\mu$ M, and 5  $\mu$ M. Cellular viability following peptoid exposure was monitored via XTT reduction as described in Section 2.14.

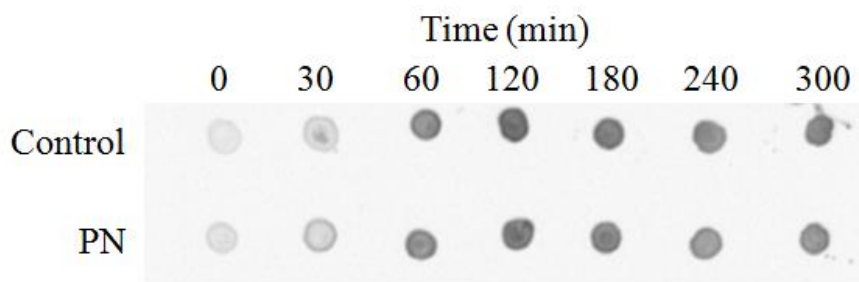
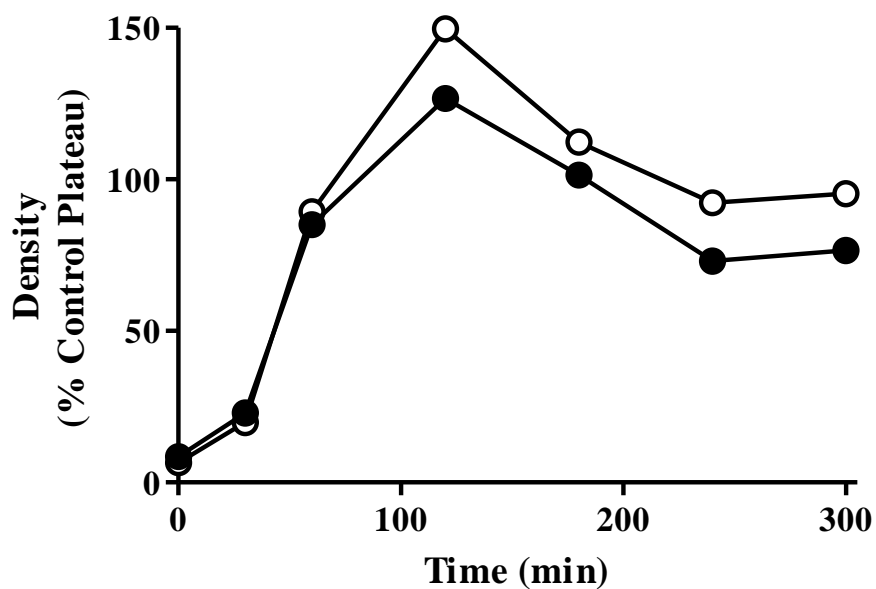
#### **4.2.6. A $\beta$ <sub>1-42</sub> Oligomer Activation of NF- $\kappa$ B**

A $\beta$ <sub>1-42</sub> oligomerization was conducted as described in Section 2.10 with the inclusion of 100  $\mu$ M PN. After 30 min, SH-SY5Y cells (Section 2.13) were incubated in the presence of end products of oligomerization reactions at an oligomer concentration of 2  $\mu$ M. Media only served as a negative control, while cells treated with 10 Units/well TNF- $\alpha$  served as a positive control. Following 15 min incubation, cells were prepared and imaged via confocal microscopy as described in Section 2.15. Image analysis was conducted as described in Section 2.16.

## 4.3. Results

### 4.3.1. Peptoid PN Inhibits A $\beta$ <sub>1-40</sub> Aggregation

To evaluate the effects of this novel peptoid on the late stages of aggregation, an A $\beta$ <sub>1-40</sub> monomer aggregation assay was employed. Monomer aggregation was induced by continuous agitation in the presence of 150 mM NaCl, and dot blotting with immunocytochemistry was used to monitor the formation of  $\beta$ -sheet amyloid aggregates. This approach has become an effective technique to monitor A $\beta$  aggregation (61; 107; 108). Antibody detection of amyloid aggregates can be classified into two categories: sequence and conformation specific. Antibodies such as 6E10, which are sequence specific, bind A $\beta$  independent of its secondary structure, and thus recognize both monomeric and aggregated forms of the protein. In contrast, conformation specific antibodies recognize structural elements to specifically label aggregate species. A common conformational specific antibody for detecting fibrillar aggregates is OC. Studies have shown that OC antibody binds to fibrillar aggregates but not to prefibrillar oligomers (109). However, the OC antibody can also non-specifically react with monomeric A $\beta$ . Therefore, LOC (like OC) antibody was developed to lower monomeric reactivity. The LOC antibody can serve as an excellent indicator of the formation of fibrillar aggregates during A $\beta$  aggregation (110-112) when ThT detection is insufficient due to binding competition or interference from potential aggregation inhibitors. Aggregation of 20  $\mu$ M A $\beta$ <sub>1-40</sub> monomer was induced in the presence of 100  $\mu$ M PN. Periodically, samples were dotted onto nitrocellulose membrane and probed with LOC (Figure 4.2A). Addition of PN resulted in a modest  $24.2 \pm 7.8\%$  reduction of the equilibrium fluorescence plateau as compared to the control (Figure 4.2B).

**A****B**

**Figure 4.2: Effect of peptoid PN on A $\beta$ <sub>1-40</sub> monomer aggregation:** A $\beta$ <sub>1-40</sub> monomer diluted to 20  $\mu$ M in 40 mM Tris-HCl (pH 8.0) was incubated alone (control,  $\circ$ ) or in the presence of 100  $\mu$ M PN ( $\bullet$ ). Monomer aggregation was induced under continuous agitation with 150 mM NaCl and monitored via immunocytochemistry by periodic dotting onto nitrocellulose membrane (A). Membranes were developed, and densitometric analysis was performed as described in Section 2.6 (B). Results are expressed as a percentage of the control plateau and are representative of two independent experiments.

### **4.3.2. Peptoid PN Alters the Size and Quantity of A $\beta$ <sub>1-42</sub> Oligomers**

To evaluate the effects of PN on the early stages of aggregation, an A $\beta$ <sub>1-42</sub> oligomerization assay was employed. A $\beta$ <sub>1-42</sub> deposits first in amyloid plaques and has been associated with the formation of early stage oligomers (113). When freshly solubilized A $\beta$ <sub>1-42</sub> was subjected to oligomerization conditions, an even distribution of oligomers appeared between 20 kDa-100 kDa and 100 kDa-250 kDa (Figure 4.3A). When PN was introduced, A $\beta$ <sub>1-42</sub> oligomers formed were fewer and smaller in size, as evidenced by smears ceasing at a lower height (Figure 4.3A). Furthermore, a dose dependent relationship is observed when PN concentration was reduced from 100  $\mu$ M to 2  $\mu$ M (Figure 4.3B). To elucidate any changes in the quantity of monomers, as well as the smallest oligomer species  $\leq$  20kDa oligomers formed in the presence of 100  $\mu$ M PN were resolved. A light band at  $\sim$ 4 kDa indicates the presence of a small quantity of unreacted monomer, while a dark band at  $\sim$ 12 kDa indicates the pronounced presence of trimers (Figure 4.4A). Interestingly, the formation of dimers at  $\sim$ 8 kDa is not observed. However, there was no significant difference in the quantity of monomers, dimers, and trimers when compared to oligomers formed in the absence of PN (Figure 4.4B).

### **4.3.3. Peptoid PN modulates A $\beta$ <sub>1-42</sub> Oligomer Structure**

To characterize changes in A $\beta$ <sub>1-42</sub> oligomer conformation due to the presence of PN, ANS fluorescence was employed. ANS is a naphthaline based compound commonly used as a fluorescent probe. When ANS is introduced to hydrophobic molecules it undergoes a conformational change resulting in both blue shift and increased quantum yield (56). A $\beta$ <sub>1-42</sub> Oligomers formed in the presence of PN exhibited increased ANS

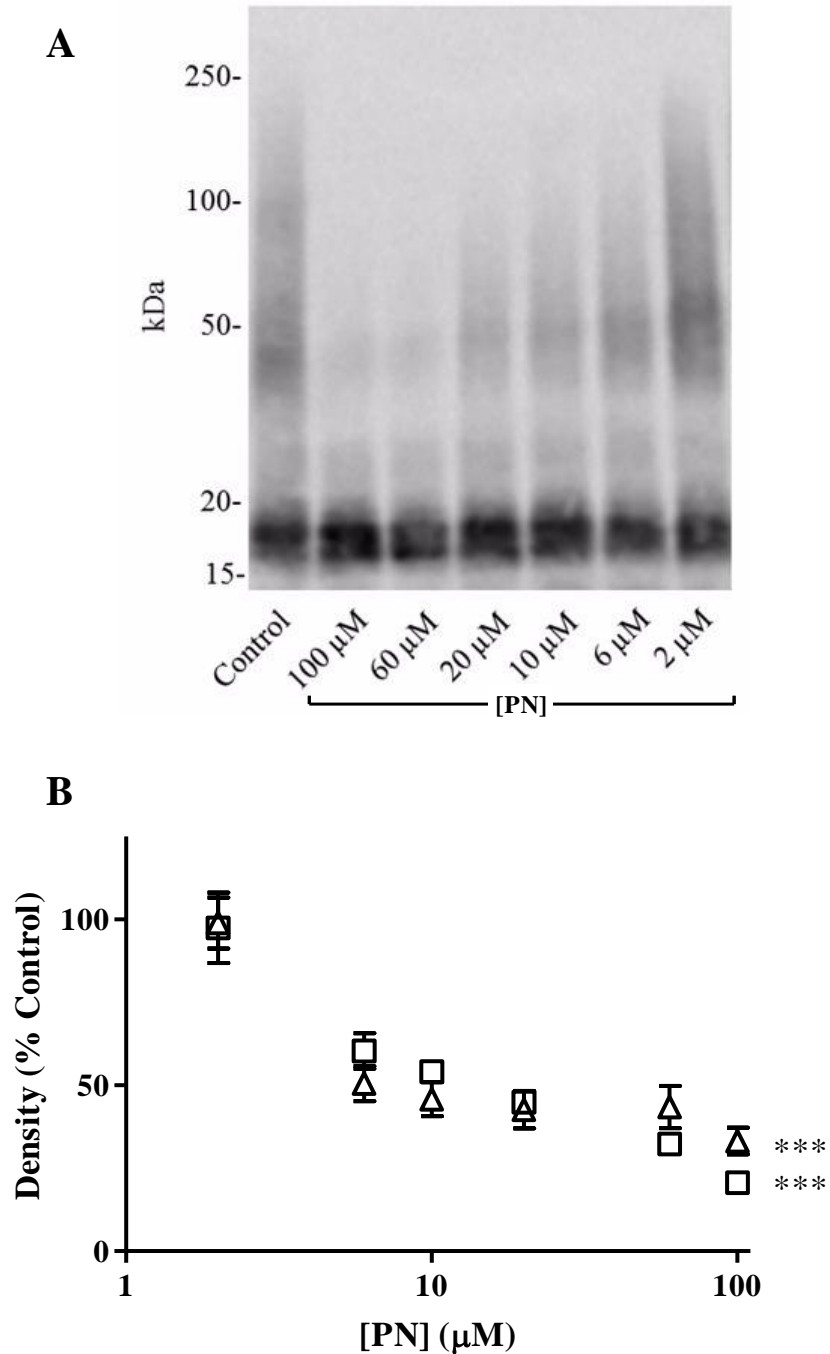


**Figure 4.3: Effect of peptoid PN on  $A\beta_{1-42}$  oligomerization:**  $A\beta_{1-42}$  oligomers were prepared, as described in Section 2.10, in the absence (control) or presence of PN. A) Oligomerization products resolved by SDS-PAGE using a 4-20% Tris-glycine gel were transferred to nitrocellulose and probed with 6E10. Image is representative of three independent experiments. B) Densitometric analysis of oligomer species within the size ranges of 20 kDa-100 kDa (□) and 100 kDa-250 kDa (Δ), reported as a percentage of the control. Error bars indicate SEM, n=3. \*\*\*p>0.001 versus control for [PN] > 2μM.

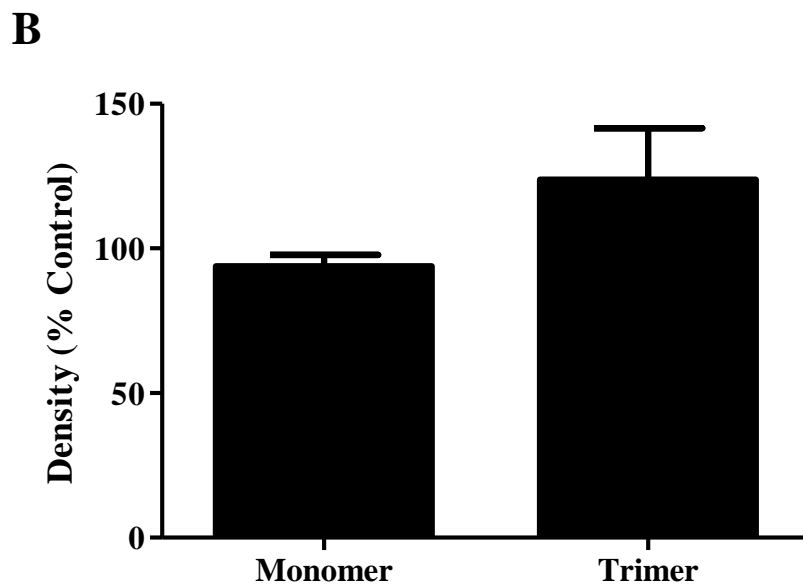
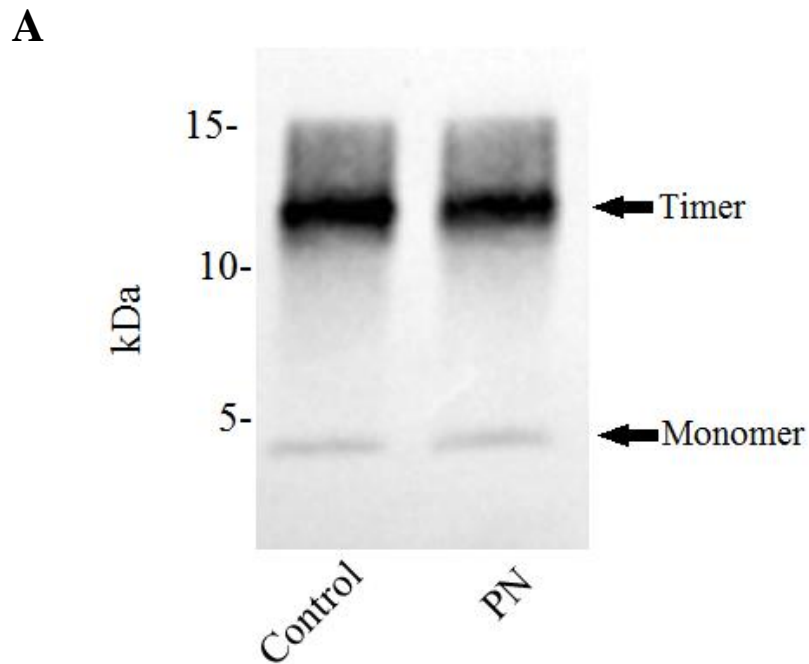


**Figure 4.4: Effect of peptoid PN on the formation of  $A\beta_{1-42}$  dimers and trimers:**  $A\beta_{1-42}$  oligomers were prepared, as described in Section 2.10, in the absence (control) or presence of PN. A) Oligomerization products resolved by SDS-PAGE using a 16.5% Tris-tricine gel were transferred to nitrocellulose and probed with 6E10 as described in Section 2.11. Results are representative of three independent experiments. B) Densitometric analysis of monomer (0 kDa-5 kDa) and trimer (10 kDa-15 kDa) species. Error bars indicate SEM,  $n=3$ .

fluorescence as compared to oligomers formed alone (Figure 4.5A, B). These results indicate that the presence of PN leads to an increased exposure of hydrophobic regions and thus an altered oligomer conformation.

#### **4.3.4. A $\beta$ <sub>1-42</sub> Oligomers Formed in the Presence of Peptoid PN Activate NF- $\kappa$ B**

A $\beta$  is known to activate NF- $\kappa$ B in neuronal cells (23-26). Under resting conditions NF- $\kappa$ B is contained mainly in the cytoplasm, as its nuclear translocation sequence is masked by I $\kappa$ B. During stressful conditions, cellular signals lead to I $\kappa$ B degradation, unmasking the NF- $\kappa$ B nuclear translocation sequence to facilitate the translocation of NF- $\kappa$ B into the nucleus where it initiates the transcription of genes involved in inflammation and immune response.

In untreated cells, NF- $\kappa$ B is located predominately in the cytoplasm with minimal levels located within the nucleus (Figure 4.6A, B). After incubation with TNF- $\alpha$ , a known activator (114), NF- $\kappa$ B translocation into the nucleus is evidenced in SH-SY5Y cells (Figure 4.6D, E). Digital removal of cytoplasmic NF- $\kappa$ B further verifies nuclear localized NF- $\kappa$ B (Figure 4.6C, F). To determine if changes in the size and structure of A $\beta$ <sub>1-42</sub> oligomers induced by PN alter NF- $\kappa$ B activation, SH-SY5Y cells were treated for 15 min with A $\beta$ <sub>1-42</sub> oligomers formed in the absence or presence of 100  $\mu$ M PN (Figure 4.7A, B, C). Compared to untreated cells, SH-SY5Y cells exposed to A $\beta$ <sub>1-42</sub> oligomers exhibited increased translocation of NF- $\kappa$ B into the nucleus (Figure 4.7D). Similar levels of NF- $\kappa$ B translocation were observed with A $\beta$ <sub>1-42</sub> oligomers formed in the presence of PN. To ensure inherent toxicity of PN is not a factor of NF- $\kappa$ B activation SH-SY5Y cells were treated for 24 h, with PN at concentrations ranging from 5-20  $\mu$ M, where 10  $\mu$ M

represents the concentration equivalent used for cell treatments to activate NF- $\kappa$ B (Figure 4.8). For all concentrations of PN tested, metabolic activity, measured via XTT reduction, was >90%, indicating no significant toxicity. These results demonstrate that alterations in A $\beta$ <sub>1-42</sub> oligomer size and structure by PN do not alter NF- $\kappa$ B activation levels as compared to natively formed oligomers.

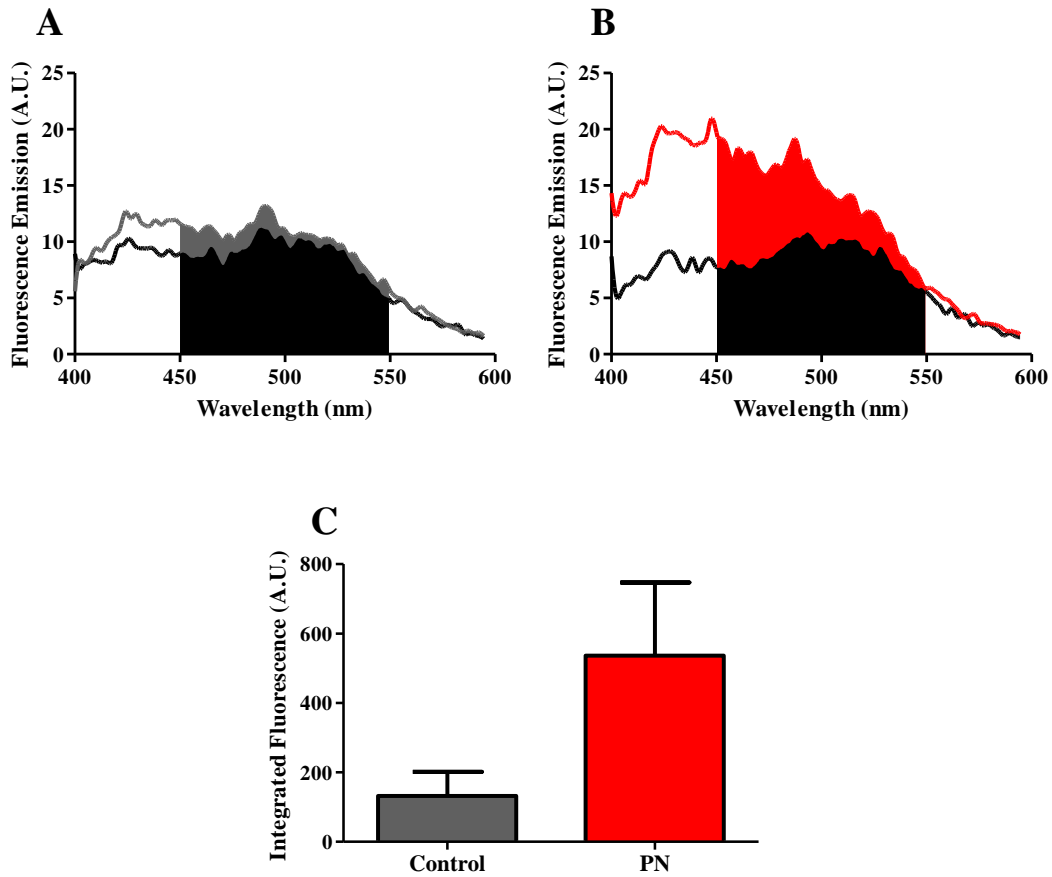


**Figure 4.5: Peptoid PN alters  $A\beta_{1-42}$  oligomer structure to expose hydrophobic regions:**  $A\beta_{1-42}$  oligomers were prepared (Section 2.10) in the absence (control, grey) or presence (red) of 100  $\mu$ M PN. Oligomers were incubated with 100  $\mu$ M ANS and fluorescence was quantified with background subtraction (black) as described in Section 2.12. Representative spectra of native oligomers (A) and oligomers formed in the presence of PN (B). C) Integrated fluorescence from 450 to 550 nm. Error bars indicate SEM, n=3.

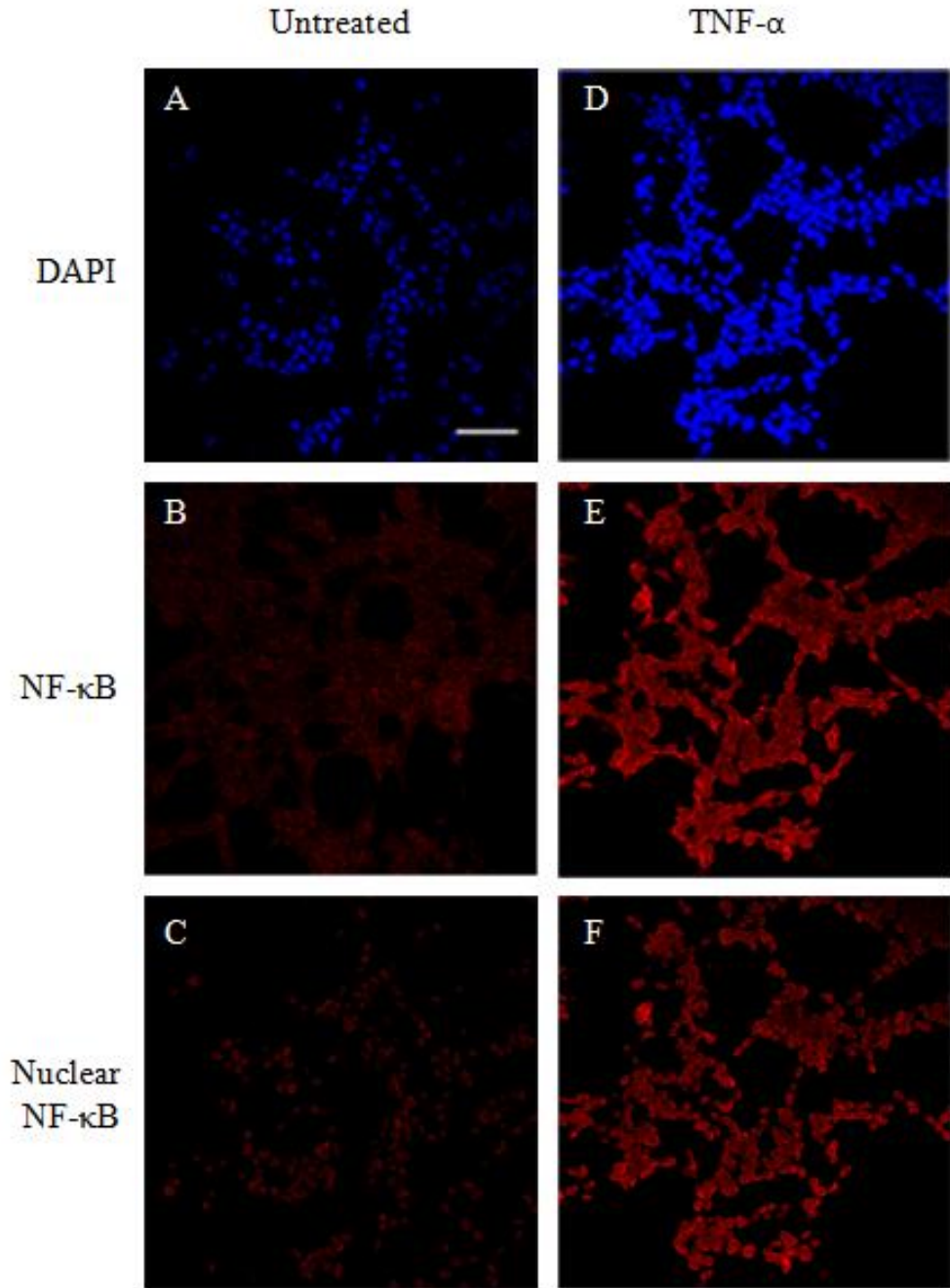


**Figure 4.6: Activation of NF- $\kappa$ B in SH-SY5Y human neuroblastoma cells:** SH-SY5Y human neuroblastoma cells were incubated for 15 min alone (untreated, A-C) or in the presence of 10 Units/well TNF- $\alpha$  (D-F). Cells were fixed, stained, and visualized by confocal microscopy as detailed in Section 2.15. Images shown depict: DAPI nuclear staining (A, D), NF- $\kappa$ B staining (B, E), or nuclear NF- $\kappa$ B staining extracted via MATLAB analysis as described in Section 2.16 (C, F). Images shown are medial sections of a z-series representative of four independent experiments. Scale bar = 50  $\mu$ m.

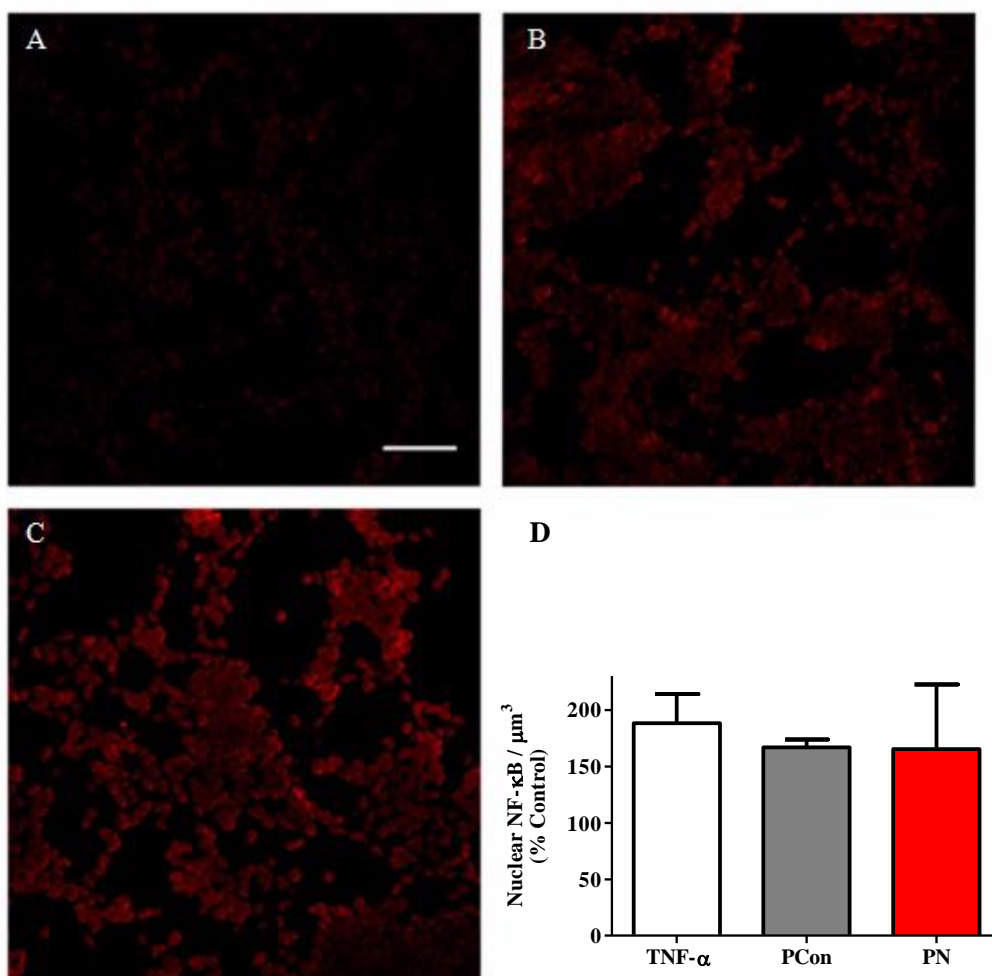


**Figure 4.7: Effect of peptoid PN on Aβ<sub>1-42</sub> oligomer induced activation of NF-κB:** SH-SY5Y human neuroblastoma cells were incubated for 15 min alone (untreated, A) or in the presence of 2 μM Aβ<sub>1-42</sub> oligomers formed in the absence (PCon, B) or presence (PN, C) of 100 μM PN. Treatment with TNF-α served as a positive control for NF-κB activation. Cells were fixed, stained, and visualized by confocal microscopy as detailed in Section 2.15. Medial section images depict nuclear NF-κB-p65 staining only, extracted via MATLAB analysis, and are representative of three independent experiments. Scale bar = 50 μm. D) Nuclear NF-κB / μm<sup>3</sup> determined by MATLAB analysis, as described in Section 2.16, and expressed as a percentage of untreated cells. Error bars represent SEM, n=3.

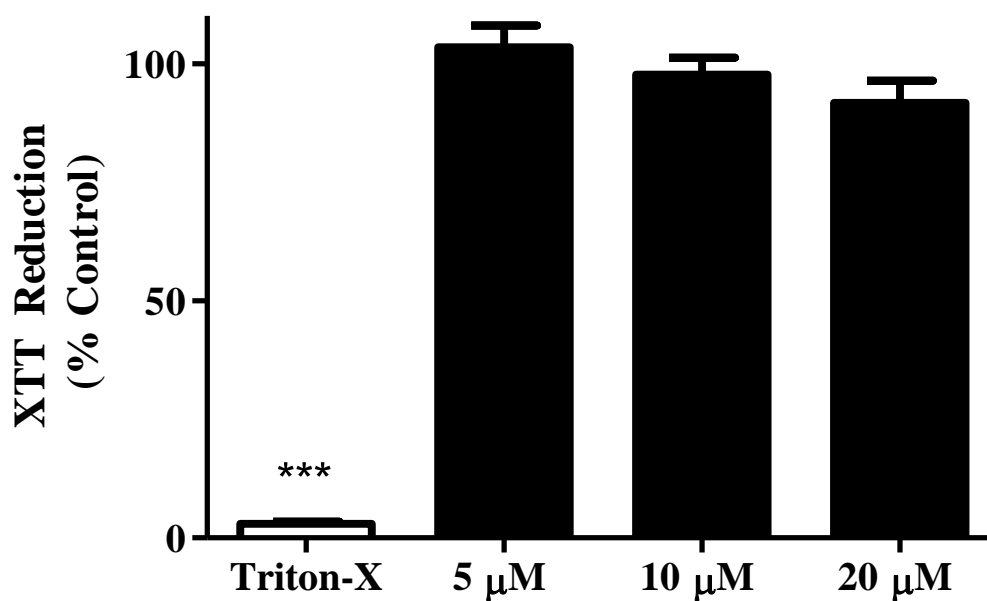


**Figure 4.8: Neurotoxicity of peptoid PN:** SH-SY5Y human neuroblastoma cells were incubated for 24 h alone (control) or in the presence of 5-20  $\mu\text{M}$  PN (closed bars). Treatment with Triton-X served as a positive control (open bar). Cellular metabolic activity was assessed using XTT reduction. Results are expressed as a percentage of the control and represent the mean of 3-4 independent experiments, each performed with 6 replicates. Error bars represent SEM. \*\*\* $p < 0.001$  as compared to control.

#### 4.4. Discussion

As there is currently no effective treatment to cure or reverse AD, there is increasing urgency to identify a therapy. One pathological characteristic of the disease, A $\beta$  aggregation, has been targeted heavily, with hopes of developing a compound to disrupt the aggregation process. Peptoids, which are poly-*N*-substituted glycines, have strong potential as a therapeutic agent. Peptoids are resistant to proteolysis, giving them an advantage over their peptide counterparts (49). While peptides homologous to the KLVFF hydrophobic core of A $\beta$  have shown promising results at abrogating A $\beta$  aggregation (97-100), their ineffectiveness *in vivo*, which results from their proteolytic degradation, renders their peptoid counterpart an excellent potential therapeutic candidate. In this study, we examined a peptoid homologous to KLVFF for its ability to alter different stages of A $\beta$  aggregation as well as associated NF- $\kappa$ B activation, which has been suggested to play an important role in inflammation.

In patients with AD, *in vivo* analysis has demonstrated that both A $\beta$ <sub>1-40</sub> and A $\beta$ <sub>1-42</sub> aggregates are present within neuronal plaques (115). While A $\beta$ <sub>1-40</sub> is the more abundant isoform, aggregates of A $\beta$ <sub>1-42</sub> form quicker and have a higher neurotoxicity (116-119). Soluble A $\beta$  oligomers have been implicated as the most neurotoxic A $\beta$  species (13), thus inhibition of the formation of oligomers could lead to reduced toxicological effects. Here, peptoid PN, mimicking the hydrophobic core of A $\beta$ , was evaluated for its ability to disrupt the formation of A $\beta$ <sub>1-42</sub> oligomers. PN reduced the size and quantity of oligomers larger than 20 kDa formed (Figure 4.3). However, PN was ineffective at eliciting changes in the formation of oligomers smaller than 20 kDa (Figure 4.4), indicating that it interacts with the protein after the initial formation of small oligomers. PN was also

evaluated for its ability to modulate A $\beta$ <sub>1-40</sub> monomer aggregation. However, it only modestly reduced the formation of fibrillar aggregates (Figure 4.2). Several studies have examined the ability of modified peptides to interfere with A $\beta$  aggregation. Findeis et al. demonstrated the ability of Cholyl-LVFFA-OH to inhibit the fibrillogenesis of A $\beta$ <sub>1-40</sub> (120). Austen et al. also demonstrated the ability of peptides to interfere with the oligomerization of A $\beta$ <sub>1-42</sub> and the aggregation of A $\beta$ <sub>1-40</sub> with the inclusion of the peptide RGKLVFFGR-NH<sub>2</sub> (121). Gordon et al. also provided evidence that N-methylated peptides analogous to the hydrophobic core of A $\beta$  can both disrupt the formation of fibrils and dissociate pre-formed fibrils (122). These results corroborate that peptide or peptoid inhibitors designed after the hydrophobic core of A $\beta$  are effective at disrupting A $\beta$  aggregation.

To gain further insight into the ability of PN to alter oligomer structure, we employed ANS spectroscopy to compare the exposure of hydrophobic residues within A $\beta$ <sub>1-42</sub> oligomers formed in the absence or presence of PN. Oligomers formed in the presence of PN exhibited enhanced ANS fluorescence, indicating an increase in solvent exposed hydrophobic regions (Figure 4.5). Changes in surface hydrophobicity of proteins can have negative effects on cells. Using two types oligomers formed from the N-terminal domain of the Escherichia coli HypF, differing in hydrophobicity, Campioni et al. discovered that oligomers with increased surface hydrophobicity disrupted SH-SY5Y cell membranes, causing an influx of Ca<sup>2+</sup>, which lead to cell death (123). Furthermore, Goransson et al. demonstrated that A $\beta$  aggregate species with increased surface hydrophobicity were responsible for cell death in cultured neuronal cells (124).

To evaluate the cellular effects of PN, oligomers formed in its presence were examined for their ability to activate NF- $\kappa$ B, which is known to play a key role in AD-associated inflammatory responses. SH-SY5Y human neuroblastoma cells exposed to A $\beta$ <sub>1-42</sub> oligomers formed in the presence of PN exhibited an increase in NF- $\kappa$ B activation similar to oligomers formed alone (Figure 4.7). Furthermore, NF- $\kappa$ B activation was not occurring due to inherent toxicity from PN, as SH-SY5Y cells treated with PN (5-20  $\mu$ M) exhibited no decrease in metabolic activity (Figure 4.8). The effects of peptoids on cultured neurons have also been observed by Chen et al. Using medium spiny neurons, <5% toxicity was induced by poly-Q binding peptoids being evaluated for their ability to inhibit Huntingtin protein in Huntington's disease (125). These results indicate that PN induced changes in oligomer size and conformation do not decrease the ability of oligomers to activate NF- $\kappa$ B.

Together, these results demonstrate that peptoid PN can alter the aggregation of A $\beta$  but not the physiological activity of aggregates formed. While PN does not significantly decrease the formation of fibrillar A $\beta$ <sub>1-40</sub> aggregates, it does lead to the assembly of fewer and smaller A $\beta$ <sub>1-42</sub> oligomers. PN was also demonstrated to alter the structure of A $\beta$ <sub>1-42</sub> oligomers by increasing the amount of solvent exposed hydrophobic residues. Finally, while PN was shown to be non-toxic to SH-SY5Y cells, oligomers formed in the presence of PN caused activation of NF- $\kappa$ B, suggesting that alterations in oligomer size and hydrophobicity by PN do not attenuate cellular responses.

## CHAPTER 5

### MODULATION OF A $\beta$ AGGREGATION BY PEPTOIDS IS EFFECTED BY CHARGED RESIDUES WITHIN THE PEPTOID SEQUENCE

#### 5.1. Introduction

Electrostatic interactions are believed to play a role in the aggregation propensity of A $\beta$  (126). Disrupting these interactions can serve as a therapeutic strategy in the rational design of A $\beta$  aggregation inhibitors. Charged small molecules have the ability to disrupt aggregate formation. Anionic sulfonate compounds (127) and Congo red (128-130) both disrupt A $\beta$  aggregation *in vitro*. Cationic surfactants, such as hexadecyl-N-methylpiperidinium bromide, also inhibit A $\beta$  fibril formation, possibly by interacting with charged A $\beta$  binding sites necessary for aggregation (131).

In Chapter 4, we demonstrated the ability of a novel peptoid to interfere with the aggregation of A $\beta_{1-40}$  and A $\beta_{1-42}$ . To enhance the effectiveness of peptoids as inhibitors of A $\beta$  aggregation, we examined the effects of modifying charged groups within the peptoid sequence. We hypothesize that the addition of charges within the peptoid sequence will increase inhibitory capabilities toward aggregation.

## **5.2. Methods & Materials**

### **5.2.1. Peptoid Synthesis**

Peptoids P<sup>+</sup> and P<sup>-</sup> were synthesized in the laboratory of Dr. Shannon Servoss (Department of Chemical Engineering, University of Arkansas) as described in Section 4.2.1. P<sup>+</sup> and P<sup>-</sup> were designed to have the same structure as PN with the neutral spacer between the two pairs of phenylalanine residues replaced by a positively charged lysine residue (P<sup>+</sup>, Figure 5.1A) or a negatively charged glutamic acid residue (P<sup>-</sup>, Figure 5.1B).

### **5.2.2. A $\beta$ <sub>1-40</sub> Monomer Aggregation**

Monomer aggregations were carried out as described in Section 2.4 with the inclusion of 100  $\mu$ M P<sup>+</sup> or P<sup>-</sup>. Aggregation was assessed via dot blot analysis as described in Section 2.6.

### **5.2.3. A $\beta$ <sub>1-42</sub> Oligomerization**

A $\beta$ <sub>1-42</sub> oligomerization was conducted as described in Section 2.10 with the inclusion of 2  $\mu$ M-100  $\mu$ M P<sup>+</sup> or P<sup>-</sup>. After 30 min incubation, oligomers were resolved via SDS-PAGE and Western blotting following procedures in Section 2.10.

### **5.2.4. Determination of A $\beta$ <sub>1-42</sub> Oligomer Structure by ANS Fluorescence**

A $\beta$ <sub>1-42</sub> oligomerization was conducted as described in Section 2.10 with the inclusion of 100  $\mu$ M P<sup>+</sup> or P<sup>-</sup>. Alterations in oligomer structure, by changes in solvent exposed hydrophobic regions, were assessed using ANS fluorescence following procedures in Section 2.12.

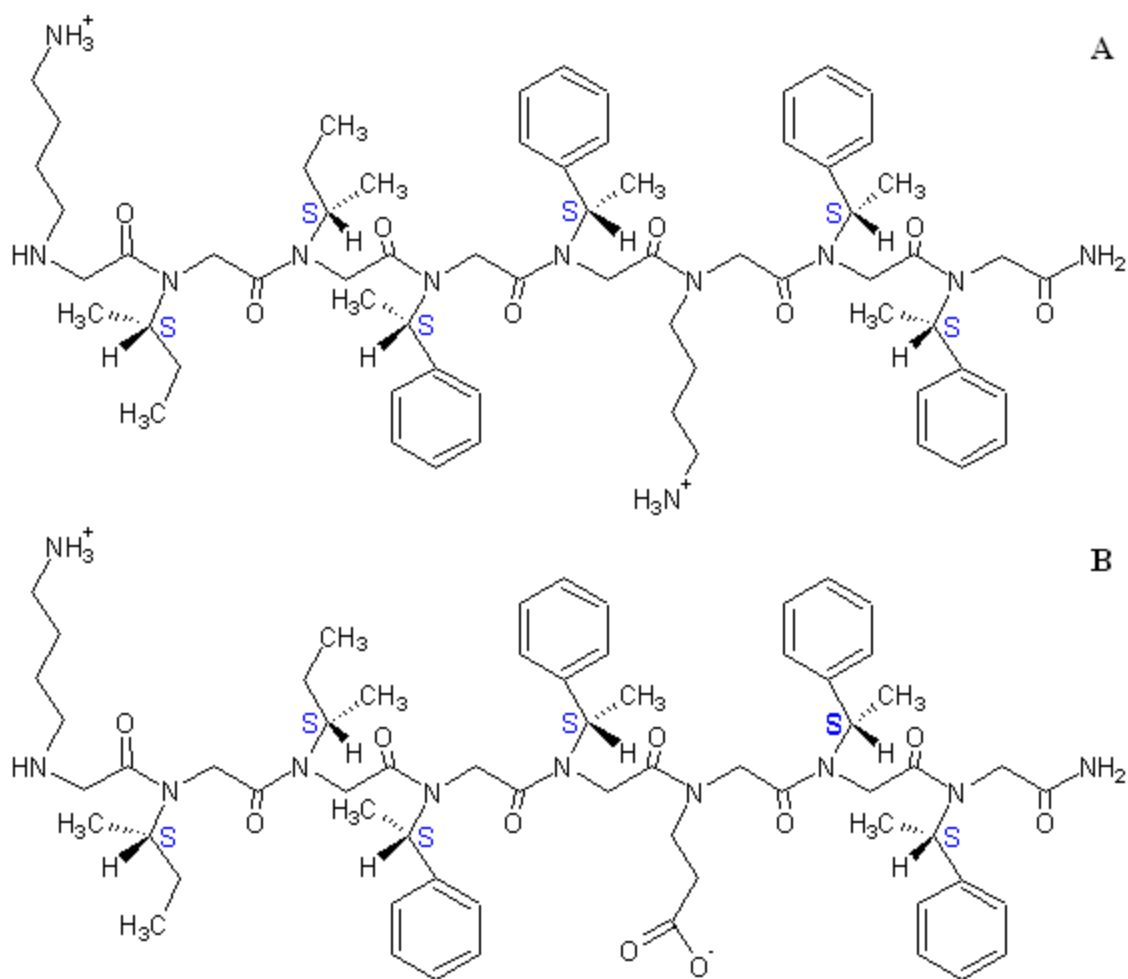


**Figure 5.1: Structure of peptoids P<sup>+</sup> and P<sup>-</sup>:** Peptoids P<sup>+</sup> and P<sup>-</sup> were synthesized analogous to KLVFF, the hydrophobic core of A $\beta$ . The first five residues of each peptoid mimic KLVFF, while the C-terminal three residues incorporate a positively charged lysine (A, P<sup>+</sup>) or a negatively charged glutamic acid (B, P<sup>-</sup>) followed by two additional aromatic phenylalanines.

### **5.2.5. XTT Reduction Assay**

SH-SY5Y human neuroblastoma cells (Section 2.13) were treated with P+ or P- at 20  $\mu$ M, 10  $\mu$ M, and 5 $\mu$ M. Cellular viability following peptoid exposure was monitored via XTT reduction as described in Section 2.14.

### **5.2.6. A $\beta$ <sub>1-42</sub> Oligomer Activation of NF- $\kappa$ B**

A $\beta$ <sub>1-42</sub> oligomerization was conducted as described in Section 2.10 with the inclusion of 100  $\mu$ M P+ or P-. After 30 min, SH-SY5Y cells (Section 2.13) were incubated in the presence of end products of oligomerization reactions at an oligomer concentration of 2  $\mu$ M. Media only served as a negative control, while cells treated with 10 Units/well TNF- $\alpha$  served as a positive control. Following 15 min incubation, cells were prepared and imaged via confocal microscopy as described in Section 2.15. Image analysis was conducted as described in Section 2.16.

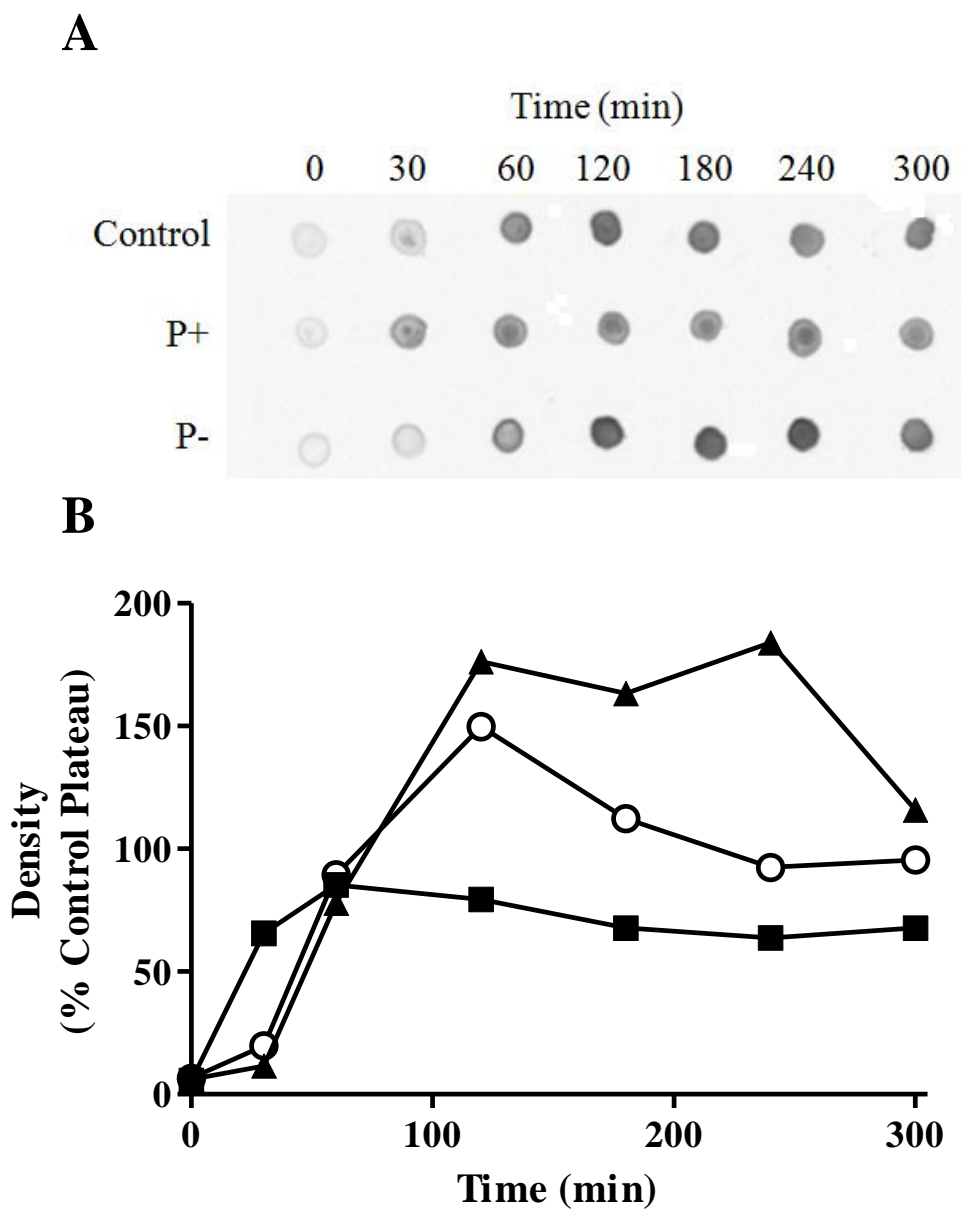
### 5.3. Results

#### 5.3.1. Peptoid P+, but not Peptoid P-, Inhibits the Fibrilization of A $\beta$ <sub>1-40</sub>

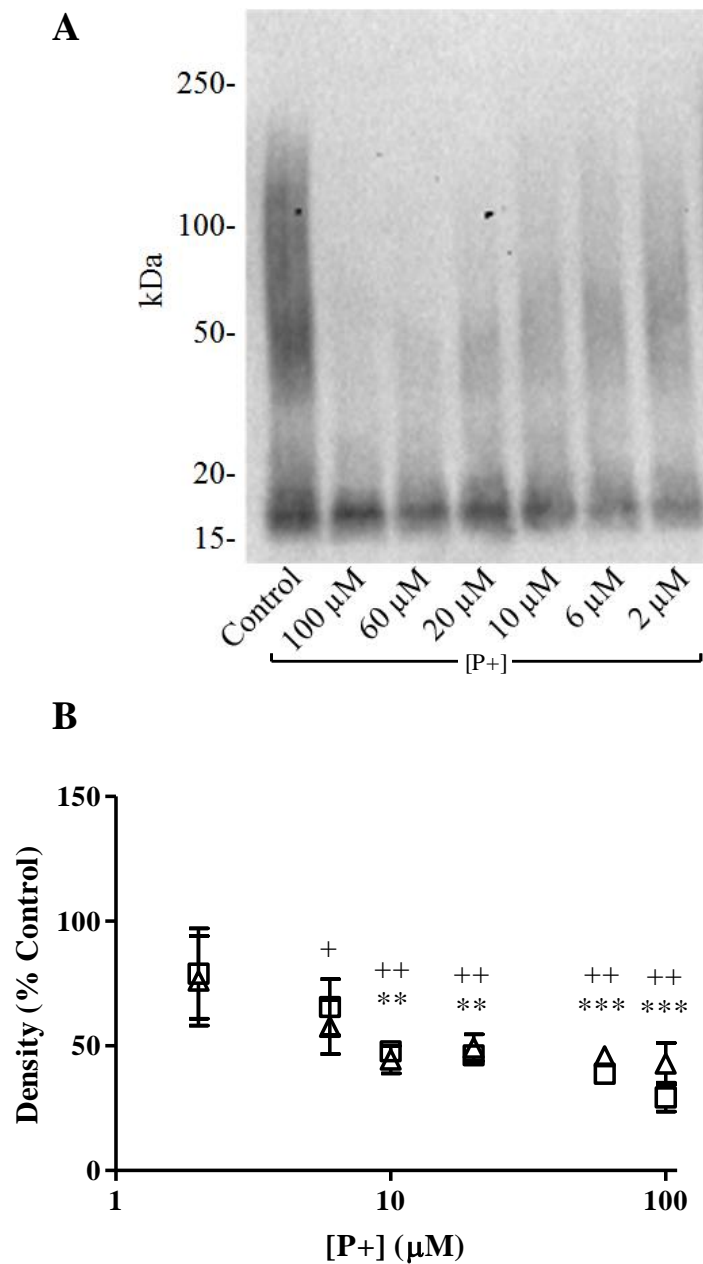
Aggregation of monomeric A $\beta$ <sub>1-40</sub> was employed to initially investigate the inhibitory capabilities of P+ and P-. Aggregation of 20  $\mu$ M A $\beta$ <sub>1-40</sub> monomer was induced via continuous agitation and 150 mM NaCl in the presence of 100  $\mu$ M P+ or P-. Periodically, samples were dotted onto nitrocellulose membrane and probed with LOC (Figure 5.2A). Addition of P+ resulted in a  $57.4 \pm 23.6\%$  reduction of the equilibrium fluorescence plateau as compared to the control (Figure 5.2B). In contrast, P- promoted the formation of fibrillar aggregates (Figure 5.2B). These results suggest that inclusion of a negative charge within the peptoid sequence removes the modest inhibitory capabilities associated with homologous peptoid PN (Figure 4.2), while inclusion of an additional positive charge imparts superior inhibition.

#### 5.3.2. Peptoids P+ and P- Both Alter the Size and Quantity of A $\beta$ <sub>1-42</sub> Oligomers

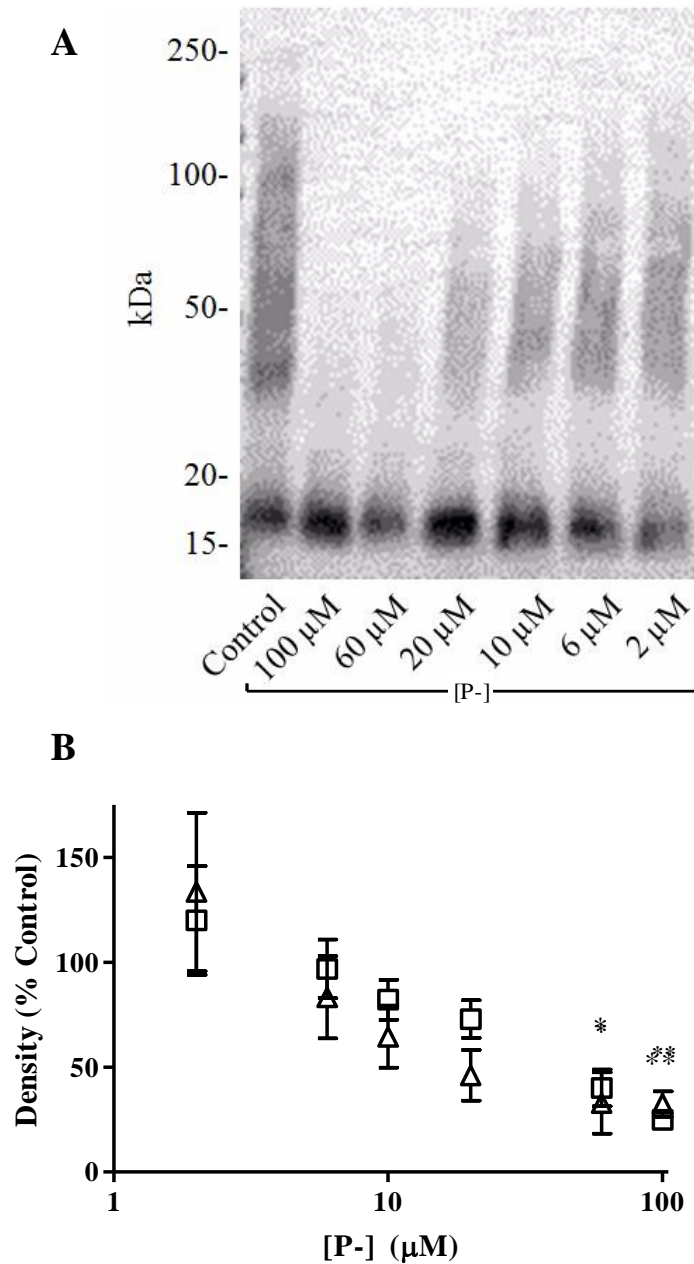
A $\beta$ <sub>1-42</sub> oligomerization was employed to examine P+ and P- for their ability to modify early stages of aggregation. When freshly solubilized A $\beta$ <sub>1-42</sub> was subjected to oligomerization conditions, an even distribution of oligomers appeared between 20 kDa-100 kDa and 100 kDa-250 kDa. A $\beta$ <sub>1-42</sub> oligomers, formed in the presence of P+ and P-, were fewer and smaller in size as compared to the control (Figures 5.3A, 5.4A). Dose dependence was observed when P+ and P- concentrations were reduced from 100  $\mu$ M to 2  $\mu$ M (Figures 5.3B and 5.4B). Furthermore, this dose dependence revealed that P- was less effective than P+ at reducing oligomer quantity. To elucidate any changes induced



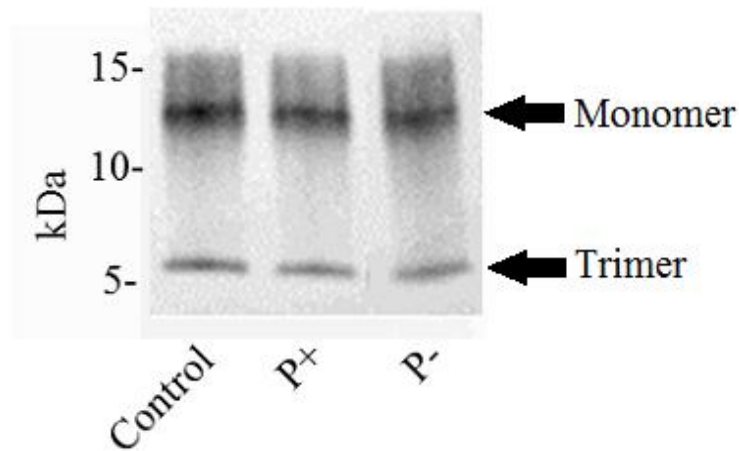
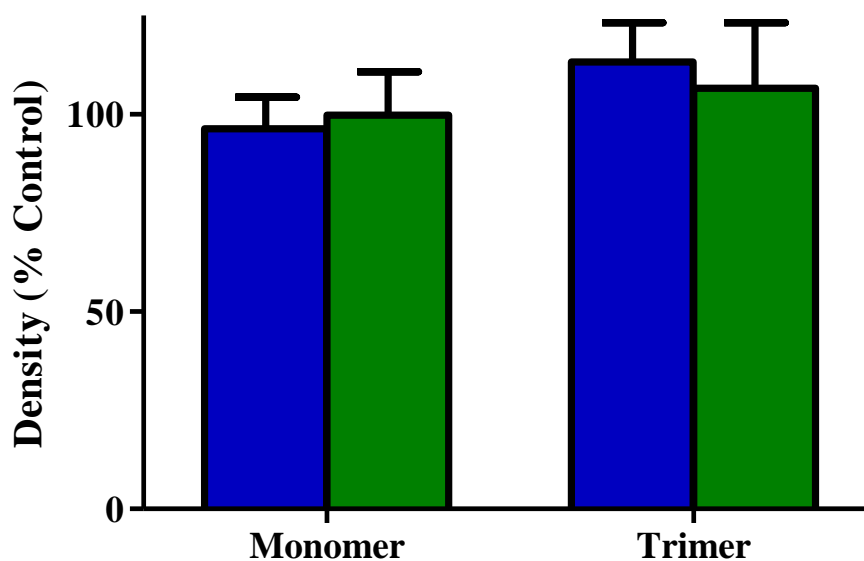
**Figure 5.2: Effect of peptoids P+ and P- on A $\beta_{1-40}$  monomer aggregation:** A $\beta_{1-40}$  monomer diluted to 20  $\mu$ M in 40 mM Tris-HCl (pH 8.0) was incubated alone (control,  $\circ$ ) or in the presence of 100  $\mu$ M P+ ( $\blacksquare$ ) or P- ( $\blacktriangle$ ). Monomer aggregation was induced under continuous agitation with 150 mM NaCl and monitored via immunocytochemistry by periodic dotting onto nitrocellulose membrane (A). Membranes were developed and densitometric analysis was performed as described in Section 2.6 (B). Results are expressed as a percentage of the control and are representative of two independent experiments.



**Figure 5.3: Effect of peptoid P+ on A $\beta$ <sub>1-42</sub> oligomerization:** A $\beta$ <sub>1-42</sub> oligomers were prepared in the absence (control) or presence of P+. A) Oligomerization products resolved by SDS-PAGE using a 4-20% Tris-glycine gel were transferred to nitrocellulose and probed with 6E10. Image is representative of three independent experiments. B) Densitometric analysis of oligomer species within the size ranges of 20 kDa - 100 kDa ( $\square$ ) and 100 kDa -250 kDa ( $\Delta$ ), reported as a percentage of the control. Error bars indicate SEM, n=3. For 20 kDa-100 kDa \*\* p<0.01, \*\*\* p<0.001; for 100 kDa-250 kDa + p<0.05, ++ p<0.01 as compared to the control.



**Figure 5.4: Effect of peptoid P- on A $\beta$ <sub>1-42</sub> oligomerization:** A $\beta$ <sub>1-42</sub> oligomers were prepared, as described in Section 2.10, in the absence (control) or presence of P-. A) Oligomerization products resolved by SDS-PAGE using a 4-20% Tris-glycine gel were transferred to nitrocellulose and probed with 6E10. Image is representative of three independent experiments. B) Densitometric analysis of oligomer species within the size ranges of 20 kDa-100 kDa (□) and 100 kDa-250 kDa (Δ), reported as a percentage of the control. Error bars indicate SEM, n=3. For 20 kDa-100 kDa \* p<0.05, \*\* p<0.01 as compared to the control.

**A****B**

**Figure 5.5: Effect of peptoids P+ and P- on the formation of Aβ<sub>1-42</sub> dimers and trimers:** Aβ<sub>1-42</sub> oligomers were prepared in the absence (control) or presence of P+ (blue) or P- (green). A) Oligomerization products resolved by SDS-PAGE using a 16.5% Tris-tricine gel were transferred to nitrocellulose and probed with 6E10. Results are representative of three independent experiments. B) Densitometric analysis of monomer (0 kDa-5 kDa), and trimer (10 kDa-15 kDa). Error bars indicate SEM, n=3.

by P+ and P- in the quantity of monomers as well as the smallest oligomers, aggregate species smaller than 20 kDa were resolved. A light band at ~4 kDa indicates the presence of a small quantity of unreacted monomer, while a dark band at ~12 kDa indicates the pronounced presence of trimers (Figure 5.5A). Interestingly, the formation of dimers at ~8 kDa is not evidenced. Unlike higher order oligomers, however, no change is observed in the quantity of monomers, dimers, or trimers formed in the presence of P+ or P- (Figure 5.5B).

### **5.3.3. Peptoid P+ but not Peptoid P- Modulates A $\beta$ <sub>1-42</sub> Oligomer Structure**

ANS fluorescence was employed to characterize changes in oligomer structure due to the presence of peptoids P+ or P-. Oligomers formed in the absence of peptoid exhibit low amounts of solvent exposed hydrophobic residues, as evidenced by low ANS fluorescence (Figure 5.6A). However, ANS fluorescence of oligomers formed in the presence of P+ was significantly increased indicating an altered structure with more exposed hydrophobic residues (Figure 5.6A, B). In contrast, P- had no significant effect on oligomer structure, with ANS fluorescence levels comparable to the control (Figure 5.6A, C).

### **5.3.4. A $\beta$ <sub>1-42</sub> Oligomers Formed in the Presence of Peptoids P+ and P- Activate NF- $\kappa$ B**

To determine whether peptoid-induced changes in the size and structure of A $\beta$ <sub>1-42</sub> oligomers can alter A $\beta$ -induced NF- $\kappa$ B activation, SH-SY5Y human neuroblastoma cells were treated for 15 min with A $\beta$ <sub>1-42</sub> oligomers formed in the absence or presence of

100  $\mu\text{M}$  P<sup>+</sup> or P<sup>-</sup>. Compared to untreated cells (Figure 5.7A), SH-SY5Y cells exposed to A $\beta_{1-42}$  oligomers exhibited increased translocation of NF- $\kappa\text{B}$  into the nucleus (Figure 5.7B). Similar levels of NF- $\kappa\text{B}$  translocation were observed with A $\beta_{1-42}$  oligomers formed in the presence of P<sup>-</sup> (Figure 5.7D), while SH-SY5Y cells treated with oligomers formed in the presence of P<sup>+</sup> demonstrated a small but insignificant increase in NF- $\kappa\text{B}$  activation as compared to the control (Figure 5.7C, E).

To ensure that inherent toxicity of P<sup>+</sup> and P<sup>-</sup>, does not account for NF- $\kappa\text{B}$  activation, SH-SY5Y cells were treated for 24 h with P<sup>+</sup> and P<sup>-</sup> at concentrations ranging from 5-20  $\mu\text{M}$ , where 10  $\mu\text{M}$  represents the concentration equivalent used for cell treatments to activate NF- $\kappa\text{B}$  (Figure 5.8). For all concentrations of P<sup>+</sup> and P<sup>-</sup> tested, metabolic activity, measured via XTT reduction, was >90%, indicating no significant toxicity. Together, these results demonstrate that size and structural differences in A $\beta_{1-42}$  oligomers induced by P<sup>+</sup> and P<sup>-</sup> do not significantly alter A $\beta$ -induced NF- $\kappa\text{B}$  activation.

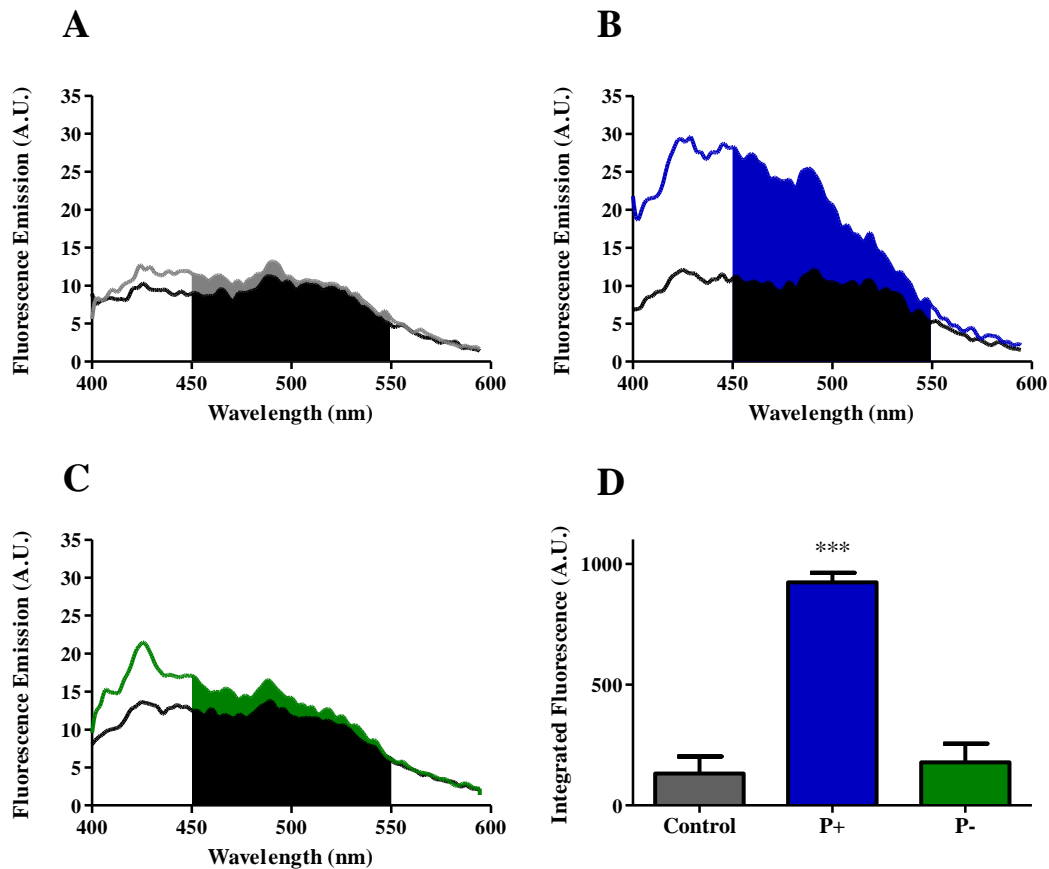


**Figure 5.6: Peptoid P+, but not peptoid P-, alters A $\beta$ <sub>1-42</sub> oligomer structure to expose hydrophobic regions:** A $\beta$ <sub>1-42</sub> oligomers were prepared, as described in Section 2.10, in the absence (control, grey) or presence of 100  $\mu$ M P+ (blue) or P- (green). Oligomers were incubated with 100  $\mu$ M ANS and fluorescence was quantified with background subtraction (black). Representative spectra of native oligomers (A) and oligomers formed in the presence of P+ (B) or P- (C). D) Integrated fluorescence from 450 to 550 nm. Error bars indicate SEM, n = 3. \*\*\*p<0.001 as compared to the control.

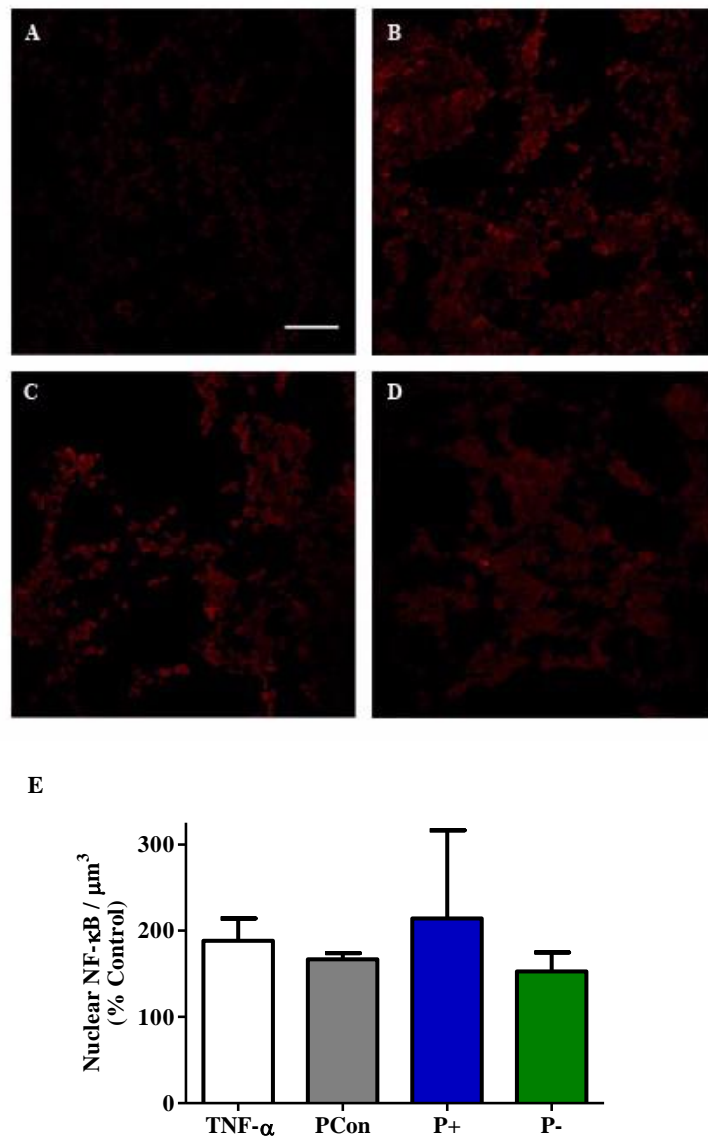


**Figure 5.7: Effect of peptoids P+ and P- on Aβ oligomer-induced activation of NF-κB:** SH-SY5Y human neuroblastoma cells were incubated for 15 min alone (untreated, A) or in the presence of 2 μM Aβ<sub>1-42</sub> oligomers formed in the absence (PCon, B) or presence of 100 μM P+ (P+, C) or 100 μM P- (P-, D). Treatment with TNF-α served as a positive control for NF-κB activation. Cells were fixed, stained, and visualized by confocal microscopy as described in Section 2.15. Medial section images depict nuclear NF-κB-p65 staining only, extracted via MATLAB analysis, and are representative of 2-3 independent experiments, each performed with 2-3 replicates. Scale bar=50 μm. E) Nuclear NF-κB / μm<sup>3</sup> determined by MATLAB analysis as described in Section 2.16, and expressed as a percentage of untreated cells. Error bars represent SEM, n=3.

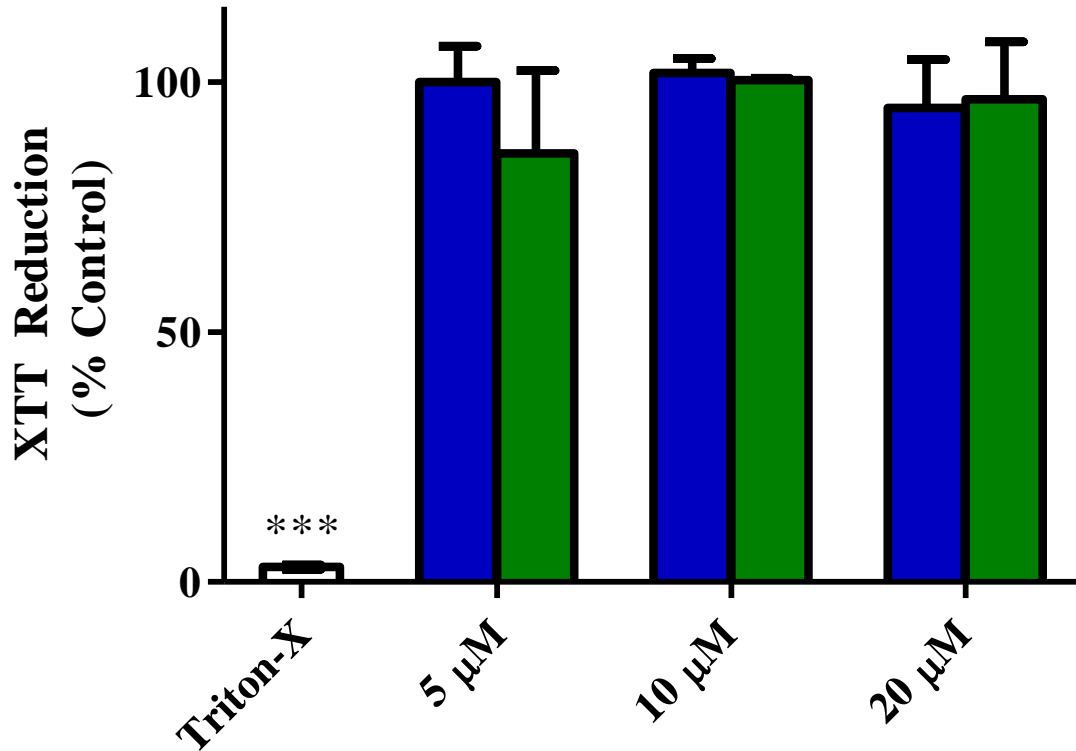


**Figure 5.8: Neurotoxicity of peptoids P+ and P-:** SH-SY5Y human neuroblastoma cells were incubated for 24 h alone (control) or in the presence of 5-20 μM P+ (blue) or P- (green). Treatment with Triton-X served as a positive control (open bar). Cellular metabolic activity was assessed using XTT reduction. Results are expressed as a percentage of the control and represent the mean of 3-4 independent experiments, each performed with 6 replicates. Error bars represent SEM. \*\*\*p<0.001 as compared to the control.

#### 5.4. Discussion

Previous studies have shown that small molecules incorporating charges can inhibit A $\beta$  aggregation through electrostatic disruptions of protein folding (126-131). Therefore, introducing additional charged residues into the structure of the peptoid PN, examined in Chapter 4, may increase inhibitory effects. In this study, we examined the effects of introducing charged residues within a peptoid homologous to KLVFF on the ability to alter different stages of A $\beta$  aggregation as well as associated NF- $\kappa$ B activation.

Inhibition of A $\beta_{1-40}$  aggregation by two peptoids incorporating charged residues was first evaluated. The peptoid incorporating an additional positive charge, P+, reduced the formation of fibrillar aggregates by  $57.4 \pm 23.6\%$ , while the peptoid incorporating an additional negative charge, P-, had no effect on aggregation (Figure 5.2). These results are in agreement with reports that charge modified KLVFF peptides can interfere with A $\beta_{1-40}$  aggregation. Bett et al. examined the abilities of various KLVFF peptides with N- and C- terminus charge additions to inhibit A $\beta_{1-40}$  aggregation (132). The addition of positively charged arginine to the C-terminus of KLVFF significantly reduced A $\beta_{1-40}$  aggregation by 80%. However, when arginine was moved to the N-terminus or contained on both termini, its effectiveness against aggregation decreased. In contrast, Lowe et al. reported that KLVFF-E<sub>4</sub>, containing negatively charged glutamic acid, promoted fibrillar aggregate growth similar to the slight promotion of aggregate formation by P- observed in the current study (98). Thus, our results corroborate prior findings that peptide mimics containing a positive charge are superior inhibitors of A $\beta_{1-40}$  aggregation, and extend these findings to include peptoid inhibitors.

To further examine the effects of charged peptoids on the A $\beta$  aggregation pathway, oligomerization of A $\beta_{1-42}$  was employed to evaluate the ability of P<sup>+</sup> and P<sup>-</sup> to interfere within early stages of aggregation. Both P<sup>+</sup> and P<sup>-</sup> were able to reduce the size and quantity of oligomers larger than 20 kDa (Figure 5.3, 5.4). In contrast, both P<sup>+</sup> and P<sup>-</sup> were ineffective at eliciting changes in the formation of oligomers smaller than 20 kDa (Figure 5.5), suggesting that these peptoids interact not with monomer, but with lower order oligomer structures. To gain further insight into the ability of P<sup>+</sup> and P<sup>-</sup> to alter oligomer structure, ANS spectroscopy was employed to compare the exposure of hydrophobic residues within A $\beta_{1-42}$  oligomers formed in the absence or presence of P<sup>+</sup> or P<sup>-</sup>. P<sup>+</sup> significantly altered the structure of oligomers formed in its presence, while P<sup>-</sup> had little effect (Figure 5.6).

To evaluate the physiological implications of peptoid modulation of A $\beta$ -induced oligomerization, A $\beta_{1-42}$  oligomers formed in the presence of P<sup>+</sup> and P<sup>-</sup> were evaluated for their ability to activate NF- $\kappa$ B. P<sup>+</sup>, but not P<sup>-</sup>, slightly but insignificantly increased oligomer activation of NF- $\kappa$ B (Figure 5.7). Like PN, P<sup>+</sup> and P<sup>-</sup> failed to alter XTT reduction in SH-SY5Y human neuroblastoma cells (Figure 5.8) demonstrating that NF- $\kappa$ B activation is not a result of peptoid toxicity. These results indicate that neither changes in oligomer size nor hydrophobicity due to the presence of charged peptoids have an effect on NF- $\kappa$ B activation.

These results demonstrate that a peptoid homologous to the hydrophobic core of A $\beta$  and incorporating an additional positive charge can alter the aggregation of A $\beta$ . This peptoid has the ability to decrease the formation of fibrillar A $\beta_{1-40}$  aggregates, as well as alter both the size and structure of A $\beta_{1-42}$  oligomers. In contrast, a similar peptoid

incorporating a negative charge reduces  $A\beta_{1-42}$  oligomer size and quantity, but is ineffective at abrogating  $A\beta_{1-40}$  aggregation or altering  $A\beta_{1-42}$  oligomer structure. Neither peptoid, however, was able to alter NF- $\kappa$ B activation by oligomeric  $A\beta_{1-42}$  aggregates. Overall, these results demonstrate that the role of charged residues in peptoid modulation of  $A\beta$  aggregation and further demonstrate that changes in oligomer size and structure are insufficient to alter  $A\beta$  aggregate physiological activity.

## CHAPTER 6

### CONCLUSIONS

Development of a treatment for AD is imperative as the number of AD diagnoses increases every year. Therapeutic intervention targeting A $\beta$  aggregation serves as one viable treatment course. In this work, we demonstrated the ability of gold nanoparticles and peptoids to act as novel inhibitors of A $\beta$  aggregation.

Within Chapter 3, we examined the ability of gold NPs with varying surface chemistries and diameters to abrogate A $\beta$  aggregation. Inhibitory capabilities exhibited a dependence on surface chemistry, including surface charge. NPs coated with the anionic polymer PAA exhibited complete inhibition of aggregation at a substoichiometric ratio of NPs:A $\beta$  of 1:2,000,000. Ratios this low have never been evidenced for potential A $\beta$  inhibitors, rendering NPs as potentially effective therapeutic agents. While cationic NPs were less effective than their anionic counterparts at inhibition A $\beta$  aggregation, they did impart mechanistic specific changes in fibril morphology. NP diameter was also evidenced to play a role in the inhibitory capabilities of NPs. As the diameter of PAA-coated NPs increased, inhibitory capabilities decreased, suggesting that smaller NPs are better suited as A $\beta$  aggregation inhibitors. With the near limitless library of NPs that can be synthesized, it is important to determine specific characteristics of NPs that enhance their ability to inhibit A $\beta$  aggregation. The results presented in this study demonstrate that surface chemistry, charge, and diameter are important characteristics to consider when designing effective NP inhibitors of A $\beta$  aggregation.

In Chapters 4 and 5, we examined the ability of peptoids to inhibit the aggregation of A $\beta$ . First, we demonstrated the ability of a peptoid homologous to the hydrophobic core of A $\beta$ , and incorporating additional aromatic phenylalanine residues, to decrease the size and quantity of A $\beta$ <sub>1-42</sub> oligomers while also altering their conformation by exposing hydrophobic residues. However, these changes in oligomer structure had no effect on diminishing A $\beta$ <sub>1-42</sub> oligomer-induced NF- $\kappa$ B activation. To further characterize properties that enhance peptoid ability to inhibit aggregation, additional positive or negative charges were incorporated within the peptoid sequence. Inclusion of a positive charge between two pairs of phenylalanine residues increased inhibitory capabilities and induced changes in oligomer conformation, while the inclusion of a negative charge at the same location reduced inhibitory effectiveness and failed to alter oligomer structure. However, these peptoids with differing effects on oligomer structure both had no effect on attenuating A $\beta$ <sub>1-42</sub> oligomer-induced NF- $\kappa$ B activation. Thus, the charge addition associated with an effective peptoid inhibitor is in contrast to that of an effective NP inhibitor, where an anionic surface charge proved to be most advantageous. This contrast suggests that NPs and peptoids disrupt A $\beta$  aggregation by different mechanisms. Overall, this study demonstrates the effectiveness of two novel inhibitors of A $\beta$  aggregation and their potential as therapeutic treatments.

## CHAPTER 7

### FUTURE WORK

The rational design of a treatment for AD must incorporate the best attributes of different potential therapeutics. PAA-coated NPs showed superior inhibitory capabilities, however their surface coating is only electrostatically contained onto the particle surface. Unfortunately, this may lead to dissociation of the particle surface coating when introduced into the body. The inherent properties of gold allow molecules to be covalently functionalized onto the particle surface through Au-S interactions. Therefore, covalent attachment of PAA onto the nanoparticle surface may increase therapeutic stability when introduced into the body.

This same functionalization also imparts NPs with the ability to covalently attach different molecules at the surface. Aggregation inhibitors, such as peptoids, can be functionalized onto a NP surface to give them access across the BBB. Also, as seen with PAA, surface functionalization of molecules onto NP surfaces can increase inhibitory capabilities by creating a high local surface concentration. Therefore, the therapeutic abilities of peptoids might be enhanced by functionalizing them onto gold NPs. Conjugation chemistry allows for the ability to control the orientation of the peptoid on the NP surface, determining orientation specific inhibitory capabilities. Also, inclusion of a PEG spacer can allow for changes in peptoid flexibility based on its distance from the NP surface. Altogether, these future design possibilities could lead to the

development of gold NP-peptoid complexes that serve as superior therapeutic agents for the treatment of AD.

## REFERENCES

1. Alzheimers A. 2012. 2012 Alzheimer's disease facts and figures. *Alzheimers & Dementia* 8:131-68
2. Selkoe DJ. 1997. Alzheimer's disease: genotypes, phenotype, and treatments. *Science* 275:630-1
3. Dahm R. 2010. Finding Alzheimer's disease. *American Scientist* 98:148-55
4. Selkoe DJ. 1996. Amyloid beta-protein and the genetics of Alzheimer's disease. *Journal of Biological Chemistry* 271:18295-8
5. Goedert M, Spillantini MG. 2006. A century of Alzheimer's disease. *Science* 314:777-81
6. Hardy JA, Higgins GA. 1992. Alzheimer's disease: the amyloid cascade hypothesis. *Science* 256:184-5
7. Glenner GG, Wong CW. 1984. Alzheimer's disease: initial report of the purification and characterization of a novel cerebrovascular amyloid protein. *Biochemical and Biophysical Research Communications* 120:885-90
8. Selkoe DJ. 1991. The molecular pathology of Alzheimer's disease. *Neuron* 6:487-98
9. Gandy S. 2005. The role of cerebral amyloid beta accumulation in common forms of Alzheimer disease. *Journal of Clinical Investigation* 115:1121-9
10. Koo EH. 2002. The beta-amyloid precursor protein (APP) and Alzheimer's disease: Does the tail wag the dog? *Traffic* 3:763-70

11. Dumery L, Bourdel F, Soussan Y, Fialkowsky A, Viale S, et al. 2001. Beta amyloid protein aggregation: its implication in the physiopathology of Alzheimer's disease. *Pathologie Biologie* 49:72-85
12. Scheuner D, Eckman C, Jensen M, Song X, Citron M, et al. 1996. Secreted amyloid beta-protein similar to that in the senile plaques of Alzheimer's disease is increased in vivo by the presenilin 1 and 2 and APP mutations linked to familial Alzheimer's disease. *Nature Medicine* 2:864-70
13. Haass C, Selkoe DJ. 2007. Soluble protein oligomers in neurodegeneration: lessons from the Alzheimer's amyloid beta-peptide. *Nature Reviews Molecular Cell Biology* 8:101-12
14. Cai HB, Wang YS, McCarthy D, Wen HJ, Borchelt DR, et al. 2001. BACE1 is the major beta-secretase for generation of A beta peptides by neurons. *Nature Neuroscience* 4:233-4
15. Nilsson MR. 2004. Techniques to study amyloid fibril formation in vitro. *Methods* 34:151-60
16. Roychaudhuri R, Yang M, Hoshi MM, Teplow DB. 2009. Amyloid beta-protein assembly and Alzheimer disease. *Journal of Biological Chemistry* 284:4749-53
17. Nichols MR, Moss MA, Reed DK, Lin WL, Mukhopadhyay R, et al. 2002. Growth of beta-amyloid(1-40) protofibrils by monomer elongation and lateral association. Characterization of distinct products by light scattering and atomic force microscopy. *Biochemistry* 41:6115-27
18. Akiyama H, Barger S, Barnum S, Bradt B, Bauer J, et al. 2000. Inflammation and Alzheimer's disease. *Neurobiology of Aging* 21:383-421
19. Tuppo EE, Arias HR. 2005. The role of inflammation in Alzheimer's disease. *International Journal of Biochemistry & Cell Biology* 37:289-305
20. Baldwin AS. 1996. The NF-kappa B and I kappa B proteins: new discoveries and insights. *Annual Review of Immunology* 14:649-83

21. Barnes PJ, Larin M. 1997. Mechanisms of disease: nuclear factor-kappa b - A pivotal transcription factor in chronic inflammatory diseases. *New England Journal of Medicine* 336:1066-71
22. Li QT, Verma IM. 2002. NF-kappa B regulation in the immune system. *Nature Reviews Immunology* 2:725-34
23. Kaltschmidt B, Uherek M, Volk B, Baeuerle PA, Kaltschmidt C. 1997. Transcription factor NF-kappa B is activated in primary neurons by amyloid beta peptides and in neurons surrounding early plaques from patients with Alzheimer disease. *Proceedings of the National Academy of Sciences of the United States of America* 94:2642-7
24. Kuner P, Schubnel R, Hertel C. 1998. Beta-amyloid binds to p75(NTR) and activates NF kappa B in human neuroblastoma cells. *Journal of Neuroscience Research* 54:798-804
25. Wang X, Chen Q, Xing D. 2012. Focal adhesion kinase activates NF-kappa B via the ERK1/2 and p38MAPK pathways in amyloid-beta(25-35)-induced apoptosis in PC12 cells. *Journal of Alzheimers Disease* 32:77-94
26. Dodel RC, Du YS, Bales KR, Gao F, Paul SM. 1999. Sodium salicylate and 17 beta-estradiol attenuate nuclear transcription factor NF-kappa B translocation in cultured rat astroglial cultures following exposure to amyloid A beta(1-40) and lipopolysaccharides. *Journal of Neurochemistry* 73:1453-60
27. Lee SY, Ha TY, Son DJ, Kim SR, Hong JT. 2005. Effect of sesaminol glucosides on beta-amyloid-induced PC12 cell death through antioxidant mechanisms. *Neuroscience Research* 52:330-41
28. He Y, Zheng MM, Ma Y, Han XJ, Ma XQ, et al. 2012. Soluble oligomers and fibrillar species of amyloid beta-peptide differentially affect cognitive functions and hippocampal inflammatory response. *Biochemical and Biophysical Research Communications* 429:125-30
29. Gonzalez-Velasquez FJ, Reed JW, Fuseler JW, Matherly EE, Kotarek JA, et al. 2010. Soluble Amyloid-beta Protein Aggregates Induce Nuclear Factor-kappa B Mediated Upregulation of Adhesion Molecule Expression to Stimulate Brain Endothelium for Monocyte Adhesion. *Journal of Adhesion Science and Technology* 24:2105-26

30. Pimplikar SW. 2009. Reassessing the amyloid cascade hypothesis of Alzheimer's disease. *International Journal of Biochemistry & Cell Biology* 41:1261-8
31. Hardy J, Selkoe DJ. 2002. The amyloid hypothesis of Alzheimer's disease: progress and problems on the road to therapeutics. *Science* 297:353-6
32. Klein WL, Krafft GA, Finch CE. 2001. Targeting small A beta oligomers: the solution to an Alzheimer's disease conundrum? *Trends in Neurosciences* 24:219-24
33. Salata O. 2004. Applications of nanoparticles in biology and medicine. In *J Nanobiotechnology*, 2:3. Number of 3 pp.
34. Faraji AH, Wipf P. 2009. Nanoparticles in cellular drug delivery. *Bioorganic & Medicinal Chemistry* 17:2950-62
35. Haes AJ, Hall WP, Chang L, Klein WL, Van Duyne RP. 2004. A localized surface plasmon resonance biosensor: first steps toward an assay for Alzheimer's disease. *Nano Letters* 4:1029-34
36. Morales-Narvaez E, Monton H, Fomicheva A, Merkoci A. 2012. Signal enhancement in antibody microarrays using quantum dots nanocrystals: application to potential Alzheimer's disease biomarker screening. *Analytical Chemistry* 84:6821-7
37. Teixido M, Giralt E. 2008. The role of peptides in blood-brain barrier nanotechnology. *Journal of Peptide Science* 14:163-73
38. Lockman PR, Mumper RJ, Khan MA, Allen DD. 2002. Nanoparticle technology for drug delivery across the blood-brain barrier. *Drug Dev Ind Pharm* 28:1-13
39. Veisheh O, Sun C, Fang C, Bhattarai N, Gunn J, et al. 2009. Specific targeting of brain tumors with an optical/magnetic resonance imaging nanoprobe across the blood-brain barrier. *Cancer Research* 69:6200-7
40. Guarnieri D, Falanga A, Muscetti O, Tarallo R, Fusco S, et al. 2012. Shuttle-mediated nanoparticle delivery to the blood-brain barrier. *Small*:n/a-n/a

41. Juszczak P, Kolodziejczyk AS, Grzonka Z. 2009. FTIR spectroscopic studies on aggregation process of the beta-amyloid 11-28 fragment and its variants. *Journal of Peptide Science* 15:23-9
42. Hilbich C, Kisterswoike B, Reed J, Masters CL, Beyreuther K. 1991. Aggregation and secondary structure of synthetic amyloid beta-A4 peptides of Alzheimer's disease. *Journal of Molecular Biology* 218:149-63
43. Milton NGN, Mayor NP, Rawlinson J. 2001. Identification of amyloid-beta binding sites using an antisense peptide approach. *Neuroreport* 12:2561-6
44. Wood SJ, Wetzel R, Martin JD, Hurle MR. 1995. Prolines and amyloidogenicity in fragments of the Alzheimer's peptide beta/A4. *Biochemistry* 34:724-30
45. Fradinger EA, Monien BH, Urbanc B, Lomakin A, Tan M, et al. 2008. C-terminal peptides coassemble into A beta 42 oligomers and protect neurons against A beta 42-induced neurotoxicity. *Proceedings of the National Academy of Sciences of the United States of America* 105:14175-80
46. Li HY, Monien BH, Fradinger EA, Urbanc B, Bitan G. 2010. Biophysical characterization of A beta 42 C-terminal fragments: inhibitors of A beta 42 neurotoxicity. *Biochemistry* 49:1259-67
47. Urbanc B, Betnel M, Cruz L, Li H, Fradinger EA, et al. 2011. Structural basis for A beta(1-42) toxicity inhibition by A beta C-terminal fragments: discrete molecular dynamics study. *Journal of Molecular Biology* 410:316-28
48. Findeis MA, Musso GM, Arico-Muendel CC, Benjamin HW, Hundal AM, et al. 1999. Modified-peptide inhibitors of amyloid beta-peptide polymerization. *Biochemistry* 38:6791-800
49. Yoo B, Kirshenbaum K. 2008. Peptoid architectures: elaboration, actuation, and application. *Current Opinion in Chemical Biology* 12:714-21
50. Zuckermann RN. 2011. Peptoid origins. *Biopolymers* 96:545-55
51. Davis TJ, Soto-Ortega DD, Kotarek JA, Gonzalez-Velasquez FJ, Sivakumar K, et al. 2009. Comparative study of inhibition at multiple stages of amyloid-beta self-assembly provides mechanistic insight. *Molecular Pharmacology* 76:405-13

52. Levine H. 1993. Thioflavine-T interaction with synthetic Alzheimer's-disease beta-amyloid peptides - detection of amyloid aggregation in solution. *Protein Science* 2:404-10
53. Biancalana M, Koide S. 2010. Molecular mechanism of Thioflavin-T binding to amyloid fibrils. *Biochimica Et Biophysica Acta-Proteins and Proteomics* 1804:1405-12
54. LeVine H. 1999. Quantification of beta-sheet amyloid fibril structures with thioflavin T. *Amyloid, Prions, and Other Protein Aggregates* 309:274-84
55. Hudson SA, Ecroyd H, Kee TW, Carver JA. 2009. The thioflavin T fluorescence assay for amyloid fibril detection can be biased by the presence of exogenous compounds. *Febs Journal* 276:5960-72
56. Cardamone M, Puri NK. 1992. Spectrofluorometric assessment of the surface hydrophobicity of proteins. *Biochemical Journal* 282:589-93
57. Wogulis M, Wright S, Cunningham D, Chilcote T, Powell K, Rydel RE. 2005. Nucleation-dependent polymerization is an essential component of amyloid-mediated neuronal cell death. *Journal of Neuroscience* 25:1071-80
58. Roehm NW, Rodgers GH, Hatfield SM, Glasebrook AL. 1991. An improved colorimetric assay for cell-proliferation and viability utilizing the tetrazolium salt XTT. *Journal of Immunological Methods* 142:257-65
59. Reed JW. 2012. *Cerebrovascular and neuronal cellular consequences of amyloid-beta induced nuclear factor-kappaB activation*. University of South Carolina. 132 pp.
60. Frid P, Anisimov SV, Popovic N. 2007. Congo red and protein aggregation in neurodegenerative diseases. *Brain Research Reviews* 53:135-60
61. Wong HE, Qi W, Choi H-M, Fernandez E, Kwon I. 2011. A safe, blood-brain barrier permeable triphenylmethane dye inhibits amyloid-beta neurotoxicity by generating nontoxic aggregates. *Acs Chemical Neuroscience* 2:645-57
62. Doig AJ. 2007. Peptide inhibitors of beta-amyloid aggregation. *Current Opinion in Drug Discovery & Development* 10:533-9

63. Takahashi T, Mihara H. 2008. Peptide and protein mimetics inhibiting amyloid beta-peptide aggregation. *Accounts of Chemical Research* 41:1309-18
64. Re F, Airoidi C, Zona C, Masserini M, La Ferla B, et al. 2010. Beta amyloid aggregation inhibitors: small molecules as candidate drugs for therapy of Alzheimer's disease. *Current Medicinal Chemistry* 17:2990-3006
65. Williams RJ, Spencer JPE. 2012. Flavonoids, cognition, and dementia: actions, mechanisms, and potential therapeutic utility for Alzheimer disease. *Free Radical Biology and Medicine* 52:35-45
66. Porat Y, Abramowitz A, Gazit E. 2006. Inhibition of amyloid fibril formation by polyphenols: structural similarity and aromatic interactions as a common inhibition mechanism. *Chemical Biology & Drug Design* 67:27-37
67. Ghosh P, Han G, De M, Kim CK, Rotello VM. 2008. Gold nanoparticles in delivery applications. *Advanced Drug Delivery Reviews* 60:1307-15
68. Kogan MJ, Olmedo I, Hosta L, Guerrero AR, Cruz LJ, Albericio F. 2007. Peptides and metallic nanoparticles for biomedical applications. *Nanomedicine* 2:287-306
69. Connor EE, Mwamuka J, Gole A, Murphy CJ, Wyatt MD. 2005. Gold nanoparticles are taken up by human cells but do not cause acute cytotoxicity. *Small* 1:325-7
70. Oyelere AK, Chen PC, Huang XH, El-Sayed IH, El-Sayed MA. 2007. Peptide-conjugated gold nanorods for nuclear targeting. *Bioconjugate Chemistry* 18:1490-7
71. Daniel MC, Astruc D. 2004. Gold nanoparticles: Assembly, supramolecular chemistry, quantum-size-related properties, and applications toward biology, catalysis, and nanotechnology. *Chemical Reviews* 104:293-346
72. Bellova A, Bystrenova E, Koneracka M, Kopcansky P, Valle F, et al. 2010. Effect of Fe<sub>3</sub>O<sub>4</sub> magnetic nanoparticles on lysozyme amyloid aggregation. *Nanotechnology* 21
73. Cabaleiro-Lago C, Lynch I, Dawson KA, Linse S. 2010. Inhibition of IAPP and IAPP((20-29)) fibrillation by polymeric nanoparticles. *Langmuir* 26:3453-61

74. Cabaleiro-Lago C, Quinlan-Pluck F, Lynch I, Lindman S, Minogue AM, et al. 2008. Inhibition of amyloid beta protein fibrillation by polymeric nanoparticles. *Journal of the American Chemical Society* 130:15437-43
75. Yoo SI, Yang M, Brender JR, Subramanian V, Sun K, et al. 2011. Inhibition of amyloid peptide fibrillation by inorganic nanoparticles: functional similarities with proteins. *Angewandte Chemie-International Edition* 50:5110-5
76. Kogan MJ, Bastus NG, Amigo R, Grillo-Bosch D, Araya E, et al. 2006. Nanoparticle-mediated local and remote manipulation of protein aggregation. *Nano Letters* 6:110-5
77. Liao YH, Chang YJ, Yoshiike Y, Chang YC, Chen YR. 2012. Negatively charged gold nanoparticles inhibit Alzheimer's amyloid-beta fibrillization, induce fibril dissociation, and mitigate neurotoxicity. *Small* 8:3631-9
78. Frens G. 1973. Controlled nucleation for regulation of particle-size in monodisperse gold suspensions. *Nature-Physical Science* 241:20-2
79. Jana NR, Gearheart L, Murphy CJ. 2001. Seeding growth for size control of 5-40 nm diameter gold nanoparticles. *Langmuir* 17:6782-6
80. Liu XO, Atwater M, Wang JH, Huo Q. 2007. Extinction coefficient of gold nanoparticles with different sizes and different capping ligands. *Colloids and Surfaces B-Biointerfaces* 58:3-7
81. Chan H-M, Xiao L, Yeung K-M, Ho S-L, Zhao D, et al. 2012. Effect of surface-functionalized nanoparticles on the elongation phase of beta-amyloid (1-40) fibrillogenesis. *Biomaterials* 33:4443-50
82. Walsh DM, Lomakin A, Benedek GB, Condron MM, Teplow DB. 1997. Amyloid beta-protein fibrillogenesis - detection of a protofibrillar intermediate. *Journal of Biological Chemistry* 272:22364-72
83. Jain PK, Huang XH, El-Sayed IH, El-Sayed MA. 2008. Noble metals on the nanoscale: optical and photothermal properties and some applications in imaging, sensing, biology, and medicine. *Accounts of Chemical Research* 41:1578-86

84. Puri A, Loomis K, Smith B, Lee JH, Yavlovich A, et al. 2009. Lipid-based nanoparticles as pharmaceutical drug carriers: from concepts to clinic. *Critical Reviews in Therapeutic Drug Carrier Systems* 26:523-80
85. Alexis F, Rhee JW, Richie JP, Radovic-Moreno AF, Langer R, Farokhzad OC. 2008. New frontiers in nanotechnology for cancer treatment. *Urologic Oncology-Seminars and Original Investigations* 26:74-85
86. Gao J, Gu H, Xu B. 2009. Multifunctional magnetic nanoparticles: design, synthesis, and biomedical applications. *Accounts of Chemical Research* 42:1097-107
87. Llevot A, Astruc D. 2012. Applications of vectorized gold nanoparticles to the diagnosis and therapy of cancer. *Chemical Society Reviews* 41:242-57
88. Khlebtsov N, Dykman L. 2011. Biodistribution and toxicity of engineered gold nanoparticles: a review of in vitro and in vivo studies. *Chemical Society Reviews* 40:1647-71
89. Yildirimer L, Thanh NTK, Loizidou M, Seifalian AM. 2011. Toxicological considerations of clinically applicable nanoparticles. *Nano Today* 6:585-607
90. Alkilany AM, Murphy CJ. 2010. Toxicity and cellular uptake of gold nanoparticles: what we have learned so far? *Journal of Nanoparticle Research* 12
91. Mironava T, Hadjiargyrou M, Simon M, Jurukovski V, Rafailovich MH. 2010. Gold nanoparticles cellular toxicity and recovery: effect of size, concentration and exposure time. *Nanotoxicology* 4:120-37
92. Ikeda K, Okada T, Sawada S-i, Akiyoshi K, Matsuzaki K. 2006. Inhibition of the formation of amyloid beta-protein fibrils using biocompatible nanogels as artificial chaperones. *Febs Letters* 580
93. Li YJ, Cao MW, Wang YL. 2006. Alzheimer amyloid beta(1-40) peptide: Interactions with cationic gemini and single-chain surfactants. *Journal of Physical Chemistry B* 110:18040-5
94. Lundqvist M, Sethson I, Jonsson BH. 2004. Protein adsorption onto silica nanoparticles: conformational changes depend on the particles' curvature and the protein stability. *Langmuir* 20:10639-47

95. Auer S, Trovato A, Vendruscolo M. 2009. A condensation-ordering mechanism in nanoparticle-catalyzed peptide aggregation. *Plos Computational Biology* 5
96. Gazit E. 2005. Mechanisms of amyloid fibril self-assembly and inhibition. *Febs Journal* 272:5971-8
97. Tjernberg LO, Naslund J, Lindqvist F, Johansson J, Karlstrom AR, et al. 1996. Arrest of beta-amyloid fibril formation by a pentapeptide ligand. *Journal of Biological Chemistry* 271:8545-8
98. Lowe TL, Strzelec A, Kiessling LL, Murphy RM. 2001. Structure-function relationships for inhibitors of beta-amyloid toxicity containing the recognition sequence KLVFF. *Biochemistry* 40:7882-9
99. Watanabe K, Nakamura K, Akikusa S, Okada T, Kodaka M, et al. 2002. Inhibitors of fibril formation and cytotoxicity of beta-amyloid peptide composed of KLVFF recognition element and flexible hydrophilic disrupting element. *Biochemical and Biophysical Research Communications* 290:121-4
100. Moss MA, Nichols MR, Reed DK, Hoh JH, Rosenberry TL. 2003. The peptide KLVFF-K-6 promotes beta-amyloid(1-40) protofibril growth by association but does not alter protofibril effects on cellular reduction of 3-(4,5-dimethylthiazol-2-yl)-2,5-diphenyltetrazolium bromide (MTT). *Molecular Pharmacology* 64:1160-8
101. Petkova AT, Ishii Y, Balbach JJ, Antzutkin ON, Leapman RD, et al. 2002. A structural model for Alzheimer's beta-amyloid fibrils based on experimental constraints from solid state NMR. *Proceedings of the National Academy of Sciences of the United States of America* 99:16742-7
102. Gazit E. 2002. A possible role for pi-stacking in the self-assembly of amyloid fibrils. *Faseb Journal* 16:77-83
103. Oyston PCF, Fox MA, Richards SJ, Clark GC. 2009. Novel peptide therapeutics for treatment of infections. *Journal of Medical Microbiology* 58:977-87
104. John H, Maronde E, Forssmann WG, Meyer M, Adermann K. 2008. N-terminal acetylation protects glucagon-like peptide GLP-1-(7-34)-amide from DPP-IV-mediated degradation retaining cAMP- and insulin-releasing capacity. *European Journal of Medical Research* 13:73-8

105. Hong SY, Oh JE, Lee KH. 1999. Effect of D-amino acid substitution on the stability, the secondary structure, and the activity of membrane-active peptide. *Biochemical Pharmacology* 58:1775-80
106. Stromstedt AA, Pasupuleti M, Schmidtchen A, Malmsten M. 2009. Evaluation of strategies for improving proteolytic resistance of antimicrobial peptides by using variants of EFK17, an internal segment of LL-37. *Antimicrobial Agents and Chemotherapy* 53:593-602
107. Chen YR, Glabe CG. 2006. Distinct early folding and aggregation properties of Alzheimer amyloid-beta peptides A beta 40 and A beta 42 - stable trimer or tetramer formation by A beta 42. *Journal of Biological Chemistry* 281:24414-22
108. Ladiwala ARA, Lin JC, Bale SS, Marcelino-Cruz AM, Bhattacharya M, et al. 2010. Resveratrol selectively remodels soluble oligomers and fibrils of amyloid A beta into off-pathway conformers. *Journal of Biological Chemistry* 285
109. Kaye R, Head E, Sarsoza F, Saing T, Cotman CW, et al. 2007. Fibril specific, conformation dependent antibodies recognize a generic epitope common to amyloid fibrils and fibrillar oligomers that is absent in prefibrillar oligomers. *Molecular Neurodegeneration* 2:11
110. Wu JW, Breydo L, Isas JM, Lee J, Kuznetsov YG, et al. 2010. Fibrillar oligomers nucleate the oligomerization of monomeric amyloid beta but do not seed fibril formation. *Journal of Biological Chemistry* 285
111. Lefterov I, Fitz NF, Cronican AA, Fogg A, Lefterov P, et al. 2010. Apolipoprotein A-I deficiency increases cerebral amyloid angiopathy and cognitive deficits in APP/PS1 delta E9 mice. *Journal of Biological Chemistry* 285:36945-57
112. Wong HE, Kwon I. 2011. Xanthene food dye, as a modulator of Alzheimer's disease amyloid-beta peptide aggregation and the associated impaired neuronal cell function. *Plos One* 6
113. Bitan G, Kirkitadze MD, Lomakin A, Vollers SS, Benedek GB, Teplow DB. 2003. Amyloid beta-protein (A beta) assembly: A beta 40 and A beta 42 oligomerize through distinct pathways. *Proceedings of the National Academy of Sciences of the United States of America* 100

114. Pregi N, Wenker S, Vittori D, Leiros CP, Nesse A. 2009. TNF-alpha-induced apoptosis is prevented by erythropoietin treatment on SH-SY5Y cells. *Experimental Cell Research* 315:419-31
115. Guntert A, Dobeli H, Bohrmann B. 2006. High sensitivity analysis of amyloid-beta peptide composition in amyloid deposits from human and PS2APP mouse brain. *Neuroscience* 143:461-75
116. Irie K, Murakami K, Masuda Y, Morimoto A, Ohigashi H, et al. 2005. Structure of beta-amyloid fibrils and its relevance to their neurotoxicity: implications for the pathogenesis of Alzheimer's disease. *Journal of Bioscience and Bioengineering* 99:437-47
117. Walsh DM, Klyubin I, Fadeeva JV, Cullen WK, Anwyl R, et al. 2002. Naturally secreted oligomers of amyloid beta protein potently inhibit hippocampal long-term potentiation in vivo. *Nature* 416:535-9
118. Gong YS, Chang L, Viola KL, Lacor PN, Lambert MP, et al. 2003. Alzheimer's disease-affected brain: presence of oligomeric A beta ligands (ADDLs) suggests a molecular basis for reversible memory loss. *Proceedings of the National Academy of Sciences of the United States of America* 100
119. Kaye R, Head E, Thompson JL, McIntire TM, Milton SC, et al. 2003. Common structure of soluble amyloid oligomers implies common mechanism of pathogenesis. *Science* 300:486-9
120. Findeis MA, Lee JJ, Kelley M, Wakefield JD, Zhang MH, et al. 2001. Characterization of cheryl-leu-val-phe-phe-ala-OH as an inhibitor of amyloid beta-peptide polymerization. *Amyloid-Journal of Protein Folding Disorders* 8:231-41
121. Austen BM, Paleologou KE, Ali SAE, Qureshi MM, Allsop D, El-Agnaf OMA. 2008. Designing peptide inhibitors for oligomerization and toxicity of Alzheimer's beta-amyloid peptide. *Biochemistry* 47
122. Gordon DJ, Sciarretta KL, Meredith SC. 2001. Inhibition of beta-amyloid(40) fibrillogenesis and disassembly of beta-amyloid(40) fibrils by short beta-amyloid congeners containing N-methyl amino acids at alternate residues. *Biochemistry* 40:8237-45

123. Campioni S, Mannini B, Zampagni M, Pensalfini A, Parrini C, et al. 2010. A causative link between the structure of aberrant protein oligomers and their toxicity. *Nature Chemical Biology* 6:140-7
124. Goransson AL, Nilsson KPR, Kagedal K, Brorsson AC. 2012. Identification of distinct physiochemical properties of toxic prefibrillar species formed by A beta peptide variants. *Biochemical and Biophysical Research Communications* 420:895-900
125. Chen XS, Wu J, Luo Y, Liang X, Supnet C, et al. 2011. Expanded polyglutamine-binding peptoid as a novel therapeutic agent for treatment of Huntington's disease. *Chemistry & Biology* 18:1113-25
126. Schmittschmitt JP, Scholtz JM. 2003. The role of protein stability, solubility, and net charge in amyloid fibril formation. *Protein Science* 12:2374-8
127. Kisilevsky R, Lemieux LJ, Fraser PE, Kong XQ, Hultin PG, Szarek WA. 1995. Arresting amyloidosis in-vivo using small-molecule anionic sulfonates or sulfates - implications for Alzheimers-disease. *Nature Medicine* 1:143-8
128. Bose PP, Chatterjee U, Xie L, Johansson J, Gothelid E, Arvidsson PI. 2010. Effects of congo red on A beta(1-40) fibril formation process and morphology. *Acs Chemical Neuroscience* 1:315-24
129. Lorenzo A, Yankner BA. 1994. Beta-amyloid neurotoxicity requires fibril formation and is inhibited by congo red. *Proceedings of the National Academy of Sciences of the United States of America* 91:12243-7
130. Podlisny MB, Walsh DM, Amarante P, Ostaszewski BL, Stimson ER, et al. 1998. Oligomerization of endogenous and synthetic amyloid beta-protein at nanomolar levels in cell culture and stabilization of monomer by congo red. *Biochemistry* 37
131. Wood SJ, MacKenzie L, Maleeff B, Hurle MR, Wetzel R. 1996. Selective inhibition of A beta fibril formation. *Journal of Biological Chemistry* 271:4086-92
132. Bett CK, Serem WK, Fontenot KR, Hammer RP, Garno JC. 2010. Effects of peptides derived from terminal modifications of the A beta central hydrophobic core on A beta fibrillization. *Acs Chemical Neuroscience* 1:661-78